SAPIENZA
UNIVERSITÀ DI ROMA

PhD Course in Biochemistry

XXXVII Cycle (2021-2024)

Engineered human ferritins for the selective delivery of bioactive molecules to pathological sites

PhD candidate:

Giada Tisci

Tutor:

Dr. Elisabetta Falvo

Supervisor:

Prof. Alberto Boffi

PhD Coordinator:

Prof. Maria Luisa Mangoni

16 December 2024

Our greatest weakness lies in giving up.
The most certain way to succeed is
always to try just one more time.
– Thomas A. Edison

Acknowledgments

At the end of these three years of PhD course I would like to thank my tutor Dr. Elisabetta Falvo who guided me, who supported me and who believed in me in this great opportunity of professional and personal growth.

Thanks to Dr. Pierpaolo Ceci for his precious scientific advice and for his support over these years. Thank you, Pierpaolo and Elisabetta for making me passionate about the world of nanoparticles day after day, and for teaching me to fuel my ideas and never give up.

I want to thank my supervisor Prof. Alberto Boffi, and the coordinators of the PhD in Biochemistry Prof. Francesco Malatesta and Prof. Maria Luisa Mangoni for their academic guidance during these years.

Special thanks are also addressed to our collaborators from: CNR-IBPM, Thena Biotech, IRE, CAST, University of Verona, University of Chieti, Czech Academy of Sciences and Università Cattolica del Sacro Cuore in Rome.

I wish to thank my lab mates, Siria, Patrizio and all the people of the of Biochemical Sciences "A. Rossi Fanelli" for their helpful encouragement and friendship. Thanks to Francesca, Benedetta and Francesca for their precious and sincere affection. Thanks to Antonella for sharing every moment of these three years with me. You made the most difficult moments easier.

I would like to thank my family for their sweety and tireless support in every moment. Dear mom, thank you for your wisdom and for your ability to calm me down. Thanks dad for teaching me perseverance, and thanks Mario for making me dream a little.

Thanks to my friend Gloria, despite the distance you are always close to me.

Thanks to my dear friend Antonio, he is like a Roman brother for me. Thank you for your advice, fun times and your constant friendship since 2014.

Last but not least, thanks to a very special person, Carmine. You have encouraged me in everything I do and I'm so grateful to have you in my life. Thank you for your love and for making me appreciate all the little things.

INDEX

1. INTRODUCTION

Cancer is a serious public health issue with a rapidly growing incidence and mortality worldwide (Sung et al., 2021). It is a particular pathological condition characterized by the development of abnormal cells that divide uncontrollably, they infiltrate and destroy normal body tissue. It is a second-leading cause of death in the world. The most diagnosed cancers worldwide were those of the lung (1.8 million, 13.0% of the total), breast (1.7 million, 11.9%), and colorectum (1.4 million, 9.7%). The prediction of numbers and trends for cancer mortality in Europe fell by 6.5% and by 4%, respectively, in men and in women from 2018 to 2024 (Santucci et al., 2024). The number of deaths is still rising, with a total of 1.270.800 predicted deaths in 2024 in the EU, due to population growth and aging (Santucci et al., 2024). The key strategies for cancer prevention are: pursue tobacco control, improve dietary patterns, eliminate alcohol intake, and implement population screening for early diagnosis. Nowadays chemotherapy, hormone, and biological therapies are used as treatment for metastatic cancers, meanwhile surgery and radiotherapy are applied for local and non-metastatic tumors. Usually, the main target of cancer drugs is the damage to nucleic acids of cells: the Ribonucleic acid (RNA) or Deoxyribonucleic acid (DNA), that are important in cell divisions. If the cancer cells are unable to divide, they die. The typical side effect of chemotherapy is due to damage to certain types of healthy cells, especially cells in the gastrointestinal tract and hair follicles. For this reason, the main challenge in the development of therapeutics is the finding of the way to obtain a more selective delivery of the drug to the pathological site by using smart carriers/vehicles. In fact, one injected, the carrier/vehicle must pass several impermeable barriers and degradative systems before reaching their sites of action by providing preferential drug accumulation at, such as

endothelial and epithelial barriers, enzymatic degradation, mononuclear phagocyte system (MPS), opsonization, interstitial transport, cell membrane, nuclear membrane (Lu et al., 2023; Perez and Fernandez Medarde 2015; Sun et al., 2014). Therefore, it would be desirable to develop highly efficient therapeutics, the so-called “magic bullets”, that can overcome biological barriers, distinguish between malignant and benign cells, selectively target the cancerous tissues, and “intelligently” respond to the heterogeneous and complex microenvironment inside a tumor for on-demand release of therapeutic agents in the optimal dosage range (Alshawwa et al., 2022; Peer et al., 2007).

Targeted delivery of anti-cancer therapeutics to cancer cells ("site-specific drug delivery") aims at enhancing accumulation of the drugs within the tumor while guiding them away from potentially healthy tissues (Arafat et al., 2024; Sun et al., 2014, Pérez-Herrero and Fernández-Medarde 2015). In recent years FDA approved many targeted cancer drugs, thus decreasing the adverse reactions and increased probability of effective treatment (Karati et al. 2024).

1.1 Tumor environment and targeting strategies

The study of tumor microenvironment (TME) is important to understand problems of drug delivery in cancer. The TME includes diverse immune cells, cancer-associated fibroblasts (CAFs), endothelial cells, and the extracellular matrix (ECM). The microscopic examination of solid tumors reveals that TME is a highly structured ecosystem containing cancer cells surrounded by diverse non-malignant cell types, collectively embedded in an altered, vascularized extracellular matrix (Karin et al., 2023). These components may vary by tissue type and co-evolve with the tumor as it progresses. The normal tissue

microenvironment can constrain cancer outgrowth through the suppressive functions of immune cells, fibroblasts, and the ECM. During the metastatic stages, the TME helps to control metastatic cell dormancy, emergence from this state, and subsequent metastatic outgrowth. Different types of proteins are involved in the remodelling and progression of TME. In the progression of malignant tumor and in the rapidly growing of malignant cells are very important two elements: the diffusion of oxygen and the absorption of nutrients. Therefore, it is necessary for the TME evolution, the formation of new blood vessels (Baban and Seymour; 1998; Jones and Harris 1998). Some important angiogenic factors are release by neoplastic tissue to increase tumor microvasculature and increase tumor size (LaRocque et al., 2009). Specific matrix metalloproteinases (MMPs) are release too. This type of enzymes are capable of degrading all kinds of extracellular matrix proteins and are tightly associated with malignant processes of tumors, such as metastasis and angiogenesis (Corry et al., 2004; Overall and Kleifeld, 2006). The resultant imbalance of angiogenic factors and MMPs within neoplastic tissues results in highly disorganized vessels, which are dilated, with numerous pores and wide gap junctions between endothelial cells (Quintero et al., 2019). Cancer cells can create a tumor-supportive environment by remodelling the vasculature and extracellular matrix (ECM). The vasculature of tumors is marked by a heterogeneous distribution of vessel sizes and shapes, generally larger vessel diameters, higher vascular density, and enhanced permeability. The size of the gaps between the leaky endothelial cells ranges from 100 to 780 nm depending on the tumor type (Hobbs et al., 1998; Rubin and Casarett 1966; Shubik 1982). This contrasts with the tight endothelial junctions of normal vessels typically of 5 to 10 nm size. In several angiogenic processes are involved some specific receptors such as αVβ3 and αVβ5 integrins, and neuropilin-1 (NRP-1) (Aman

et al., 2023; Niland et al., 2019; Rizzolio et al., 2011). These types of proteins are abundantly present in tumor vasculatures and cells. Therefore, the tumor vasculature can be considered as the target of tumor diagnosis and treatment.

ECM and interstitial fluid are two compartments that form tumor interstitium. It is composed of an elastic network of collagen fibers filled with hydrophilic fluid which has high interstitial pressures offering resistance to the internal flux of molecules (Jain 1987; Heldin et al., 2004).

For transporting drugs in the interstitium is important the combination of external interstitial pressure and the properties of the diffusing drug including particle size and configuration, hydrophobic nature, and electrical charge. Solid tumors have high interstitial fluid pressure (IFP) derive from tumor properties such as the vessel leakiness and the poorly working lymphatic vessels (De Visser et al., 2023). The pressure causes fluids to flow out of tumors, which limits diffusion of carriers to opposite direction. The absence of a relevant lymphatic system inside a tumor is responsible of insufficient drainage, and for the elongation of retention time in tumor interstitium by drugs. This phenomenon of leaky vasculature and impaired lymphatic drainage has been referred to as the enhanced permeability and retention effect (EPR) (Maeda et al., 2000, Maeda 2001; Subhan et al., 2021; Vannucci et al., 2014). In general, drug-carrier compounds can be delivered to tumors by two strategies: passive and/or active targeting (**Figure 1**).

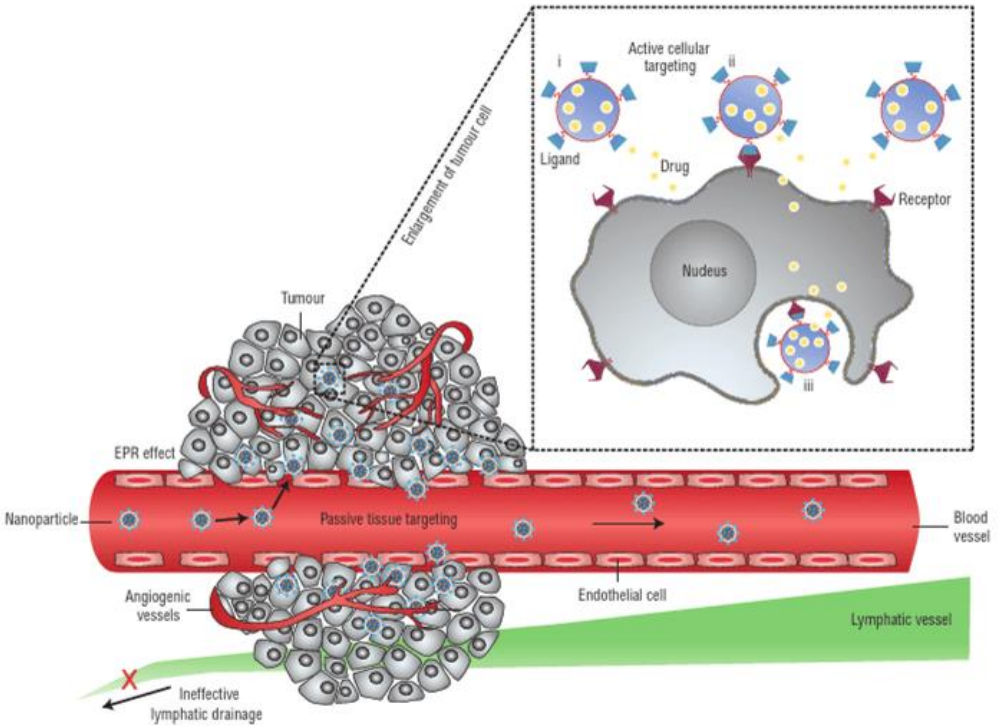

Figure 1. Nanoparticles, as an example of drug carriers, as promising transporters of anticancer drugs to tumors by passive tissue targeting and active cellular targeting. Passive tissue targeting uses the increased permeability of tumor vasculature and the poor lymphatic drainage of tumors (EPR effect), allowing the release of chemotherapeutic agents in the vicinity of the tumor. Active cellular targeting is achieved by functionalization of the surface of nanoparticles, containing chemotherapy drugs, with targeting moieties that provide selective recognition of different receptors or antigens overexpressed in cancerous cells, increase their therapeutic efficacy, and overcomes the multiple-drug resistance. Nanoparticles, once in the vicinity of the tumor, can: (i) release their cytotoxic content next to the cancer cells; (ii) bind to the membrane of the cancer cells and release their content in a sustained way; (iii) be internalized into the cell (Peer et al., 2007).

1.1.1 Passive targeting

In tumors, the passive targeting of drug-carrier compounds is due to the enhanced permeability and retention effect (EPR). This phenomenon is linked to extravasation of macromolecules through the leaky and poorly differentiated neo-vascular tumor system and, at the same time, the lack of an effective lymphatic drainage (**Figure 1**). The result of EPR is the accumulation of extravasated materials at the tumor site (Danhier et al., 2010; Matsumura and Maeda 1986).

As the endothelial pore size of tumor vessels varies from 10 to 1000 nm (5-10 nm in normal vessels), carriers with the size of about 10-150 nm are considered being able to extravasate and accumulate in the tumor in the interstitial space. Moreover, inefficient lymphatic drainage system inside a tumor facilitates accumulation of large particles in the TME (Chehelgerdi et al., 2023; Maeda 2001; Maeda et al., 2013; Perrault and Chan 2010). This condition further leads to an increased interstitial pressure and a reduced intra-extravascular gradient (Baronzio et al., 2012). Therapeutic particles entering the tumor microenvironment and are captured and are thus accumulated and retained inside the tumor. Using this mechanism, a very high local concentration of drug-loaded carriers can be delivered to the tumor site at, for instance, a 5–50-fold higher rate than in normal tissue within few days (Din et al., 2017). Despite the potential of the EPR effect in targeted drug delivery with carriers, some limitations related to the nature of tumors have been recognised. Solid tumors have high interstitial fluid pressure (IFP) that is assumed to result from tumor properties such as the poorly working lymphatic vessels and heterogeneity of vessels formed through angiogenesis. For example, hypo vascular tumors such as prostate and pancreatic cancers are very difficult to reach, there are differences in the vascular permeability in the same single

tumor. Moreover, in some parts of unhealthy tissue, macromolecules as large as 200 nm are able to extravasate and penetrate, whereas in other parts, even molecules of about 15 nm are unable to enter the interstitium. Another limitation can be the presence of necrotic areas, especially in larger neoplasms (Rossin et al., 2005). Therefore, to efficiently target tumors, it is necessary to coupled passive and active targeting at the same time. Active targeting occurs only after passive accumulation in tumors.

1.1.2 Active targeting

Active targeting is an example of a way to overcome limitations of passive targeting (**Figure 1**). In an actively targeted system, a targeting moiety (such as antibodies, peptides, aptamers or small molecules) is present on the carrier surface in order to bind the particle to the receptors expressed on the tumor/endothelial cell surface (Arap et al., 1998; Leamon and Reddy 2004; Sudimack and Lee 2000; Wu et al., 2010). If the targeting moiety is not naturally present on the carrier surface, it could be possible to functionalize the relative surfaces through: hybridization methods (Aubin-Tam 2013; Yu et al., 2012) or bioconjugation strategies (direct conjugation, linker chemistry, physical interactions) (Shi et al., 2023).

For systems based on proteins, as protein-based nanoparticles (NPs), it is possible a more powerful and reproducible conjugation method: a genetic engineering approach. Genetic engineering allows to obtain NPs with the same architecture in a simple and reproducible way, better than chemical modifications (Obozina et al., 2023).

For this type of approach, it is necessary to genetically insert the peptide sequences in the amino acid protein sequence to build a specific and homogeneous construct and avoid repeated and expensive chemical reactions (De la Rica and Matsui 2010; Vannucci et al., 2014). Targeted particles are then internalized by a receptor-mediated endocytosis. In particular, after receptor-binding, the antigen-ligand complex can enter into the cell by forming an endocytotic vesicle that detaches from the membrane and moves inside the cell compartments. This receptor-mediated endocytosis is necessary for the bypassing of the recognition of P-glycoprotein, one of the main drug resistance mechanisms (Allen 2002; Maeda 2001). In fact, a variety of mechanisms at the cellular level contribute to drug resistance. These include the presence of drug efflux proteins on the cell membrane, an example of which is the membrane bound P-glycoprotein (P-gp), which decreases the intracellular concentration of cancer drugs (Links and Brown 1999; Krishna and Mayer 2000). P-gp may also be present on the nuclear membrane limiting drug transport into the nucleus (Calcabrini et al., 2000). Additionally, drugs showing intracellular access may be trapped in cytoplasmic vesicles, not released, and then degraded, or externalized from the cell still contained in the exocytosed vesicle (Vasir and Labhasetwar 2005). In receptor-mediated endocytosis mechanism, there are some main steps: the recognition and the binding between targeted carriers and the specific receptor, formation of endosome around ligand-receptor complex and the transfer of this new endosome to specific organelles for the enzymatic or acidic release of drugs. Active targeting of particles allows carriers to bind with high affinity and selectivity some molecules overexpressed by tumor cells (Danhier et al., 2010; Friedman et al., 2013). Active drug targeting is generally realized to improve target cell recognition, cell uptake and restoring the body immunological response against cancer.

Peptides, small organic molecules, oligosaccharides, and monoclonal antibodies (mAbs) belong to the targeting ligands category (Friedman et al., 2013). The mAbs have been widely used as tumor-homing molecules for the targeted delivery of NPs; however, several limitations including large size, difficulty in conjugation to NPs and high manufacturing costs have hampered their use. For this reason, NPs was decorated with smaller-sized ligand (including peptides) to obtain major selectivity (Talekar et al., 2011). In general, three cellular targets can be distinguished in the active targeting strategy: (a) the targeting of cancer cell and (b) the targeting of tumor vasculature (c) the targeting of receptors involved in the immune response. Thanks to the active targeting, drug carriers have more chances to reach their targets, with lower limitations due to extravasation or tumor interstitium (Bedi et al., 2013; Sakhrani and Padh 2013; Wang et al., 2011).

1.2 Drug delivery based on nanoparticles

Nanoparticles have emerged as a promising alternative to conventional cancer therapies and for cancer imaging. They can be triggered by specific stimuli and target-specific sites with precise capability to co-delivering therapeutics and diagnostic reagents. This type of system has been intensively studies with the aim to overcome limitations associated with conventional cancer diagnosis and therapy, such as rapid clearance, insolubility under aqueous conditions and lack of selectivity (Bao et al., 2013; Howell et al., 2013; Rossin et al., 2005). An ideal multifunctional nanocarrier would allow for the simultaneously loading of therapeutics, ligands for cell specific targeting and fluorescent materials for ease of detection. Targeting cancer therapeutics to solid tumors is facilitated by particle delivery systems capable of escaping phagocytic

clearance by the reticuloendothelial system (RES) (Aggarwal et al., 2009; Fan et al., 2023; Moghimi and Patel 1998; Papisov 1998). In desirable conditions, nanocarriers preferentially extravasate the tumor vasculature and accumulate in TME (Maruyama et al., 1999). Thanks to the "target-design" of NPs they reduce their accumulation in healthy organs (Moghimi and Patel 1998; Paciotti et al., 2005; Papisov 1998), consequently, the drug's therapeutic index increases. Research on NPs also works to develop new methods to overcome problems linked to the cellular resistance mechanisms (Baban et al., 1998; Hobbs et al., 1998; Jain 2001; Jones et al., 1998; Shubik 1982; Salmaso and Caliceti 2013). Other optimizations in the field of nanocarriers concern the process of production of this type of particles. For the production, it is necessary the homogeneous synthesis of nanocarriers in size, shape, and chemistry. The ideal nanoparticles size should be somewhere between 10 and 100 nm, for efficient extravasation and to avoid the filtration by the kidneys. In this context, the charge of the NPs should be neutral or anionic to obtain an efficient evasion of the renal elimination, as well as of the RES-based phagocytosis (Gullotti and Yeo 2014; Malam et al., 2009). Therefore, to promote a prolonged circulation in the bloodstream, NP surface should be functionalized. In the past, a common functionalization method was the procedure called PEGylation, a coating of the NP surface with polyethylene glycol (PEG). The coating of the surface of NPs with PEG chains often results in a significant increase of the blood circulation half-life by several orders of magnitude (10-100) (Essa et al., 2011; Ferrari et al., 2013; Pozzi et al., 2014). The steric repulsion forces of the hydrophilic protective layer around NPs, repel the absorption of opsonin proteins, thereby blocking and delaying the opsonization process (Romberg et al., 2008; Sant et al., 2008; Xie et al., 2007). Some more recently approaches to extend life span of the NPs by slowing

clearance from the body, exploit other types of surface modifications: polysaccharide dextran decoration, PASylation, XTEN and CTP (carboxyl terminal peptide) conjugation (Fares et al., 2007; Köber et al., 2015; Kotagiri et al., 2013; Lee et al., 2017; Schlapschy et al., 2013). The last three approaches involve genetic or chemical fusion of the random polypeptide sequences composed of the amino acids Proline, Alanine, and Serine (for PASylation), or Alanine, Glutamate, Glycine, Proline, Serine and Threonine (for XTEN) or derived from the carboxyl terminal of human chorionic gonadotropin β subunit (for CTP). The random amino-acid PAS sequence is a more efficient alternative to PEG, because it has lower disadvantages link to development and pharmaceutical production (Harari et al., 2014; Schlapschy et al., 2013; Strohl et al., 2015). The highlights of these two sequences attached to existing proteins and material, are represent by: the elongation of retention time in the blood, the extension of NPs life span, and the maintenance of biological activity during time (Fares et al., 2007; Schlapschy et al., 2013). Therefore, thanks to the recombinant DNA techniques, it is possible to obtain PAS, XTEN or CTP-modified proteins with inferior levels of production complexity and costs. Examples of biocompatible nanocarriers include those composed of liposomes, polymers, micelles, engineered multi-functional antibodies, and nanoparticles that can be composed of metals (e.g., gold, silver), polymer, quantum dots, dendrimers, fullerenes, proteins, DNA, other biological molecules or combinations of these materials (Alexis et al., 2010; Ding et al., 2013; Lammers et al., 2012; Nie et al., 2007).

1.3 Protein-based systems

Protein-based nanoparticles represent an important platform of nanotechnology in drug delivery systems. The great interest in this type of nanocarriers, comes from their exceptional characteristics, namely biodegradability, solubility, functionalization versatility and their extraordinary binding capacity to various drugs. In the nanomedicine field, natural or synthetic protein systems are used for drug delivery, including viral capsids, monoclonal antibodies, heat shock proteins, albumin, transferrin and ferritin (Ft) (**Figure 2**). Important advantages of using protein-based nanoparticles as nanocarrier are due to the possibility of targeting specific type of cells (for example cancer cells), and to their excellent capacity of conjugation with several drugs. Recombinant antibodies loaded with drugs, also called antibody-drugs conjugates (ADCs), have been investigated linked to their high target specificity, and an extensive pharmaceutical development is ongoing (Birrer et al., 2019; Carter and Lazar 2018; Hong et al., 2020). Other protein classes are used as nanocarriers due to their stability in the human blood and to their specific internalization through membrane receptors over-expressed on cancer cells, mainly serum albumin (Park et al., 2012), transferrin (Daniels et al., 2012) and ferritin proteins (Fan et al., 2013). Thanks to its structural and biochemical peculiarities, ferritin represents one of the most appealing drug-nanocarrier.

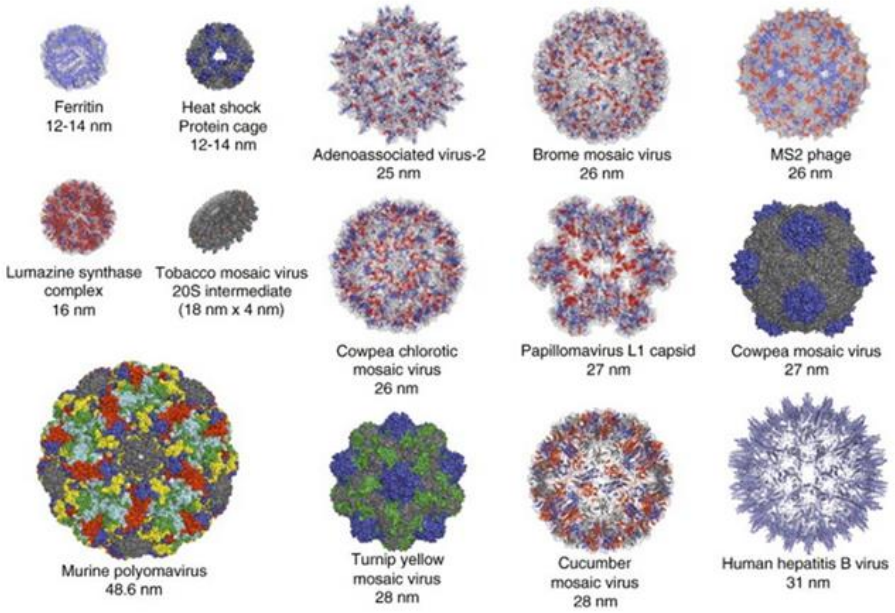

Figure 2. Types of protein cage structures currently being developed for applications in bio nanotechnology applications.

1.4 Ferritins

Human ferritins represent one of the most popular protein-based nanoparticles in drug-delivery studies. This is due to its unique cage-like structure, important for encapsulation processes, and to its other advantageous features. This nanoparticle is a natural protein, with intrinsic targeting ability and excellent biosafety. Ferritin drug carrier (FDC) has sparked great interest among researchers and shown promising application potential in the biomedical field (Zhang et al., 2021).

1.4.1 Structural and functional properties

Ferritin consists of 24 subunits that form a globular protein, assemble into a shell-like molecule enclosing a hollow cavity with external and internal diameters of 12 nm and 8 nm, respectively (Harrison and Arosio 1996). A non-toxic, water soluble, yet bioavailable iron core, often consisting in a ferric oxy-hydroxide mineral, is stored within the ferritin hollow shell. Ferritin protein without loaded iron is also referred as apoferritin (Ceci et al., 2012). The single subunits of the 24-mer cage of all these proteins are folded in a characteristic four-helical bundle, formed by four antiparallel helices (A-D, named in order from the amino terminus), and a shorter helix on the top of them (E) in the carboxy-terminal end lying at a 60° angle with respect to the four-helix bundle (**Figure 3**).

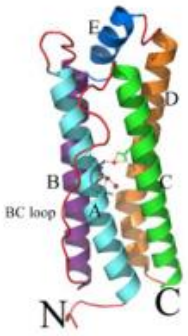

Figure 3. Monomeric fold of Human H ferritin.

The subunits related by 3- and 4-fold symmetry form at their junction pores that traverse the protein shell in order to allow the passage of ions and small molecules (**Figure 4**).

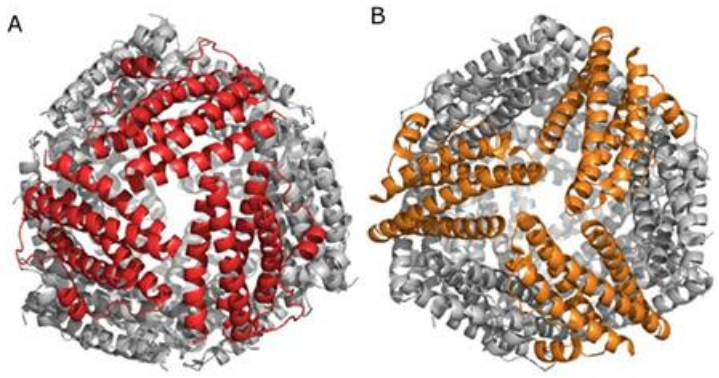

Figure 4. Quaternary assembly of ferritin from Pyrococcus furiosus (PDB code: 2JD7). **A**. View along the four-fold axis. **B**. View along the three-fold axis. The subunits forming the four- and three-fold interfaces are indicated in orange and red, respectively, the other subunits are grey.

The threefold pores are hydrophilic, being lined with negatively charged residues, and are involved in the uptake of Fe (II) ions. In particular, the entrance of iron ions in the channels are guided to the 3-fold pores by a negative electrostatic gradient, and reaches specific catalytic sites, named the ferroxidase sites, where it is oxidized by molecular oxygen. Fe (III) thus produced moves to the protein cavity where the iron core nucleates and grows at specific iron binding/nucleation sites to encompass up to 4,000 iron atoms (**Figure 5**).

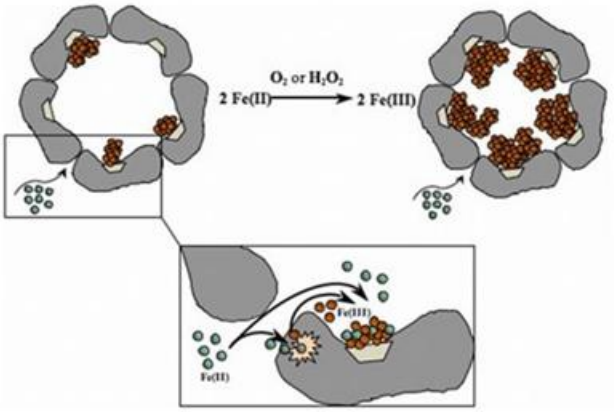

Figure 5. A schematic illustration of the most widely accepted mechanism for iron incorporation in ferritin proteins. Briefly, Fe (II) atoms (green) enter the cavity enclosed by protein subunits (dark grey) via the hydrophilic pores. From these pores, Fe (II) atoms are driven to the ferroxidase centre (light pink) where they are oxidized to Fe (III). Fe (III) atoms (brown) move to the iron nucleation sites (light grey), where Fe (III)-mineral formation is initiated. When the Fe (III)-mineral reaches a sufficient size, Fe (II) atoms can also get oxidized directly on the surface of the growing mineral.

All animal ferritins are assembled from two subunit types, the heavy (H chain; 21 kDa) and light chains (L chain; 20 kDa). H chains contain the catalytic centres and are more abundant in tissues with an active iron metabolism. L chains contain many nucleation sites and are more abundant in iron storage tissues like spleen (horse spleen ferritin, for example contains ~15% H and ~ 85% L chains). In contrast, bacterial ferritins contain a single subunit type that resembles the H chains. The quaternary structure of ferritin (i.e., the globular protein shell) is well-conserved. The N-terminal ends of each subunit are located on the ferritin surface and the C-terminal ends point toward the inner cavity (**Figure 6**).

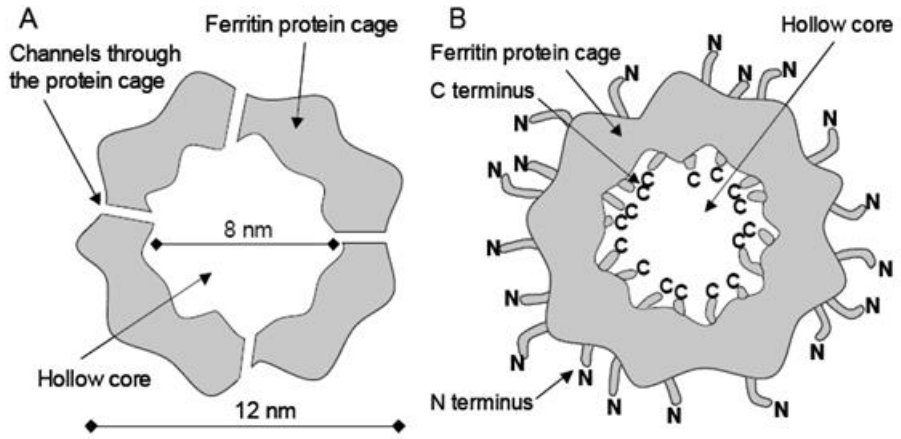

Figure 6. Schematic representations of ferritin (cross section). **A**. Ferritin is globular, hollow protein with outer and inner diameters of 12 nm and 8 nm, respectively. The protein coat is perforated by several small channels. **B**. Ferritin consists of 24 subunits, the amino-termini (denoted with N) of which protrude from the protein outer surface. The carboxy-termini (denoted with C) are located in the inner cavity of the protein.

1.4.2 Ferritins for human applications *in vivo*

Ferritin nanoparticles have been used in several applications in biomedical field. Nanocarriers based on the heavy chain of the human protein ferritin (HFt) show interesting features and advantages for active targeting drug-delivery.

In physiological conditions, HFt is stable and soluble, and it is present both inside cells and, at low levels (about 20 μg/L), in the bloodstream. HFt is exploited as a nanocarrier for delivery of drugs thanks to its great ability to bind transferrin receptor 1 (TfR1 or CD71), that it is overexpressed by several solid and hematological tumors (Li et al., 2010). Furthermore, Ft cage structure is resistance to a wide range of temperatures (up to 80 °C) and pH (2–10). These aspects allow for: pH-dependent encapsulation of drugs inside the Ft cavity and large-scale production at a low cost through recombinant

techniques. For example, under extreme environments, such as strong acidic pH, the quaternary structure of ferritin disassembles but, interestingly, reassembles once pH returns to physiological conditions. Thus, by manipulating the disassembly and reassembly of ferritin, it is possible to encapsulate therapeutic drugs inside its cage-structure (**Figure 7**). In fact, due to its 8-nm diameter inner cavity, ferritin has the potential space to encapsulate many drug molecules, thus offering protection from degradation as well as limiting potential side effects to healthy cells.

Figure 7. Schematic illustration of nanoparticles synthesis using ferritins as nano-reactors (see text for details). Ferritin-drug loading approach using the assembly-disassembly approach.

Other important features of HFt are linked to the particle dimensions, because HFt NPs are small (< 20 nm), so they can pass human body barriers to reach specific targets, but at the same time they are large enough to avoid rapid clearance through the kidney (the ideal diameter being lower than 30 nm and greater than 6–8 nm, respectively).

Thanks to genetic engineering and chemical conjugation, which involved many chemical groups naturally exposed to both the external and internal protein (primary amines, carboxylates, thiols), it is possible to easily functionalize HFt. In this way, the exterior surface is another platform to be used for drugs loading, such as chemotherapeutics, toxins and cytotoxic

peptides. Different studies have begun to design the external surface of ferritin NPs as a carrier to deliver drugs for the purpose of therapy (Choi et al., 2021; Kang et al., 2021; Kwon et al., 2012; Lee et al., 2017; Liu et al., 2022; Tesarova et al., 2020; Wang et al., 2019; Xin et al., 2024).

1.4.3 Tumor targeting using ferritin-based NPs

For drug-delivery applications, the development of molecules endowed with the ability to specifically direct NPs to selected cells and tissues would be of great value. In this direction, the exterior surface of the ferritin assembly possesses all the features necessary to operate as an appropriate platform for specific cell targeting/delivery. As mentioned above, modification of the protein exterior surface can be achieved either chemically or genetically (**Figure 8**). Several examples are present in literature where human ferritin was chemically or genetically modified to produce an efficient drug-delivery system (Khoshnejad et al., 2018).

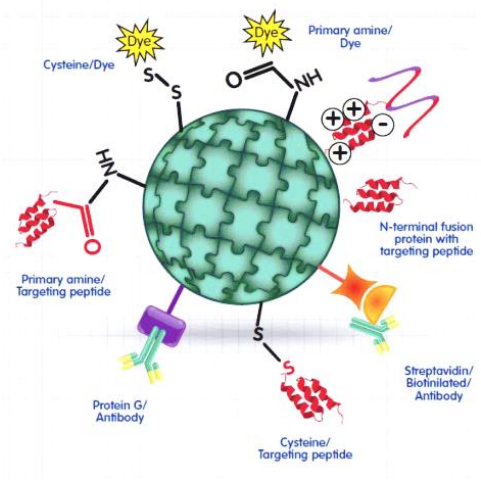

Figure 8. Ferritin external surface can be functionalized by attaching different molecules chemically or genetically (Truffi et al., 2016).

1.4.4 Intrinsic targeting ability of the HFt: the Transferrin Receptor 1 (TfR1/CD71)

TfR1(or CD71) is one of many molecules involved in the process of iron transport and utilization. This receptor is a universally expressed cell entry carrier whose primary function is to import Transferrin-bound iron in response to variations in intracellular concentration of this essential element (Gammella et al., 2017). It is a homodimeric type II transmembrane protein composed of a small cytoplasmic domain (in humans, residues 1-60), a single-pass transmembrane region (residues 61-88), and a dimeric extracellular domain (residues 89-760). Each monomer of the ectodomain, whose total molecular weight is 150 kDa, is in turn subdivided in a protease-like domain (P) in contact with the cell membrane, a helical domain (H) comprising the dimer contact regions, and an apical (A) domain (Lawrence et al., 1999) (**Figure 9**).

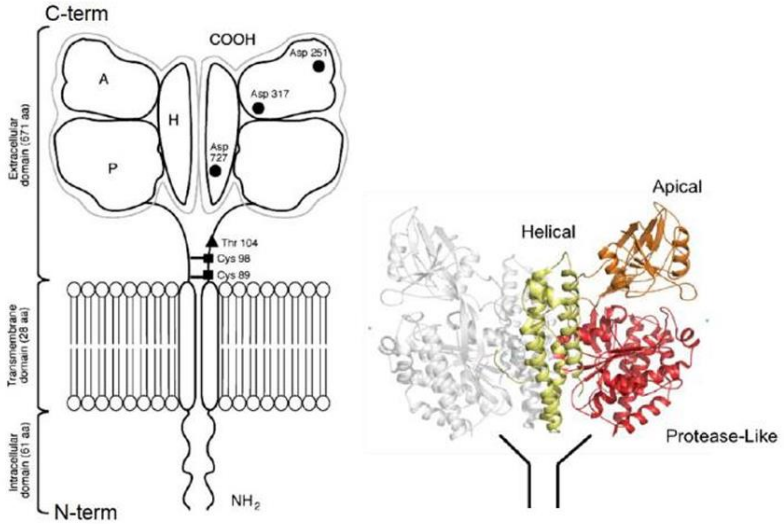

Figure 9. Human Transferrin Receptor 1 (hTfR1 or CD71). Left: cartoon structure of the whole protein, divided in intracellular, transmembrane and extracellular domains (Daniels et al., 2012). Right: crystallographic structure (pdb 3KAS, visualized with Chimera (Pettersen et al., 2004) of the sole ectodomain, subdivided in protease-like, helical and apical domains.

The ectodomain displays binding sites for diverse ligands (**Figure 10**). Its basal portion (formed by P and H domains) binds transferrin (Tf), while the H domain forms a complex with the Hereditary Hemochromatosis factor (HFE): these proteins are both involved in iron homeostasis. HFE negatively regulates iron uptake by competing with Tf for CD71: its association lowers the affinity of hCD71 for Tf up to 50-fold (Bennett et al., 2000; Lebrón et al., 1998).

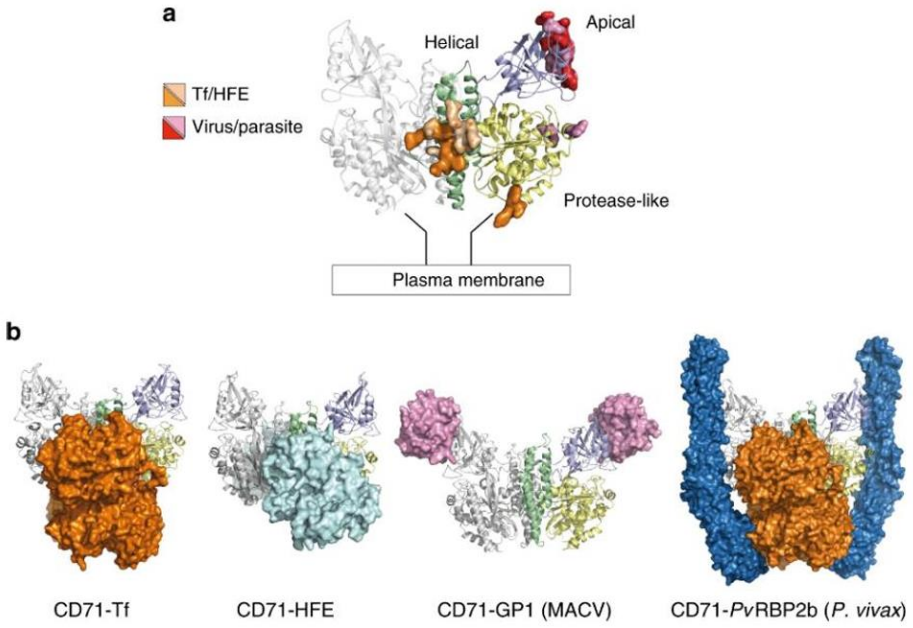

Figure 10. CD71 ligand recognition epitopes and binding modes that are to date known. A. CD71 residues identified as recognition epitopes for iron-regulating proteins Tf/HFE, and viruses/parasite are represented as orange/wheat and red/pink surfaces, respectively. B. CD71 receptor is shown bound to Tf (orange surface, pdb 1SUV (Cheng et al., 2004)), 30 HFE (cyan surface, pdb 1DE4 (Bennett et al., 2000)), GP1 protein of MACV (pink surface, pdb 3KAS (Abraham et al., 2010)), Tf and PvRBP2b from P. vivax (orange and blue surfaces, pdb 6D04 (Gruszczyk et al., 2018)). Figure obtained with Chimera (Pettersen et al., 2004).

Pivotal research by Li et al. in 2010, highlighted that HFt has the ability to bind to CD71 and effectively target cancer cells. In fact, only HFt (but not the light chain of human ferritin, LFt) can bind CD71, that it is highly express on the cancer cell surfaces. CD71 is upregulated on these types of cells (up to 100-fold higher than in normal cells) due to its involvement in iron homeostasis and cell growth regulation (**Figure 11**).

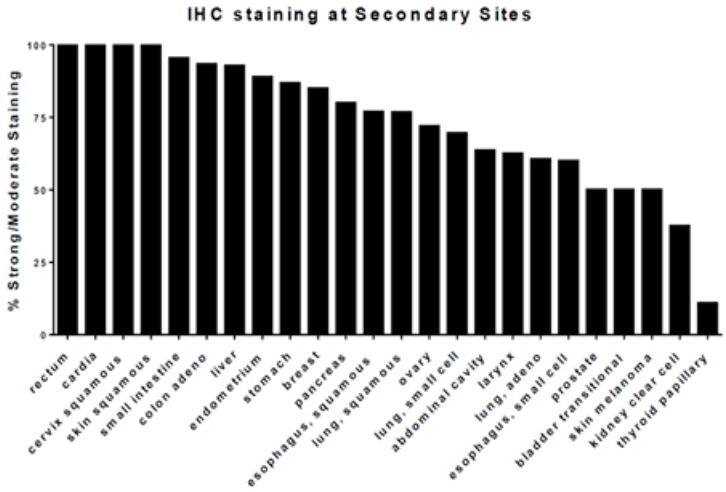

Figure 11. CD71 immunohistochemistry (IHC) staining in different tissues show that it is highly overexpressed in many metastatic cancers (Singh et al., 2016).

Recently, HFt was shown to be internalized by CD71 in more than 474 clinical tissue specimens and specifically recognize several types of tumor (i.e. liver, lung, pancreas, colon, cervical, ovarian, prostate, breast, sarcoma and thymus cancers) over non-tumor tissues with 98% sensitivity and 95% specificity (Fan et al., 2012). The high expression of CD71 in tumor cells (Daniels et al., 2006) is probably linked to the enhanced request of DNA synthesis in dividing cells in presence of ribonucleotide enzyme. In fact, this enzyme uses iron as

cofactor. Interestingly, it was reported that HFt is able to delivery substances or drugs directly to the cell nucleus. Papers by Zhang et al., (2015) and Bellini et al., (2014) underline the selective capability of HFt, but not LFt to shuttle doxorubicin molecules (DOXO) to the cell nucleus. In this case, HFt nanocages loaded with DOXO could behave like a "Trojan horse", called back within the nucleus for the purpose of defence it through the well-reported HFt antioxidant activity (**Figure 12**). On the contrary, once reached the cell nucleus, HFt can release cytotoxic drugs poisoning the cancer cell.

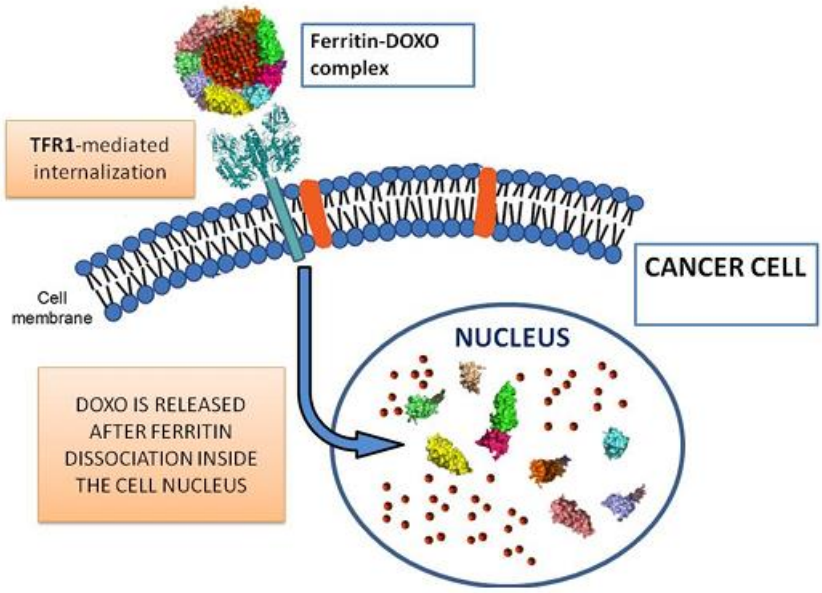

Figure 12. Schematic representation of the nuclear delivery of DOXO in HFt (DOXO) complex.

In 2019, our research group, collaborated with Montemiglio's team in the work that led to the resolution of the structure of the HFt/CD71 complex (Montemiglio et al., 2019) with Cryo-EM techniques (**Figure 13**).

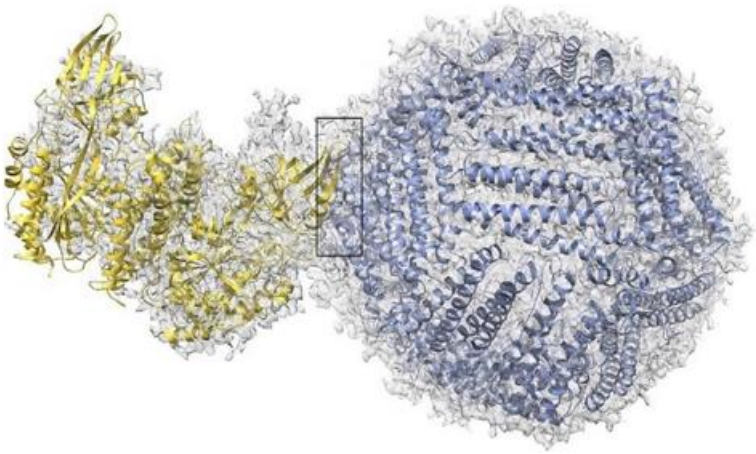

Figure 13. CD71/HFt complex final cryo-EM map (resolution 3.9 Å) with crystallographic structures fitted in (yellow: CD71, pdb 3KAS; purple: HFt, pdb 3AJO). The close-up view is in **Figure 14**.

HFt binds CD71 in a "virus-like" fashion, covering an overall area of ≈1900 Å2 (**Figure 14**).

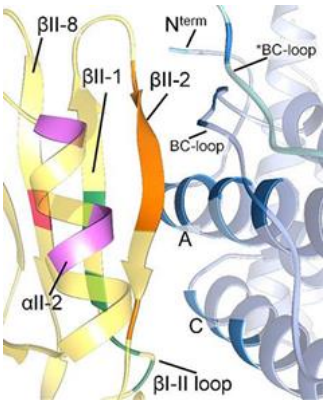

Figure 14. CD71/HFt binding region with crystallographic structures fitted in the cryo-EM map (yellow: CD71, pdb 3KAS; purple: HFt, pdb 3AJO), colored according to the text.

CD71 interacts through four specific regions on the apical domain, highlighted in different colors: i) the βI-II loops and the βII-1 strand (S195, E197, S199, I202: green); ii) a residue on the βII-8 strand (K374: magenta). These are specific on CD71 for HFt, and we refer to them as "exclusive contacts". Additional residues are: iii) six amino acids on the βII-2 strand (R208-L212 and N215: orange); iv) residues E343, K344 and N348 on the αII-2 helix (purple). We refer to these as "common contacts" on CD71, since they represent the key structural determinants for binding. The HFt binding counterpart regions are three: i) the external BC loop (R79, F81, Q83, K86, K87); ii) the N-terminus of the A-helix (T5, Q14, D15, E17-A19, N21, R22, N25); iii) the C-terminus of the C helix (E116, K119, D123). The interactions between exclusive contacts and HFt are: i) CD71 βII-1 strand and HFt A helix (**Figure 15 left**); ii) CD71 βI-II loop and HFt C helix (**Figure 15 left**); iii) K374 CD71 with Q14 and D15 (**Figure 15 right**).

Finding the residues involved in this contact is of major importance for providing the structural basis that govern HFt-CD71 interaction, beyond nanotechnological applications.

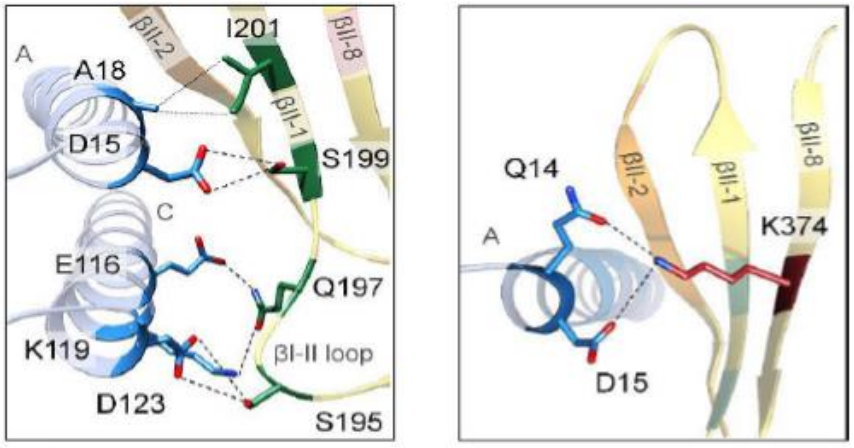

Figure 15. Contacts involving CD71 epitopes that are exclusive for HFt binding.

1.4.5 Pasylated ferritins

In spite of its many advantageous features, an important weakness of HFt should be tackled in order to harness its full potential as drug-delivery system. HFt plasma half-life after systemic injection (i.e., about 2 h) may be too short to attain sufficient accumulation at the tumor level, a problem shared by most other first-generation protein therapeutics. One way to improve the *in vivo* half-life of native HFt, its loading capacity, and its stability is represented by the functionalization of the HFt surface with the PAS polypeptide sequence. Our research group have developed novel HFt-based constructs, named HFt-MP-PAS, suitable for drug delivery. In these constructs, the N-terminus of each HFt subunit was genetically fused to: i) a PAS polypeptide sequence, i.e., a sequence rich in proline (P), alanine (A) and serine (S) residues; (Falvo et al., 2015, Fracasso et al., 2016) and ii) a tumor-selective sequence (MP) responsive to proteolytic cleavage by tumor proteases (MMPs), inserted between each HFt subunit and the outer PAS polypeptide (**Figure 16**).

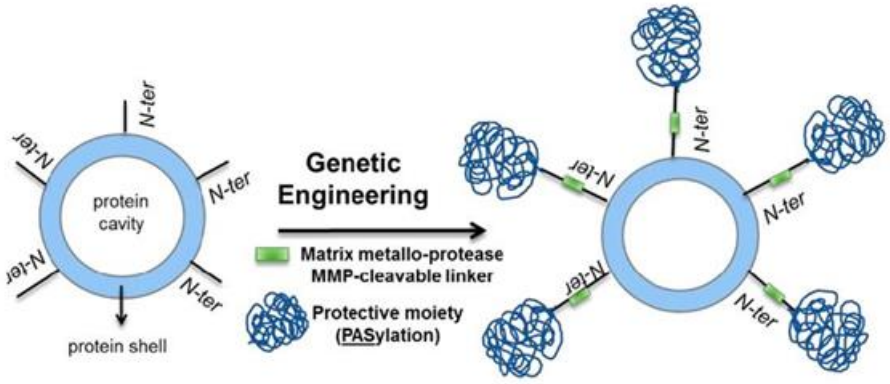

Figure 16. Schematic representation of the synthesis of HFt-MP-PAS40 (Falvo et al., 2016).

Thanks to the PAS mask, it is reduced the internalization of drug-loaded HFt in normal cells, already limited by their lower expression of the receptor CD71. Surface plasmon resonance experiments quantified this lower interaction between PAS-masked HFt and its receptor CD71 by a factor five (Fracasso et al., 2016). In tumor microenvironment, in presence of specific MMPs, the MP sequence is cleaved and, consequently, the PAS shield is removed. The unmasked HFt can interact with CD71 receptor, overexpressed by cancer cells, for the internalization. The HFt-MP-PAS constructs proved to i) encapsulate in the internal cavity three times more doxorubicin (DOX) than wild-type HFt, ii) form more stable complexes (i.e., drug leakage was negligible) and iii) possess higher *in vivo* circulation time. Importantly, DOX-loaded HFt-MP-PAS (HFt-MP-PAS-DOX) displayed excellent therapeutic efficacy either in a human pancreatic and a head and neck cancer models *in vivo*, significantly increasing overall animal survival (Damiani et al., 2017; Fracasso et al., 2016). The PAS sequence allows a better DOX encapsulation and delivery than

canonical HFt. The effectiveness of this delivery system is related to a useful PAS removal by tumor specific MMPs, that subsequently permit an excellent DOX delivery in cell nucleus, also confirm by confocal microscopy studies (Fracasso et al., 2016).

To further optimize plasma persistence and tumor/organs accumulation *in vivo* of the PASylated ferritin technology, other studies have been carried out. Some evidence suggests that the charge of NPs stemming from distinct surface chemistries influences opsonization, circulation times and interaction with resident macrophages of organs comprising the mononuclear phagocyte system (MPS), with slightly negatively charged NPs have longer circulation lifetimes and less accumulation in liver and spleen organs of the MPS (Xiao et al., 2011). This reduced binding of membrane receptors may be due to the fact that most cell surfaces, as well as extracellular matrix components, are also negatively charged. For this reason, we designed a novel PASylated ferritin introducing negative glutamate residues (E) in the PAS sequence and named it HFt-MP-PASE (Falvo et al., 2018). Thanks to surface plasmon resonance experiments, it was observed that the binding of HFt-MP-PASE to CD71 dropped by 10/15-fold (a factor 3 with respect to the HFt-MP-PAS construct). This results in a significant improvement of the plasma persistence and tumor accumulation of the HFt-MP-PASE construct in a xenogenic human pancreatic cancer model (PaCa44) *in vivo*. Moreover, HFt-MP-PASE efficiently encapsulates the anti-cancer drug mitoxantrone (MIT). MIT is a synthetic anthracenedione developed to improve the therapeutic profile of anthracyclines and a clinically well-established anticancer agent which targets DNA topoisomerase I and ubiquitin-specific peptidase 11 (USP11) enzyme, a component of the DNA repair complex. The resulting MIT-loaded nanoparticles (HFt-MP-PASE-MIT) proved to be more soluble and

monodispersed than the HFt-MP-PAS counterparts (Falvo et al., 2018). The efficiency of this construct was tested *in vitro* and *in vivo* (Conti et al., 2021). It was demonstrated that when MIT is delivered to tumor mass by HFt nanocage, the growth of subcutaneous induced tumor is much slower, thereby prolonging the overall survival rate of treated mice.

Recently, our group proposed a first-in-class nanoparticle named The-0504 that incorporates in a single formulation many advantages of classes of cancer therapeutics, and at the same time has been carefully designed to minimize hurdles (Falvo et al., 2021; Falvo et al., 2021). The-0504 is based on the HFt-MP-PASE protein that by spontaneous self-assembly entraps large molar amounts of a selected, cytotoxic drug named Genz-644282 (**Figure 17**).

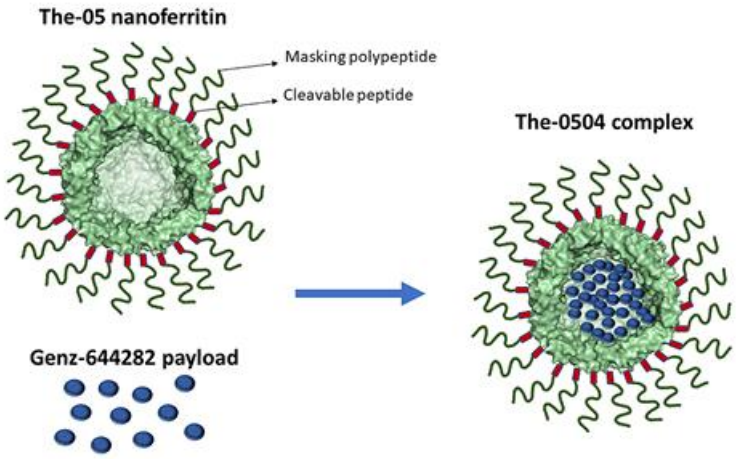

Figure 17. Schematic representation of The-0504. The-05 (the ferritin nanocage) contains N-terminal PASE repeats (from the single-letter amino acid codes) and proteolytic cleavage sites (both indicated). The payload is entrapped within the nanoferritin hollow cavity that in nature carries iron. The picture has been generated with PyMol and GNU Image Manipulation Program.

Genz-644282, a topoisomerase I inhibitor, had previously showed an appreciable killing efficacy (i.e., IC90 in the sub micromolar range) on different cancer cell lines, including camptothecin resistant cell lines (Houghton et al., 2012; Kurtzberg et al., 2011). Genz-644282 has already done a clinical trial dose-escalation in humans (NCT00942799). Therefore, like chemotherapy, the cytotoxic agent of The-0504 has a wide spectrum of activity against many human tumors. As opposed to standard chemotherapy, The-0504 can spare most of the normal cells because it is a conditionally activated masked drug, unmasked by tumor-associated proteases, thereby promoting the engagement of the target mainly in the tumor milieu. Specifically, The-0504 incorporates the safe-lock mechanism based on the tumor-restricted metalloproteases (MMP-2/9) release, favouring local concentration of the therapeutic effect.

A preliminary evaluation of The-0504 in terms of safety and efficacy outlined the strong anti-tumor activity (i.e. delay in tumor growth or durable complete remissions) as well as manageable toxicities of the nanoferritin compound.

1.5 Delivery of multiple bioactive peptides (BAPs), antisense oligonucleotides (ASOs), and small interfering RNAs (siRNAs)

Ferritin-based system could have applications for the selective delivery of molecules different from chemotherapeutics. For example, the transport of Multiple Bioactive Peptides (BAPs) still represents an unresolved issue in the field of drug-delivery. BAPs are a unique class of peptides known for their extensive physiological functions, and their role in enhancing human health (Daliri et al., 2017; Du et al., 2024). These peptides can regulate important biological functions through their myriad activities, including antihypertensive, antimicrobial, antithrombotic, immunomodulatory, opioid,

antioxidant, and mineral binding functions. Despite their promising activity *in vitro* and *in vivo,* short BAPs also have disadvantages, including weak binding affinity, low persistence in blood, and susceptibility to degradation (Wang et al., 2022). It is necessary to delivery multiple copies of distinct BAPs to elicit a strong and long-lasting biological effect (e.g. for enhanced drug delivery or checkpoint blockade).

Other unsolved delivery issue involves the transport of nucleic acids (NAs), fundamental in the process calls RNA interference (RNAi). RNAi has become a widely used tool for the *in vitro* downregulation of specific gene expression in molecular biological research. This basically involves a complementary RNA that binds a target sequence to affect its transcription or translation process. Currently there are two main approaches used to target RNA: double stranded RNA-mediated interference (dsRNA) and antisense oligonucleotides (ASO). Both approaches are currently in clinical trials for targeting of RNAs involved in various diseases, such as cancer and neurodegeneration (Soutschek et al., 2004; Juliano et al., 2008; Rubin et al., 2008; Karlsson et al., 2019; Yuan et al., 2022). Small interfering RNA (siRNA) (usually 20-24 bp) induces gene silencing by forming RNA-induced silencing complexes (RISC) and cleaving targeted mRNA molecules. Antisense oligonucleotides (ASOs) are synthetic, single stranded DNA molecules that have been chemically modified to downregulate gene expression by exploiting endogenous cellular machinery to induce RNA interference.

Although the great potential of these systems, the delivery of siRNA and ASOs turns out to be problematic. Difficulties are linked to poor pharmacokinetic, intracellular uptake, enzymatic degradation, and high toxicity. siRNAs and ASOs reach the peak of accumulation in 3-4 h after subcutaneous injection,

then their plasma concentration decrease, and they are eliminated (Collotta et al., 2023). Their passive diffusion into cells is limited by the fact that they are large molecules (single-stranded ASOs are 4–10 kDa, double-stranded, siRNAs are 14 kDa), and have a negatively charged surface because of phosphate groups, resulting in electrostatic repulsion with the cell membrane (Roberts et al., 2020). Another problem is linked to the enzymatic degradation of the nucleic acids, by intracellular nucleases. Intracellularly, nucleases are found in the cytosol, endoplasmic reticulum, nucleus, and especially in lysosomes. DNase II and RNase T2 are well-characterized lysosomal nucleases that are capable of hydrolyzing endocytosed nucleic acids (Zhang et al., 2024). The toxicity of NAs is due to excessive pharmacological effects that occur between the NA and the target, non-specific effects due to complementary or partial recognition of unwanted transcripts (Batista-Duharte et al., 2020), tissue accumulation in the kidney and liver, proinflammatory and immunostimulatory effects (Zhang et al., 2024).

One possible way to overcome some limitations due to delivery of NAs and BAPs, and to exploit their high therapeutic potential, it is to combine these types of molecules with a specific nanocarrier. However, this approach requires careful selection of the system with proven carrier ability, strong tropism for multiple tumors, resilient three-dimensional folding, tolerance to multiple simultaneous substitutions in different regions, a controlled release safelock, and an effective, industrial-grade biomanufacturing pipeline. PASylated ferritins, thanks to their great characteristics, could represent an intriguing platform as a nanocarriers for this type of molecules.

2. AIMS OF THE WORK

The research in our laboratory is focused on the study of engineered HFt. HFt represent a potential multi-functional protein with different roles in normal and in cancer cells. It is involved in proliferation, angiogenesis, antioxidation, and immunosuppression (Bhavyata et al., 2023). Its structure, the possibility of genetic engineering this protein, and its internalization by CD71 (Li et al., 2010), make HFt an interesting platform in cancer drug delivery studies. We proposed a first-in-class nanoparticle named The-0504. The-0504 is based on the recombinant homopolymeric HFt protein that by spontaneous self-assembly entraps large molar amounts of a selected, cytotoxic drug named Genz-644282. Genz-644282, a topoisomerase I inhibitor, had previously showed an appreciable killing efficacy (Houghton et al., 2012; Kurtzberg et al., 2011).We evaluated this nanoformulation in terms of safety and efficacy outlined the strong anti-tumor activity as well as manageable toxicities of the nanoferritin compound (Chang et al., 2023; Chen et al., 2016; Conti et al., 2021; Falvo et al., 2021; Falvo et al., 2016; Inoue et al., 2021; Inoue et al., 2011).

The first aim of this PhD thesis is to extend our previous studies on The-0504 by demonstrating therapeutic efficacy on additional xenograft mouse models. We also want to demonstrate DNA-damaging properties and favourable pharmacokinetics of The-0504 engender comparable therapeutic effects on lower dosages. Therefore, The-0504 may complement naked cytotoxic drugs, ADCs and other nanoparticle-based (Manivasagan et al., 2023; Manohar et al., 2023; Manohar et al., 2022) aiming at milder, on-target, low-side-effects chemotherapeutic applications.

The second aim of this PhD thesis is to develop a new engineered HFt construct for the delivery of bioactive peptides (BAPs). We focused our attention on two peptide sequences with specific biological activity. We have grafted them into the ferritin structure for a selective delivery and a specific release in TME. In that way, we attempted to obtain new construct that acts as a therapeutic booster for co-administered drugs in solid tumors. Furthermore, this construct has been characterized using biochemical and biophysical methods. Subsequently, during this project, its biological activity has been characterized both *in vitro* and *in vivo*.

The third aim of this PhD thesis is to exploit engineered HFt as a platform for the selective delivery of small nucleic acids involved in RNA interference mechanisms. In particular, we decided to work with siRNA implicated in silencing of specific genes in Crouzon Syndrome (CS). CS is a rare genetic disorder characterized by craniosynostosis and midface deformities (Conrady and Patel 2021), due to heterozygous missense mutations in the fibroblast growth factor receptor 2 (FGFR2) gene. Furthermore, we investigated the delivery of antisense oligonucleotides (ASOs). We aspire to deliver long noncoding RNA MB3 (lncMB3), in Medulloblastoma pathology. Medulloblastoma (MB) is a cancerous brain tumor that starts in the lower back part of the brain (Cerebellum).

Overall, the work of this thesis investigated the following aspects:

1. Design, production and purification of the HFt-based genetic variants as recombinant proteins expressed in *Escherichia coli*.

2. Biophysical characterization of the HFt variants using different biophysical techniques like size-exclusion chromatography (SEC), and dynamic light scattering (DLS).

3. Assessment of the binding affinity of the new HFt construct to its specific receptors (PDL1, integrins, Neuropilin-1, etc.) by Surface Plasmon Resonance (SPR).

4. Assessment of the selective release of specific BAPs due to enzymatic cut and internalization tests with live imaging on cancer cells.

5. Assessment of the anti-tumor and toxicity effects of the HFt-based construct *in vivo*, in animal models of cancer.

6. Characterization and assessment of the stability of ferritin-Nucleic Acid complexes with different techniques like SEC and agarose gel electrophoresis.

7. Assessment of the levels of CD71 receptor, MMP 2 and MMP 9 enzymes on specific cells with molecular biology techniques (e.g. quantitative Real Time PCR). Next, cellular uptake of engineered ferritin variants evaluated by confocal laser scanning microscopy and Incucyte-Live cell analysis system.

8. Assessment of the levels of gene silencing *in vitro* (Real time PCR and Western blot).

3. MATERIALS AND METHODS

3.1 The-0504 therapeutic efficacy on additional xenograft mouse models

3.1.1 The-05 Construct Design and Production

To effectively encapsulate the anti-cancer drug Genz-644282, which is expected to bear positive charges at physiological pH values, we designed a variant of the previously reported HFt-MP-PASE construct (see above) with an enhanced negative charge of the HFt internal surface. To this end, we analysed the three-dimensional (3D) structure of HFt which has been experimentally determined by X-ray crystallography (Lawson et al., 1991) and is available from the Protein Data Bank archive (PDB ID: 1FHA). Structure visualization and analysis was performed with Insight II (Accelrys Inc., San Diego, CA, US) and PyMol. We chose to introduce the negatively charged glutamic acid residue (Glu) in place of four native HFt residues, namely Lys53, Lys71, Thr135, and Lys143. These residues were selected because they satisfy the following criteria: (i) their side-chains are solvent accessible on the internal surface of the HFt cavity; (ii) they are not involved in interactions, either within the monomer or at inter-monomer interfaces, whose alteration might undermine the stability of the tertiary structure or quaternary assembly, respectively; (iii) they are not involved in metal binding at the ferroxidase center of HFt; (iv) the three Lys side-chains are positively charged, and therefore their removal contributes to the generation of a negatively charged surface; (v) their relative distance in the 3D structure is high enough that Glu residues introduced at these positions are not expected to give rise to unfavourable interactions, either with their surrounding residues or with one

another. Finally, structure superposition between mutated and wild-type HFt structures available from the PDB indicates that introduction of mutations at positions 53 (i.e., Lys53Cys, PDB ID: 4DZ0) and 143 (i.e., Lys143Cys, PDB IDs: 3ERZ, 2Z6M, 3ES3) does not determine detectable changes in either the monomer fold or multimeric assembly. The variant of the HFt-MP- PASE construct bearing the Lys53Glu, Lys71Glu, Thr135Glu and Lys143Glu mutations was named The-05. It was obtained via recombinant protein technology, as previously reported. In brief, the expression vector pET-17b containing the The-05 gene was assembled by GENEART AG (Germany). Gene synthesis was performed taking into account codon-optimization for high level expression in *Escherichia coli*. The recombinant protein The-05 was expressed in *E. coli*, purified and quantified as previously reported (Falvo et al., 2020).

3.1.2 The-0504: Genz-644282 encapsulation in the The-05 nanovector

Genz-644282 Trifluoroacetic acid (TFA) salt (MedKoo Biosciences) was encapsulated in The-05 using the ferritin disassembly/reassembly procedure previously described for other drugs resulting in a 120:1 molar ratio between the drug and The-05 protein (Falvo et al., 2018). The final product was named The-0504. Briefly, solutions of The-05 (2 mg/mL) in 15 mM NaCl was incubated for 10 min at pH 3.1 (pH adjusted with HCl). Protein disassembly/reassembly was achieved by dropwise addition of NaOH to pH = 7.5. After 20 min of stirring at room temperature, the product was filtered to eliminate insoluble particles. An excess of unbound drug was removed using 100 kDa Amicon Ultra-15 centrifugal devices, in 20 mM Tris-HCl at pH 7.5. Finally, the solution was sterile filtered and stored at 2–8°C in the dark. The

obtained system, made of The-05 containing Genz-644282 in the internal cavity, was named The-0504. Genz-644282 content of the samples was determined by UV-vis spectroscopy, after extracting the drug in 0.1 N HCl. Genz-644282 was quantified by using the calculated molar extinction coefficient ε = 10,000 M^{-1} cm^{-1} at 345 nm, with a linearity comprises between 0.25–0.45 AU. Protein content was also determined by UV-vis spectroscopy applying the following correction for the absorbance at 280 nm: A280nm - (A345nm x 4.2). The-0504 was stored as lyophilized powder at 2–8° C and checked monthly for its stability. The-0504 production and formulation process development studies were carried-out in collaboration with Thena Biotech and BSP pharmaceuticals (Latina, Italy).

3.1.3 Immunofluorescence microscopy detection of γH2AX

The experiment was carried out essentially as described in Sooryakumar et al., 2011. MiaPaCa-2 cells were seeded at a concentration of 3.5×10^5 /well into 6-well dishes in Dulbecco's Modified Eagle's Media (DMEM) and treated with 1 μM Genz-644282 or The-0504 for 6h and 24h. Then, cells were fixed with 4 % formaldehyde solution and permeabilized with 0.01 % Triton X-100 in PBS containing 1 % BSA for 10 min. Cells were incubated with primary rabbit anti-γH2AX antibody (Phospho-gamma-H2AX Ser139 Antibody A300-081A, Thermo Fisher Scientific, Waltham, MA USA) followed by incubation with Alexa fluor 488 (rabbit) conjugated secondary antibodies (Thermo Fisher Scientific). Then, nuclei were counterstained with Hoechst 33,342 (Thermo Fisher Scientific) and were mounted with Vectashield (DBA, Milan, Italy). Cells were visualized under fluorescence confocal microscopy (Zeiss, Wetzlar, Germany). Immunofluorescence intensity was quantified by the ImageJ

software plugin. Error bars indicate means ± SEM. **p < 0.01 and ***p < 0.001 as determined by Student's t-test.

3.1.4 Pharmacokinetics of The-0504 in rat

The exposure to the test item The-0504, after a single intravenous administration in rat, was investigated in a study carried-out at the European Research Biology Center (ERBC, Pomezia, Italy) on 18 Wistar Hannover rats (6 females per group), 7–8 weeks old, body weight approximately 176–225 g. Blood pharmacokinetic time-points were taken from all animals according to the following schedule: pre-dose (0), 2 and 30 min, 6, 24, 48, 72, 96 and 144 h from the end of dosing. Two bioanalytical methods were applied for orthogonal kinetic assessments of the HFt-based carrier (The-05) and the drug, respectively: (a) an ELISA method using a polyclonal antibody antiThe-05 (developed by us), and the purified carrier protein The-05 as standard; and (b) an LC/MS method, using Genz-644282 as reference item. The lower limits of quantitation were 50 ng/mL and 250 ng/mL for the ELISA and LC/MS methods, respectively. The-0504 was intravenously administered at two different doses of 1.5 mg/kg and 3.0 mg/kg, as Genz-644282 concentration, corresponding to about 30 mg/kg and 60 mg/kg as The-05 protein concentration, respectively. The cytotoxic product Genz-644282 was used as reference item and administered at dose of 3.0 mg/kg. The following pharmacokinetic parameters were obtained or calculated for the injected compounds, when appropriate, from the mean plasma values: Cmax: maximum (peak) observed plasma concentration; Tmax: time to reach peak or maximum concentration; AUC(0-inf): area under the plasma concentration-time curve from time zero to infinity; T1/2: elimination half-life associated

with terminal slope (λZ) of a semi logarithmic concentration-time curve; Cl: Clearance.

3.1.5 Cultured cells

The human cancer cell lines MiaPaca2, HT-1080, MDA-MB 157, MDA-MB 468, H1339, A549 were obtained from American Type Culture Collection (ATCC). PaCa44 cells were provided by Prof. Scarpa (Department of Diagnostics and Public Health University of Verona, Italy). All cell lines were grown as described (Falvo et al., 2021), or as per supplier's instructions.

3.1.6 Pre-clinical activity of The-0504 on tumor xenotransplants mouse models

The-0504 was administered at MTT lab srl, (Trieste, Italy) or at University of Chieti to athymic nude mice carrying tumor xenotransplants of the following human tumor cell lines: PaCa44 and MiaPaca2 (pancreas), HT-1080 (fibrosarcoma), MDA-MB 157 and MDA-MB 468 (breast cancer, triple-negative subtype), H1339 and A549 (lung). Mice were marked with Uno Pico-ID Transponders (1.25 mm × 7 mm) (UNO BV, AA Zevenaar, Netherland) by s. c. Injection, using specific implanter one week prior to the study for accurate individual monitoring. After the acclimatization period, 5×10^6 tumor cells were inoculated subcutaneously in the right flank of each athymic nude mouse. Mice were observed at least once a day. After a week from cell inoculation, tumor growth was measured by a caliper. Treatments were started when tumor sizes averaged at about 60–100 mm^3. Before treatment, all mice were weighted, and the size of all tumors was measured. Animals were semi-randomly assigned to the study groups based on the initial tumor size. Animals

were divided 4 per cage. The treatment dose normalized to Genz-644282 concentration was 2.0 mg/kg (twice a week) or 1.5, 3.0 or 6.0 mg/kg (once a week). Mice (n = 5 or 6) were treated intravenously once or twice a week for three weeks. All mice were culled by cervical dislocation at the end of the study or when they reached the endpoint tumor volume (i.e., 1500–1700 mm^3). A gross autopsy was also performed. A protocol approved by the Institutional Animal Care and Use Committee of the University of Udine or University of Chieti and authorized by the Italian Ministry of Health (Protocols no. 414/2021-PR and 457/2018-PR) was used for the animal studies. This was in accordance with the principles laid down in the European Community Council Directives (86/609/EEC).

3.1.7 Response determination

Response codes of the efficacy studies were as reported (Falvo et al., 2021), e.g. progressive disease (PD); stable disease (SD); partial response (PR); and complete response (CR). The study period was set at 2 weeks from the last treatment. For treated groups only, the percentage of tumor growth inhibition (% TGI) was defined as 100x (MTV control-MTV treated)/MTV control, where MTV is the median tumor volume. The objective response rate (ORR) represents the percentage of treated animals that show a significative response (PR or CR) to therapy.

3.1.8 Statistical analysis

A linear mixed-effects model was used to test the tumor volume change rate over time among different groups.

3.2 THE-10: Development of a new engineered HFt construct for the delivery of bioactive peptides (BAPs)

3.2.1 Design of the THE-10 nanovector

The *THE-10* gene is a variant of the HFt-MP-PASE gene previously reported (Falvo et al., 2018). THE-10 includes, C- to N-terminus: (a) a first domain comprising the amino acid sequence of the native human ferritin HFt; (b) a second domain comprising: (i) the amino acid sequence LQKTPKQ as PD-L1 binding peptide, which is conjugated to the N-terminal of said first domain through the amino acid sequence of a matrix metalloproteinase (MMP) cleavage site PLGLAG, and (ii) the amino acid sequence RGDKGPD as tumor penetrating peptide, which is conjugated to said amino acid sequence LQKTPKQ through the amino acid sequence of the MMP cleavage site; (c) a third N-terminal domain consisting of proline, serine, alanine and glutamate (PASE): ASPAAPAPASPAEPAPSAPAASPAAPAPASP AEPAPSAPA**.**

3.2.2 Cloning, overexpression and purification of THE-10 construct

The *THE-10* sequence was codon-optimized for high level expression in *Escherichia coli*, generated by whole-gene synthesis at GENEART AG (Germany), cloned into the expression vectors pET-27b (Thermo Fisher Scientific Waltham, USA), and expressed in the BL21(DE3) bacterial host (New England BioLabs, Ipswich, USA). *E. coli* cells were grown to OD600 1.0 at 37°C in 1 L of terrific broth medium (Grisp, Porto, Portugal) containing kanamycin (Serva, Heidelberg, Germany) at a final concentration of 0.03 mg/mL. Gene expression was induced by addition of 1 mM isopropyl-1-thio-ß-D-galactopyranoside (IPTG), and *E. coli* were incubated overnight at 37°C.

The cells were harvested by centrifugation at 5000 rpm for 20 minutes at 4°C. The recovered pellet was suspended in 90 mM Tris-HCl, 50 mM NaCl and EDTA 0.5 mM at pH 9 and incubated at 60°C for 15 minutes. After thermal treatment, the enzyme DENARASE (c-LEcta GmbH, Leipzig, Germany) was added at 15 U/mL to cleave DNA and RNA impurities, and then the cells were disrupted by sonication. The lysate was centrifuged at 14,000 rpm for 50 minutes at 4°C and the supernatant was further treated at 72°C for 8-10 minutes. The solution was centrifuged 14,000 rpm for 50 minutes at 4°C. The supernatant was dialyzed overnight against phosphate-buffered saline (PBS) pH 7.5, concentrated by means of 100 kDa Amicon Ultra-centrifugal filter devices (Millipore, Billerica, USA) and loaded on a strong basic anion-exchange filter, Sartobind Q (Sartorius, Goettingen, Germany), previously equilibrated with the same buffer. THE-10 preparations were eluted from the column, whereas other *E. coli* impurities were retained by the filter. Finally, the THE-10 samples were sterile-filtered and stored at 4 °C (short-term) or -20°C (long-term).

3.2.3 Protein characterization of THE-10

The purity of all the preparations was assessed by Sodium Dodecyl Sulphate - PolyAcrylamide Gel Electrophoresis (SDS-PAGE), running the samples on 15% gels and staining with Coomassie brilliant blue. Protein concentrations were determined spectrophotometrically at 280 nm, using a molar extinction coefficient (on a 24-mer basis) of 4.54×10^5 M^{-1} cm^{-1} (ProtParam sofware, http//www.expasy.org). Size-Exclusion Chromatography (SEC) was performed using a Superose 6 gel-filtration column equilibrated with PBS at pH 7.4. All samples were prepared at 1 mg/mL in PBS pH 7.4. All the traces

of SEC experiments were analyzed with QtiPlot (IONDEV SRL, Bucuresti, Romania).

3.2.4 *In vitro* release of PASE and multiple peptides from THE-10 in the presence of MMP2/9 proteases

To assess the peptides, release after enzymatic cleavage, THE-10 cleavage was studied in the presence of the specific proteasesMMP-2/9. Collagenase IV (Collagenase Type 4 containing MMP2 and 9, *Clostridium histolyticum*, Pan-biotech, Leipzig, Germany) was previously suspended in Tris HCl 50 mM, NaCl 50 mM, and $CaCl_2$ 5 mM. pH 7.4, to obtain 2 mg/mL stock. THE-10 protein was mixed with Collagenase IV stock at molar ratio 1:1. This mix was incubated at 37 °C for 2 h. It was concentrated by means of 100 kDa Amicon Ultra-centrifugal filter devices (Millipore, Billerica, USA), and Collagenase IV was thus removed. Samples were then analysed by SEC using a Superose 6 gel-filtration column equilibrated with PBS at pH 7.4, and by SDS-PAGE gel chromatography. SDS PAGE was stained with Coomassie brilliant blue R-250.

3.2.5 Testing of the THE-10 fusion protein binding ability by Surface Plasmon Resonance experiments

Surface Plasmon Resonance (SPR) was carried out to assess the thermodynamic and kinetic parameters of the interaction between the construct THE-10 (analyte) and its specific receptors (ligands): αVβ3, NRP-1 (αVβ3 #IT3-H52E3, his-tagged human #NR1-H5228; ACROBiosystem, Germany), and PD-L1 (C-terminal his-tagged human PD-L1 #10084-H08H, Sino Biological Europe GmbH, Germany) in a Biacore X-100 apparatus. The ligands were immobilized on a Sensor Chip nitrilotriacetic acid (NTA). The

NTA group was activated by nickel ions (Ni2+) to bind selectively histidine-tagged ligands. Ligands (αVβ3 or NRP-1: 25 μg/mL and PD-L1: 50 μg/mL) were stripped by sequestering nickel ions with EDTA (regeneration phase). After ligand immobilization, THE-10 was injected at different concentrations: αVβ3 and NRP-1: 96, 192, 384 (tested twice to ensure reproducibility of the results), 768 and 1536 nM; PD-L1: 6.25, 12.5, 25, 50, 100 and 200 nM.

3.2.6 Testing Flow cytometry analysis

To assess surface markers, A375 cells were stained with anti-HER2 Trastuzumab (provided from the hospital pharmacy of the Regina Elena Cancer Institute) or with the following fluorescently labeled monoclonal antibodies (mAbs): anti-human CD51/CD61 FITC (23C6) from eBioscience and anti-human CD304 PE (12C2) from Biolegend, respectively. Cells were stained with anti-CD51/CD61 or anti-CD304 mAbs (1:20) or with anti-Her-2 (10 μg/ml) in cold PBS-2% FBS solution, 30 min on ice. Appropriate Goat anti-Human IgG (H+L) Secondary Antibody, FITC (1:100) was added to Trastuzumab stained cells. All acquisitions were performed with Attune NxT Acoustic Focusing Cytometer (Invitrogen, Thermo Fisher) and data analyzed with the FlowJo software v10.

3.2.7 Uptake and internalization experiments

Uptake and internalization were assessed using an Incucyte S3 live-cell analysis system (Sartorius, Goettingen, Germany). The test compound (recombinant antibody trastuzumab obtained from injectable preparations for human infusion, Roche Pharmaceuticals) was conjugated with the pH-sensitive dye pHrodo using the Deep Red Antibody Labeling kit (#P35355,

Invitrogen, Thermo Fisher scientific), according to the manufacturer's instructions. Human melanoma cells A375 (obtained from the American Type Culture Collection, ATCC) were seeded at a density of $3x10^3$ cells/well in 96-well plates one day before the addition of Trastuzumab-pHrodo (10 μg/mL), alone or combined with THE-10 (1.0 mg/mL). Phase contrast and fluorescence images of cells cultured under standard conditions (37 °C, 5% CO2, RPMI 1640 medium, 10% fetal bovine serum, 1% penicillin–streptomycin and 1% glutamine) were captured at 20X magnification every 60 min for 48 hours and mounted in the time-lapse mode by on-board software. Red integrated fluorescence (from pHrodo-labeled antibodies internalized in acidic intracellular compartments) was elaborated by the integrated, automated Incucyte software, and quantitated after background subtraction. Data were plotted and analysed by onboard software. Internalization was expressed as per cent of baseline (time 0) fluorescence over incubation time.

3.2.8 Testing of the THE-10 fusion protein activity on cultured cells: anti-proliferative effect stimulation

To assess proliferation, human melanoma A375 cells were seeded at a density of $1x10^3$ cells/well in 96-well plates (Costar #3595). On the following day, Trastuzumab Deruxtecan (T-DXd, MedChemExpress, USA), alone or combined with THE-10 (1.0 mg/mL), was added, and cells were grown under standard conditions. Cell viability was measured by the Cell Titer-Glo 2.0 kit (Promega, Madison, WI, USA). Each experimental condition was assessed in triplicate. After 96 hours of treatment, 100 μL of Cell Titer-Glo reagent were added to each well. Plates were incubated for 10 minutes at room temperature in the dark, and luminescence was determined on a Synergy/LX multimode

reader (Biotek), using the Gen5 3.10 Imager software. Results were plotted as mean +/- SD and analyzed by GraphPad Prism 9.

3.2.9 *In vivo* studies authorizations and response determination

Protocols for animal studies were approved by the Institutional Animal Care and Use Committees of the University of Udine (Italy), University of Chieti (Italy), and the Institute of Microbiology of the Czech Academy of Science (Prague, Czech Republic): Italian Ministry of Health IDs no. 414/2021-PR and 391/2022-PR; and ID 111/2019, respectively. Experiments were compliant with the principles laid down in the European Community Council Directives (86/609/EEC). In all experiments, tumor volume was measured twice a week with a digital caliper and mouse weight was monitored. Animals were sacrificed at the end of the study period or when the tumor had reached a volume ≥1000 mm^3. For treated groups only, the percentage of tumor growth inhibition (% TGI) was defined as 100x (MTV control-MTV treated)/MTV control, where MTV is the median tumor volume.

3.2.10 *In vivo* anti proliferative enhancement effect of THE-10 using KPC pancreatic cancers

Seven-week-old female C57BL/6 mice (Charles River Laboratories, Lecco, Italy) were injected subcutaneously (i.e., right flank) with $0.5x10^6$ pancreatic KPC cells resuspended in in a 1:3 (v:v) solution of PBS:Matrigel in a final volume of 200 µL. Three different experiments were carried out using this cancer model. In the first experiment, as test cytotoxic drug compound was evaluated the small molecule Gemcitabine (MedChemExpress, USA). When tumors had reached a volume of about 100-200 mm^3, mice were randomized

in groups of six animals and injected with 200 µL of physiological saline (intravenously, i.v.), 200 µL Gemcitabine (100 mg/Kg; intraperitoneal, i.p.) or 200 µL Gemcitabine (100 mg/Kg; i.p.) plus 200 µL THE-10 (130 mg/Kg; i.v.). THE-10 was injected 24 hours before treatments. Mice were injected twice a week for two weeks. In the second experiment, as test cytotoxic drug compound the large macromolecule THE-0504 nanoferritin (Thena Biotech Srl) was evaluated (Falvo et al., 2021, Falvo et al., 2020; Marrocco et al., 2024). When tumors had reached a volume of about 200-250 mm^3, mice were randomized in groups of six animals and injected i.v. with 200 µL of physiological saline (i.v.), 100 µL THE-0504 (1.0 mg/kg), 100 µL THE-0504 (1.0 mg/kg) plus 100 µL iRGD peptide (3.0 mg/Kg; MedChemExpress, USA) or 100 µL THE-0504 (1.0 mg/kg) plus 100 µL THE-10 (130 mg/Kg, corresponding to 3.0 mg/kg in iRGD peptide). Mice were injected twice a week for three weeks. In the third experiment, as test cytotoxic drug compound the large macromolecule Sacituzumab govitecan (IMMU-132; MedChemExpress, USA) was evaluated. When tumors had reached a volume of about 100 mm^3, mice were randomized in groups of six animals and i.v. injected with 200 µL of physiological saline (i.v.), 100 µL Immu-132 (45 mg/Kg) or 100 µL Immu-132 (45 mg/Kg) plus 100 µL THE-10 (130 mg/Kg). THE-10 was injected 5-10 minutes before the treatments with Immu-132. Mice were injected every 3-4 days for three times.

3.2.11 *In vivo* effects of THE-10 in CT26 colorectal cancers

Eight- to ten-week-old male Balb/c mice (AnLab, Prague, Czech Republic) were subcutaneously injected with $1x10^6$ syngeneic colorectal adenocarcinoma cells CT26 (ATCC, USA). When tumors reached a volume

about 50-100 mm^3, mice were randomly subdivided into groups of 6 animal each. In the first experiment, animals were injected with 200 µL of saline (i.v.) or THE-10 (120 mg/Kg) two times per week for a total of four injections. In the second experiment, animals were injected with 200 µL of saline (i.v.), 300 µL of irinotecan (100 mg/Kg) (i.p.) or 300 µL of irinotecan (i.p.) plus THE-10 (120 mg/Kg) (i.v.), two times per week for a total of four injections. THE-10 was injected 24 hours before the treatment with irinotecan.

3.2.12 *In vivo* antiproliferative enhancement effect of THE-10 using MiaPaca2 pancreatic cancer

Four-week-old female athymic nude mice (Envigo, Italy) were injected subcutaneously (i.e., right flank) with $5x10^6$ pancreatic MiaPaca2 cells resuspended in 200 µl of DMEM medium plus 1% BSA. When tumors had reached a volume of about 80-100 mm^3, mice were randomized in groups of six animals and injected i.v. with 200 µL of physiological saline (i.v.), 100 µL THE-0504 (1.0 mg/kg), or 100 µL THE-0504 (1.0 mg/kg) plus 100 µL THE-10 (130 mg/Kg). Mice were injected twice a week for three weeks.

3.2.13 Statistical analysis

Values are presented as the means and standard deviation. Data analysis was performed by GraphPad Prism version 5. Statistical analysis of tumor growth curve and tumors weights at the sacrifice were done using one-way ANOVA analysis, adopting the Kruskal-Wallis's test and using Dunn's Multiple Comparison test for coupled comparisons. Differences at $p<0.05$ were considered to be statistically significant.

3.3 Delivery of short RNA interfering: delivery of siRNA in Crouzon Syndrome

3.3.1 Allele-specific siRNA design

The specific siRNA to be complexed with ferritin nanocarriers was provided by our collaborator at the Università Cattolica del Sacro Cuore (Prof. Wanda Lattanzi). Briefly, the heterozygous *FGFR2* mutation found in each Crouzon syndrome (CS) patient enrolled was used to drive the design of different siRNA sequences using *ad hoc* bioinformatic tools (Integrated DNA technologies, IDT, USA). Each siRNA sequence has been designed and synthetized as asymmetric 27-mer RNA duplex with two-base 3' overhang on the antisense strand, whereas the sense strand of 25 nucleotides in length presented a 3' blunt end modified with two DNA bases (Rose et al., 2005). Specifically, the guide strand of each siRNA fully matched the corresponding mutated *FGFR2* mRNA sequence, thus containing a single base difference (mismatch) with wild-type *FGFR2* mRNA. A set of four to seven siRNAs was designed for each allelic variant, introducing the mismatch at different positions from 5' end of each siRNA guide-strand, based on previous works.(Huang et al., 2009; Schwarz et al., 2006).

3.3.2 *In vitro* siRNA treatment

The allele-specific silencing effects of the designed siRNAs was then evaluated in patients calvarial mesenchymal stromal cells (CMSCs).

Specifically, siRNAs were first tested for 48 hours in CMSC culture grown in standard proliferative condition (GM) to identify the most effective molecules for each allelic *FGFR2* variant-positive case. To this aim, cells were seeded at a density of $5x10^4$ cells *per* well and grown to ~50-60% confluency, then

transiently transfected with siRNA using Lipofectamine RNAiMAX Transfection Reagent (Invitrogen, Carlsbad, CA, USA), according to the manufacturer's instructions. All siRNAs were tested either individually or in an equally proportioned mixed pool using scalar concentrations. Briefly, siRNA molecule(s) was diluted in culture medium (DMEM high glucose) to reach the final treatment concentration (from 0.1 nM to 10 nM); whereas 7.5 µl of Lipofectamine RNAiMAX were added in 100 µl of culture medium. To allow the formation of stable siRNA/transfectant complexes, Lipofectamine solution was incubated with the diluted siRNA(s) for 5 minutes at room temperature. Then, cells in GM were incubated with the resultant solution for 48 hours. CMSCs treated with Lipofectamine were used as controls.

Subsequently, given the pre-determined and finite number of population doublings due to primary cells senescence, cells from a single use case (patient#1) were chosen for further validation of our siRNA design strategy. To this purpose, to evaluate the effect of the previously selected siRNA for patient#1 (named si4) on cell differentiation, CMSCs derived from patient#1 were pre-treated with GM supplemented with 1 nM of si4 for 48 hours. Followed this, cell were treated with osteoinductive medium (OM) supplemented with 1 nM of si4 for 5 days. The OM was changed every 2 days, with siRNA added each time. Cells cultured in OM without siRNA served as positive controls for differentiation. The silencing efficiency of siRNA molecules was assessed by Real-Time PCR expression analysis of mutant and wild-type *FGFR2* mRNA as well as of osteogenic markers.

3.3.3 Design of the HFt-HIS-PASE nanovector

To bind and deliver selected siRNA molecules, a novel ferritin-based construct was developed. The new *HFt-HIS-PASE* gene is a variant of the HFt-MP-PASE

gene previously reported (Falvo et al., 2018). The design of HFt-HIS-PASE protein includes, C- to N-terminus: (a) a first domain comprising the amino acid sequence of the native human ferritin HFt modified through the inclusion of a 5 histidine peptide sequence, inserted in the external loop (referred as CD loop) of the ferritin surface; (b) a second N-terminal domain comprising the amino acid sequence of the matrix metalloproteinase (MMP) cleavage site (PLGLAG) followed by a Proline, Serine, Alanine, and Glutamate (PASE) sequence (ASPAAPAPASPAEPAPSAPA).

3.3.4 Production of HFt and HFt-HIS-PASE

The expression vector pET-27b containing the HFt gene was purchased by GENEART AG (Thermo Fisher Scientific Waltham, USA). Recombinant HFt was expressed and purified from *E. coli*, as previously described (Falvo et al., 2013). The expression vectors pET-27b containing the *HFt-HIS-PASE* gene was assembled by GENEART AG (Thermo Fisher Scientific). Gene synthesis was performed taking into consideration the codon optimization for high level expression in *Escherichia coli*. BL21 (DE3) (New England BioLabs, Ipswich, USA) cells harboring the recombinant gene were used for the expression of HFt-HIS-PASE protein. *E. coli* cells were grown first at 23°C o.n. and then at 37°C the next day to reach an optical density of 1.0 at 600 nm. Cells were grown in 1 L of terrific broth medium (Grisp, Porto, Portugal), containing kanamycin at a final concentration of 0.03 mg/mL (Serva, Heidelberg, Germany). After induction with IPTG (Isopropil-β-D-tiogalattopiranoside) 1 mM (PanReac, Monza, Italy), *E. coli* cells were incubated at 30°C for 2 hours. Cells were harvested by centrifugation at 5,000 rpm for 20 minutes at 4°C. The recovered pellet was suspended in PBS, NaCl 150 mM and 20 mM imidazole at pH 7.4, and mixed with protease inhibitor tablets (Thermo scientific,

Rockford, USA) and Phenylmethylsulfonyl fluoride 1 mM (PMSF Thermo scientific, Rockford, USA). Then, the DNAse enzyme (Sigma-Aldrich, St. Louis, USA) was added at a final concentration of 0.1 mg/mL and then cells were disrupted by sonication. Cell lysate was incubated at 37°C for 40 minutes and was centrifuged at 14,000 rpm for 50 minutes at 4°C. The supernatant was recovered and loaded in a His-Trap column (Cytiva, Uppsala, Sweden), for metal affinity chromatography, previously equilibrated with the same buffer. HFt-HIS-PASE samples were eluted with an elution buffer containing imidazole 100 mM, to separate it from *E. coli* proteins and DNA contaminants. The samples were dialyzed overnight against PBS pH 7.5, concentrated by means of 100 kDa Amicon Ultra-15 centrifugal filter devices (Millipore, Billerica, USA). Finally, the HFt-HIS-PASE samples were sterile filtered and stored at 4 °C (short-term) or -20°C (long-term).

3.3.5 Protein characterization of HFt-HIS-PASE

The purity of all the HFt-based preparations was assessed by SDS-PAGE (Sodium Dodecyl Sulphate - PolyAcrylamide Gel Electrophoresis), running the samples on 15% gels and staining the proteins with Coomassie brilliant blue**.** Protein concentrations were determined spectrophotometrically at 280 nm using a molar extinction coefficient (on a 24-mer basis) of 4.56 10^5 M^{-1} cm^{-1} (ProtParam sofware, http//www.expasy.org).

Size-Exclusion Chromatography (SEC) experiments were performed using a Superose 6 gel-filtration column equilibrated with PBS at pH 7.4. All samples were prepared at 1 mg/mL in PBS at pH 7.4. All the traces for SEC experiments were analyzed with QtiPlot (IONDEV SRL, Bucuresti, Romania).

3.3.6 Fluorescent labelling of proteins

To obtain fluorescetly-labeled NPs, HFt and HFt-HIS-PASE (HFt A and HFt B) protein solutions (1 mg/mL) were incubated with 1 mM of of Fluorescein-5-Maleimide (λex 491 nm, λem 518 nm; Thermo Scientific) in PBS, pH 7.0 for 2 hours and room temperature under stirring in the dark. Subsequently, the sample was filtered, dialyzed and exchanged with H_2O_{dd} and PBS by using 100 kDa Amicon Ultra-15 centrifugal filter devices to remove excess reagents. The samples were sterile filtered and stored at 4° C in the dark. The number of dye molecules linked per protein was determined by absorbance spectroscopy, in accordance with the manufacturer's instructions, applying the Lambert–Beer law (Falvo et al., 2013).

3.3.7 Allele-specific siRNA design optimization

To produce HFt-HIS-PASE/siRNA complexes, we chemically optimized the siRNA molecule designed for its conjugation onto NPs surface. To this aim, siRNA sequence (si4), selected as the most efficient in patient#1 cells by our collaborators, has been chemically modified by introducing Locked nucleic acid (LNA) bases and a reactive amino group at 3' end of siRNA strand (NH_2-si4).

Modified NH_2-si4 molecule has been tested in patient#1-derived CMSCs to confirm their allele-specific targeting effect. Briefly, cells were treated with scalar concentration of NH_2-si4 molecule (0.1 nM, 1 nM, 10 nM) for 48 h, using lipofectamine as transfection reagent. Real time PCR was carried out to evaluate the expression of mutant and wild-type *FGFR2* alleles.

3.3.8 Formulation and characterization of HFt-HIS-PASE-siRNA complexes

The efficiency of the developed HFt-based constructs as a siRNA delivery system has been assessed by producing and testing HFt-HIS-PASE-siRNA complexes.

To this aim, chemically modified si4 molecules were conjugated to HFt NPs by exploiting the complexation of the reactive amino group at 3' end of siRNA strand (NH_2-si4; as previously described) with the thiol groups present on HFt-HIS-PASE surface through the use of the SPDP (N-succinimidyl 3-(2-pyridyldithio) propionate) cleavable crosslinker (Thermo Scientific, Rockford, USA). We used a 30:1 SPDP-to-NH_2-si4 ratio in the solution that was incubated for 30 minutes at 20°C. To remove reaction byproducts and excess nonreacted SPDP reagent, a desalting column PD MiniTrap G-25 (Cytiva, Uppsala, Sweden), equilibrated with PBS, was used. Then about four excesses of this reactive solution was mixed with the HFt-HIS-PASE protein. The reaction mixture was incubated overnight at 20°C to allow protein-siRNA complex formation. The resulting solution was ultra-filtered at pH 7.4 and exchanged with PBS by using 100 kDa Amicon Ultra-15 centrifugal filter devices to remove unbound molecules. The HFt-HIS-PASE/ si4 complex was characterized through 1.8% agarose gel electrophoresis (AGE) to demonstrate the successful binding of NH_2-si4 to the protein external surface. The gel was run at 90V for 60 min and subsequently imaged using ChemiDoc™ (Bio-Rad, USA). The amount of si4 bound to the ferritin nanoparticles was evaluated with the software Image J (https://imagej.net/ij/), enabling the calculation of the area and value statistics of pixels, in user-defined selections objects based on intensity. Standards of siRNA (as NH_2-si4) were used as reference. The gel was stained with Nucleic acid SYBR Gold staining for DNA/RNA visualization.

The same analysis was used to evaluate the concentration of the protein using standards of HFt-HIS-PASE as reference after gel staining with Coomassie dye. Purity and hydrodynamic volume of the complex HFt-HIS-PASE/si4 were determined by SEC. SEC experiments were performed as already described above. Stability of HFt-HIS-PASE/si4 complex was evaluated after storage at 2-8°C (three months) and in the presence of Denarase (c-LEcta GmbH, Leipzig, Germany) at $12.5x10^3$ U/mL. Denarase is able to cleave DNA and RNA impurities.

3.3.9 Analysis of CD71, MMP2 and MMP9 expression

To evaluate the potential application of the functionalized HFt-HIS-PASE construct in our cellular model, we have investigated the expression level of CD71 and of MMP2 and MMP9 on the selected cells. To this aim, the expression of CD71, MMP2 and MMP9 on osteogenic differentiated CMSCs was evaluated during different time points (0-5-10-15 days of osteogenic induction), using Real time PCR.

3.3.10 Cellular uptake and trafficking of HFt-NPs

To analyze the ability of the wild-type HFt nanovector and HFt-HIS-PASE (named HFt A and HFt B, respectively) to recognize CMSCs we performed the following experiment. CMSCs were seeded at a density of 2×10^4 cells/well in a 24-well plate (Corning, New York, USA) and cultured with standard growth medium for 24h. Subsequentely, cells were treated with 0.1 mg/mL and 0.3 mg/mL of fluorescently-labeled HFt A and HFt B constructs and placed into Incucyte® Live-Cell Analysis system incubator (Sartorius, Gottinga, Germany) for 6 days. Fluorescent signals were detected using phase contrast

and green (300-ms exposure) channels in the Incucyte platform. Specifically, for each condition, 9 image sets from distinct regions per well were taken every 15 min for the first 2 hours and then every 4 hours for 6 days using a 10X objective. The efficiency of HFt entry was evaluated by measuring the average number of green objects resulting from 9 images per well at different time points. Each condition has been repeated in triplicate (n=3). Images of untreated cells were selected as negative control for background correction. Graphics were generated with IncuCyte Basic Software graph/export functions.

3.3.11 Tracking of lysosomes

To investigate the difference between HFt and HFt-HIS-PASE nanovectors (HFt A and HFt B) in escaping the endosomal compartment, we performed the following experiment. Briefly, cells were seeded at a density of $15x10^3$ in a 8 well chamber slide (Ibidi, Munich, Germany) and cultured in standard growth medium for 24h. Then, cells were incubated with prewarmed (37°C) Lysotracker Deep Red (Invitrogen)-containing medium, according to manufacturer's instructions. After 2 hours, the medium was replaced with fresh medium and cells were treated with 0,1 mg/mL of fluorescently-labeled HFt A and HFt B. After 3h and 24h of incubation, images of live cell were acquired with confocal laser scanning microscopy (Nikon A1 MP+, Nikon). The experiments were repeated in triplicate.

3.3.12 *In vitro* testing of HFt-HIS-PASE-si4 constructs

The construct consisting of modified NH_2-si4 molecule selected for CS patient#1 conjugated onto HFt surface (HFt-HIS-PASE/si4) has been tested in

patient#1 cells to evaluate siRNA delivery and release efficiency. To this aim, CMSCs derived from CS patient#1 were plated at a density of $5x10^4$ cells/well in a 6-well plate and cultured in growth medium until they reached 50-60% confluence. Then, CMSCs were treated with 5 nM of NH_2-si4 delivered by HFt-HIS-PASE NPs (HFt-HIS-PASE/si4) for 48 hours. Cells treated with naked HFt-HIS-PASE were used as controls. Each experimental condition was performed in triplicate. The effects of the described treatment were investigated through Real-Time PCR expression analysis of mutant and wild-type *FGFR2* mRNA.

3.3.13 Statistical analysis

Data were analysed using GraphPad Prism software version 10 (San Diego, CA, USA). The graphs were reported as means with standard deviation (SD) of the mean. Unpaired Student's t-test and One-way ANOVA test were performed for determining statistical differences between groups and probability values $p< 0.05$ were considered significant.

3.4 Delivery of antisense oligonucleotides (ASOs)

3.4.1 Cell Culture

All cell lines were obtained from ATCC. Semi adherent D283 Med cells were cultured in MEM medium (M2279, Sigma-Aldrich) supplemented with 20% of heat-inactivated foetal bovine serum (USA origin), 1% sodium pyruvate, 1% non-essential amino acid solution, 1% L-glutamine, and 1x penicillin/streptomycin. Adherent HD-MB03 cells were cultured in RPMI medium (R0883, Sigma-Aldrich) supplemented with 10% of heat-inactivated foetal bovine serum (USA origin), 1% penicillin/streptomycin.

3.4.2 Cell Propagation

D283 Med floating cell subpopulation was collected, whereas adherent cell fraction was washed with 1x PBS w/o Ca^{++}/Mg^{++} and detached by incubation in 1x Trypsin/EDTA (T4299, Sigma-Aldrich) for 5 min. Cell fractions were centrifuged at 800 RPM for 5 min and resuspended in fresh culture medium. HD-MB03 cells were washed, detached, centrifuged and resuspended as described above. Cells were counted on a CytoSMART Cell Counter (CLS6749, Corning, Sigma-Aldrich) and replated at the desired concentration.

3.4.3 Evaluation of Viable Cell Number

D283 Med cells and HD-MB03 cells were seeded in plates, treated according to experimental plans (GapmeR/plasmid transfection and/or chemotherapeutic treatment) and counted at different time points. Specifically, 10 µL cell aliquots

were thoroughly suspended, mixed to 10 µL of trypan blue dye and counted by CytoSMART Cell Counter for cell population quantifications.

3.4.4 Transfections

LNA GapmeRs control (LG00000002, Qiagen) or specific LNA GapmeRs (Qiagen) were transfected one or three times (every 24 hours) in D283 Med or HD-MB03 cells at a concentration of 100 nM with Lipofectamine 2000 (11668-019, Invitrogen, ThermoFisher Scientific), in opti-MEM I medium (31985070, Gibco, ThermoFisher Scientific), according to manufacturer's instructions. LNA GapmeR sequences are gap_scr AACACGTGTATACGC, gap_lncMB3 ACGGTGAGGAGTTAAC (GapmeR #1) and gap_lncMB3(2) (GapmeR #2) GGTGTCCCTCTGTCTG.

Control (empty epB puroTT) and Δ16 plasmids were transfected in D283 Med cells at 100 ng with Lipofectamine 2000 (11668-019, Invitrogen, ThermoFisher Scientific), in opti-MEM I medium (31985070, Gibco, ThermoFisher Scientific), according to manufacturer's instructions. Doxycycline 100 ng/mL (D9891, Sigma Aldrich, Merck KGaA) was added in the complete growing medium.

Five g of control (sh_SCR) and sh_HMGN5 plasmids were transfected twice (24 and 48 hours after cell seeding) in D283 Med cells with Lipofectamine 2000 (11668-019, Invitrogen), in opti-MEM I medium (31985070, Gibco, ThermoFisher Scientific), according to manufacturer's instructions.

3.4.5 RNA Extraction and Analysis

Total RNA was extracted by Direct-zol RNA MiniPrep (R2052, Zymo Research). For quantitative real-time PCR (qRT-PCR) assay, cDNA was synthesised by Takara PrimeScript RT Reagent Kit (RR037A, Takara-bio). qPCR detection was performed using SensiFAST SYBR Lo-ROX Kit (BIO-94020, Bioline) on a 7500 Fast Real-Time PCR (Applied Biosystem). GAPDH or ATP50 was used as a reference target.

For RNA-sequencing TruSeq Stranded mRNA Library Prep Kit (Illumina) was used to obtain sequencing libraries from polyA+ RNA extracted. The sequencing reaction produced 100 nucleotide-long paired-end reads and was performed on a Novaseq 6000 sequencing system (Illumina) with a depth of more than 20 M reads. To remove adapter sequences and low-quality end bases Trim Galore188 (version 0.6.4_dev) software was used; the minimum read length after trimming was set to 20. Alignment to human GRCh38 genome primary assembly was performed using STAR (version 2.7.9a189).

3.4.6 Design, production, characterization and fluorescent labelling of the HFt-HIS-PASE nanovector

The design, production, characterization and fluorescent labeling of HFt-HIS-PASE nanovector are the same of the previous paragraphs: 3.3.3, 3.3.4, 3.3.5, 3.3.6.

3.4.7 Production of HFt-HIS-PASE-GapmeR complex

The lncMB3-specific GapmeR #1 was encapsulated within the internal cavity of the HFt-HIS-PASE using reversible, pH-dependent cage dissociation (acid pH) and re-association (neutral pH), in the presence of the bioactive payload.

HFt-HIS-PASE dissociation into subunits was achieved by lowering pH to 2.8 by 0.1 M HCl. LncMB3-specific GapmeR was added to the disassembled protein solution at a molar ratio of 1:1. The pH was then adjusted to 7.4 by 0.1 M NaOH, the solution was ultra-filtered at pH 7.4 and exchanged with PBS by 100 kDa Amicon Ultra-15 centrifugal filter devices to remove unbound molecules.

3.4.8 Characterization of HFt-HIS-PASE-GapmeR complex

Electrophoresis on 1.8% agarose gel (AGE) of the purified ferritin-GapmeR complexes was used to demonstrate the loading of GapmeRs in the protein cavity. The gel was run at 90V for 60 min stained with Nucleic Acid SYBR Gold for DNA/RNA visualisation and imaged by ChemiDoc™ (Bio-Rad, America). The amount of GapmeR bound to the ferritin nanoparticles was evaluated by the Image J software (https://imagej.net/ij/), by calculating the area and statistics value of pixels in user-defined selection-objects based on intensity. The same analysis was used to evaluate the concentration of the protein using standards of HFt-HIS-PASE as reference after gel staining with Coomassie dye. Purity and hydrodynamic volume of the HFt-HIS-PASE-GapmeR complex were determined by SEC experiments.

To verify GapmerR encapsulation and protection, HFt-HIS-PASE-GapmerR sample was incubated at 37°C for 1 hour and overnight with $12.5x10^3$ U/mL Denarase (c-LEcta GmbH) to digest DNA and RNA impurities. AGE was used as previously described to determine the GapmeR intensity of each sample. AGE was also employed to check the stability of HFt-HIS-PASE-GapmerR nanoparticles stored at 4 °C for three months.

3.4.9 HFt-HIS-PASE-GapmeR delivery

HFt-HIS-PASE-empty and HFt-HIS-PASE-GapmeR complexes were added to D283 Med cell complete growing medium at a concentration of 200 nM and maintained for 48 hours. To better understand the transduction pathways that lead to apoptosis in D283 cells, our collaborators conduced an experiment of double treatment on D283 with HFt-HIS-PASE-GapmeR and Cisplatin (DDP). In HFt/ DDP double treatment experiments 5 μM DDP was added to cells 2 hours after HFt-HIS-PASE-GapmeR administration. Then they valuated cells viability.

3.4.10 GapmeR stability, serum stability and nanoparticle stability

To verify that GapmerR molecules were encapsulated and protected from external damage, HFt-HIS-PASE-GapmerR sample was incubated with $12.5x10^3$ U/mL Denarase (c-LEcta GmbH, Leipzig, Germany). This enzyme is able to efficiently cleave DNA and RNA impurities when incubated at 37°C for an hour. AGE was used to determine the GapmeR intensity of each sample. To check the stability of HFt-HIS-PASE-GapmerR NPs stored at 4 °C for three months, 1.8 % AGE was used. The gel was run at 90V for 60 min and subsequently imaged using ChemiDoc™ (Bio-Rad, America).

4. RESULTS AND DISCUSSION

4.1 The-0504 therapeutic efficacy *in vitro* and *in vivo*

4.1.1. The-0504 production

The-0504 is based on a modified, recombinant human ferritin molecule, named The-05, that instead of iron contains about 70 molecules of the cytotoxic drug Genz-644282, entrapped in its hollow cavity (**Figure 17**). The production and characterization of the The-0504 protein-drug complex has been thoroughly described (Falvo et al., 2020). The-05 is produced at high yield in *E. coli,* and after purification process, this NP is functionalized with a specific anticancer drug. The-0504 was found to be highly pure and monodispersed in solution with a zeta-potential value of − 4.5 ± 0.9 mV (Falvo et al., 2020; Falvo et al., 2021). The mean diameter was about 19.0 nm as assessed by dynamic light scattering (17.0 ± 0.7 nm) and transmission electron microscopy (19.7 ± 1.5 nm). Stability data using size-exclusion liquid chromatography assays did not disclose compound aggregation or drug loss following The-0504 formulation as lyophilized powder, storage at 2–8 ◦C for 12 months, and reconstitution in water (**Table 1**).

Time (months)	Free Genz-644282 (%)	Purity of The-0504 by size-exclusion chromatography (%)
0	4.7	98.3
1	4.4	98.5
3	4.1	98.4
6	5.3	97.7

9	4.4	98.5
12	4.3	98.6

Table 1. Free-drug content in lyophilized The-0504 after storage at 2–8 ◦ C for 12 months.

4.1.2. Generation and persistence of γH2AX foci in MiaPaca2 cells in response to Genz-644282 and The-0504

We have previously demonstrated that adding the "masking" PASE polypeptide at the N-terminus of ferritin reduces its binding to the human CD71 receptor by sharply increasing the dissociation constant (Kd) from 10 nM to 120 nM for native HFt and The-05 based compounds, respectively (Falvo et al., 2018). Of special applicative interest, binding is restored to the original Kd value of 10 nM after *in vitro* incubation of the purified proteins with site-specific metalloproteases (MMP 2/9) cleaving the proteolytic site immediately downstream of PASE. Thus, reduction in CD71 binding was made transient, reversible, and conditional. In addition, we demonstrated that PASE-masked HFt compounds massively accumulate in the nucleus 3 h after treatment of cell lines at 37 ◦C (Falvo et al., 2018). In analogy with previous descriptions (Bellini et al., 2014; Zhang et al., 2015), it then appears that HFt-drug complexes bind CD71 at the cell surface, and are internalized in the endosomal compartment, where a mildly acidic pH (pH 5.5) favours some drug release/translocation in the cytoplasm, diffusion to the nucleus and initial DNA damage (Falvo et al., 2018; Zhang et al., 2015). This mechanism can further trigger nuclear translocation of HFt-based molecules, due to the well documented DNA-protective activity of HFt itself. Therefore, HFt-based

molecules are likely to act as “Trojan horses” delivering high amounts of the drug right to the site of action of the drug itself (cell nucleus).

To expand on the mechanism of action of The-0504, we further investigated DNA damage. It was hypothesized that the Topo 1 inhibitor Genz-644282, delivered as The-0504 complex into the nucleus, might induce DNA double-strand breaks (DSBs). DSBs are lethal DNA injuries that can be caused by cytotoxic chemical agents as well as environmental and physical damage. They were assessed by staining cells with an antibody to histone H2AX (S139 phosphorylation), that is a specific DSBs marker. Human pancreatic cancer MiaPaca2 cells were treated with 1 μM of Genz-644282 or The-0504. Immunofluorescence staining revealed clear γH2AX foci after 6 h of treatment with both compounds (**Figure 18A**), but H2AX phosphorylation was more evident with The-0504 than free Genz-644282 (**Figure 18B**). This reflects relative cytotoxicity of The-0504 and Genz-644282 in this specific cell line (Falvo et al., 2020). Drugs were washed out after 6 h, but this did not affect DSBs at 24 h, e.g. DNA damage response persists after drug removal. Free Genz-644282 results are in full agreement with previous observation with the naked drug (Sooryakumar et al., 2011). Notably, DSBs are more persistent upon treatment with HFt-encapsulated Genz-644282 than with the free drug (**Figure 18C**). These results altogether are fully consistent with the elective ability of H-ferritins to route and deliver drugs to the nuclear compartment of the cell (Bellini et al., 2014; Falvo et al., 2018; Zhang et al., 2015).

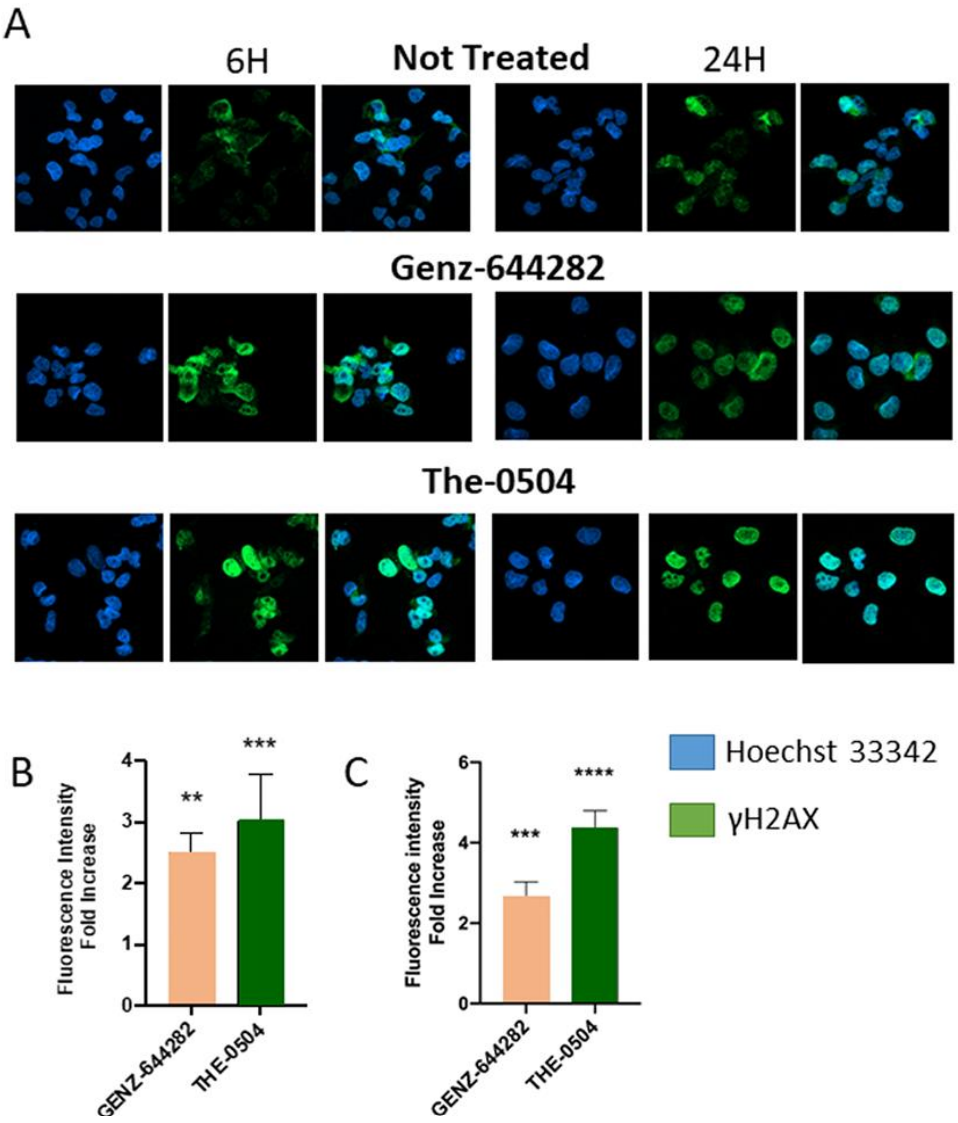

Figures 18. Phosphorylation of H2AX in MiaPaca2 cells treated with either free Genz-644282 or the fully encapsulated The-0504 formulation. Treat ment was for 6 h (1 M in Genz-644282 for both the free and encapsulated drug). γH2AX staining: 6h (end of treatment) and 24 h. **A**. Immunofluorescence microscopy images of γH2AX foci of MiaPaca2 cells mock-treated vs Genz-644282 vs The-0504 at the indicated times. γH2AX staining: green, nuclei counterstained in blue. **B**. and **C**. Same results

expressed as fold-increase relative to control at 6 and 24 h, respectively. Fluorescence outside the nucleus was considered background and subtracted.

4.1.3. The-0504 efficacy *in vivo*: pancreas, breast, lung and sarcoma xenotransplants

In vivo experiments were performed in collaboration with Thena Biotech, University of Verona and University of Chieti. In previous studies, The-0504 was evaluated on different human tumor xenotransplant models (triple-negative breast cancer, liver hepatocarcinoma, colorectal and pancreatic cancers) (Falvo et al., 2020; Falvo et al., 2021). Here, we expand our testing on 8 additional *in vivo* tumor models. The first model was a subcutaneous tumor xenograft of HT-1080 human fibrosarcoma. The-0504 was administered intravenously at the dose of 1.9 mg/kg (adjusted on the dosage of the active principle Genz-644282), twice a week for three consecutive weeks, and was compared with equimolar administrations of free Genz-644282. These are the same doses and regimens previously used to treat other tumor types. Like in these previous studies, the anticancer activity of The-0504 was very high, leading to complete regression of all HT1080 tumors, with 100 % values of both Tumor Growth Inhibition (TGI) and Objective Response Rate (ORR) (**Figure 19** and **Table 2**). Free Genz-644282 also showed antitumor activity, but much lower, failing to achieve complete regression (TGI value of 20.0 % and 0 % ORR; **Figure 19** and **Table 2**). Combined with the summary in **Table 2** and previously published observations of ours (Falvo et al., 2021), these results demonstrate remarkably similar The-0504 efficacy on mesenchymal, treatment-refractory fibrosarcoma and aggressive epithelial xenografts, despite these are usually treated by different drugs in the clinical setting. It is also remarkable that in both cases antitumor responses are complete only with The-

0504 but not free Genz-644282, clearly showing the considerable added value of delivering wide-spectrum chemotherapy through a CD71-targeted approach.

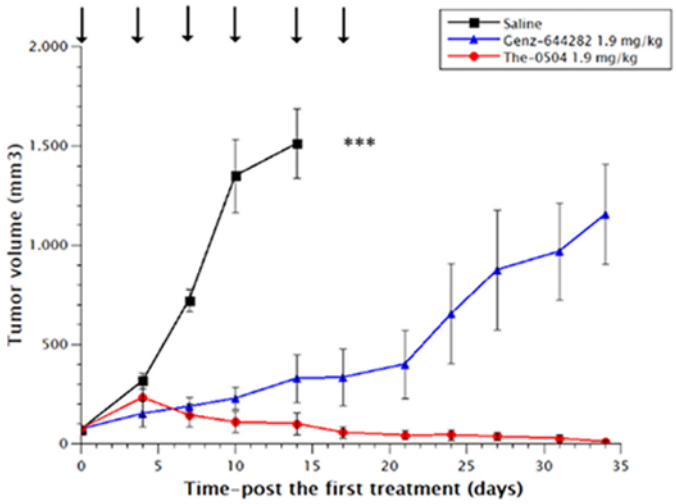

Figure 19. Anti-tumor activity of The-0504 vs free Genz-644282 on HT-1080 (fibrosarcoma) mouse xenografts. Statistical differences (Student's t-test) are as follows. The-0504 1.9 mg/kg vs control: ***p

Inferiority of free Genz-644282 prompted us to apply the 3R principles of animal ethics. Therefore, no free Genz-644282 treatment groups were planned for the following seven experiments on breast, lung and other pancreatic cancers, that were carried out with The-0504 only. Triple-negative breast cancer is usually more aggressive, harder to treat, and more likely to recur than other breast cancers (hormone receptor-positive or HER2-positive). Two tumor xenografts models were assessed, with similar results. The-0504 displayed a clear antitumor activity on both MDA-MB 468 and MDA-MB 157, complete response (CR), partial response (PR) and stable disease (SD) being equally

distributed among the six treated animals (**Figure 20**). Overall, the TGI and ORR values for The-0504 in both models were 92.2% and 66.7%, respectively.

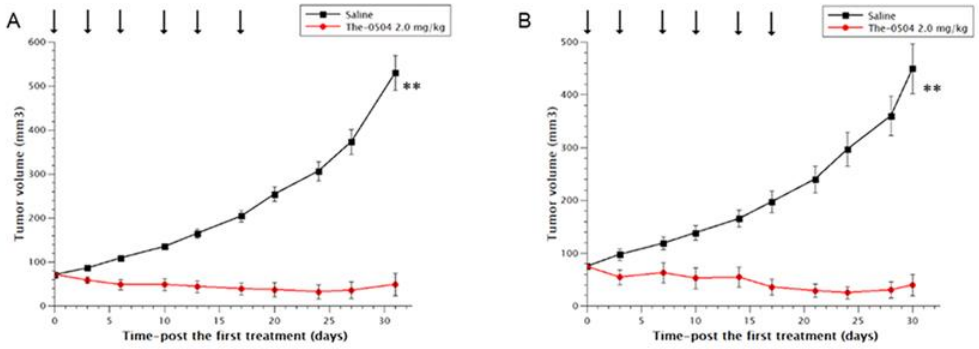

Figure 20. Anti-tumor activity of The-0504 on human breast cancer xenografts. **A**. MDA-MB 468; **B**. MDA-MB 157. Control vs The-0504 2.0 mg/kg **p < 0.005 (Student's t-test). Arrows: administrations.

The-0504 anticancer activity was also explored in two different histotypes of lung cancer: a small-cell lung cancer cel line (H1339) and a non-small cell lung cancer (A549), the latter of neuroendocrine origin (Kawasaki et al., 2023). Anticancer activity was observed, although at lower levels than in previous cancer models evaluated (**Figure 21**). This is particularly true for the A549 model, where the TGI and ORR values for The-0504 were 89.0 % and 33.3 %. In contrast, the TGI and ORR values for The-0504 in the H1339 model were 96.5 % and 66.7 %, respectively. The slightly lower response in the A549 model cannot be ascribed to low expression of the CD71 receptor, as a substantial high expression in this model was previously reported (Huang et al., 2017). Primary resistance is more likely and needs further evaluation.

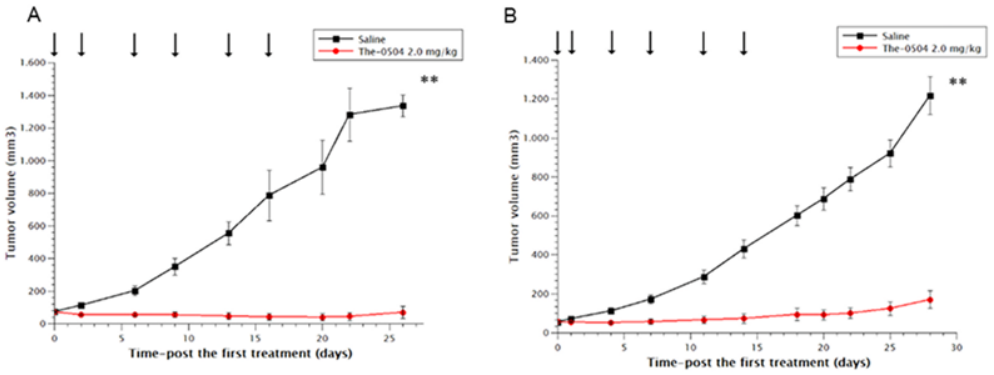

Figure 21. Anti-tumor activity of The-0504 on human lung cancer xenografts. **A**. H1339; **B**. A549. Control vs The-0504 2.0 mg/kg **p < 0.005 (Student's t-test). Arrows: administrations.

Finally, we tested The-0504 also on the pancreatic MiaPaca2 tumor cells, using the same regimen of 2.0 mg/kg bi-weekly used in the earlier panel of experiments. Like in previous studies on different pancreatic cancer models, e.g. PaCa44 and HPAF II (Falvo et al., 2020; Falvo et al., 2021), the anticancer activity of The-0504 was very high, leading to a 100 % values of both TGI and ORR, confirming that pancreatic cancer is a highly responsive model to The-0504 compound (**Figure 22** and **Table 2**).

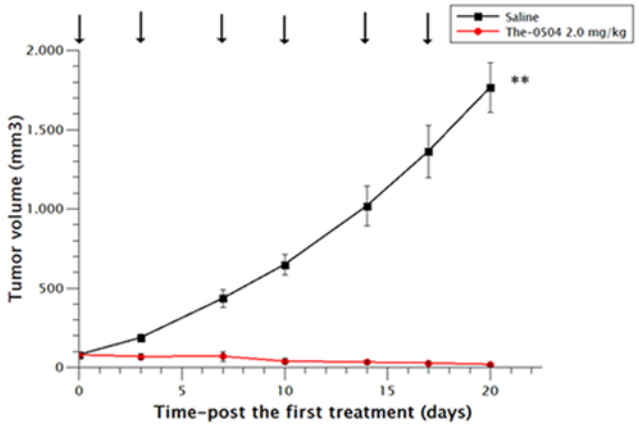

Figure 22. Anti-tumor activity of The-0504 on MiaPaca2 pancreas cancer xenografts. Control vs The-0504 2.0 mg/kg **p < 0.005 (Student's t-test). Arrows: administrations.

TUMOR MODEL DOSE (mg/kg)	**TGI (%)** **ORR (%)**		**RESPONSE (%)**	
	Genz-644282	***The-0504***	***Genz-644282***	***The-0504***
Pancreatic (PaCa44) 1.9 mg/kg (Falvo et al., 2021)	64.2 16.7	100 100	33.3 SD 66.7 PD	100 CR
Pancreatic (HPAF II) 1.9 mg/kg (Falvo et al., 2020)	33.3 0	93.3 83.3	33.3 SD 66.7 PD	16.7 CR 50.0 PR 16.7 SD
Pancreatic (PDX)* (Falvo et al., 2021)	0 0	93.6 83.3	100 PD	50 CR 33.3 PR 16.7 SD
Colorectal (HT29)	na 16.6	na 100	33.3 SD 66.7 PD	66.7 CR 33.3 PR

1.9 mg/kg (Falvo et al., 2021)				
Breast **(MDA-MB 231)** 1.9 mg/kg (Falvo et al., 2021)	70.1 0	100 100	16.7 SD 83.3 PD	100 CR
Liver **(HepG2)** 1.9 mg/kg (Falvo et al., 2021)	55.5 25.0	100 100	25.0 PR 75.0 PD	100 CR
Fibrosarcoma **(HT-1080)** 1.9 mg/kg	20.0 0	100 100	100 PD	100 CR
Breast **(MDA-MB 157)** 2.0 mg/kg	na	92.2 66.7	na	33.3 CR 33.3 PR 33.3 SD
Breast **(MDA-MB 468)** 2.0 mg/kg	na	92.2 66.7	na	33.3 CR 33.3 PR 33.3 SD
Lung **(H1339)** 2.0 mg/kg	na	96.5 66.7	na	16.7 CR 50.0 PR 16.7 SD 16.7 PD
Lung **(A549)** 2.0 mg/kg	na	89.0 33.3	na	33.3 PR 50.0 SD 16.7 PD
Pancreatic **(MiaPaca2)** 2.0 mg/kg	na	100 100	na	66.7 CR 33.3 PR
Pancreatic **(PaCa44)**** 3.0 mg/kg	na	100 100	na	100 CR
Pancreatic **(PaCa44)**** 6.0 mg/kg	na	100 100	na	100 CR
Pancreatic **(MiaPaca2)**** 1.5 mg/kg	na	92.2 66.6	na	16.6 CR 50.0 PR 33.3 SD

Regimen= BIWx3
*Nab-paclitaxel at 10 mg/Kg instead of Genz-644282 was used in Patient-Derived Xenograft (PDX) model

** Regimen= Q7dx3

Table 2. Summary of The-0504 and Genz-644282 efficacies in tumor-bearing mice models of several human cell lines using different administration schedules.

4.1.4. Pharmacokinetics in rats

In all the *in vivo* studies, The-0504 was administered two times a week for three weeks. The rationale for this frequency was essentially dictated by the fast growth kinetics of tumors in murine models. In light of a future use in humans, dosages and schedules will likely require optimization. As a first step to obtain crucial information, we resorted to pharmacokinetic experiments in Wistar Hannover rats and a non-rodent model (cynomolgus monkey). Herein, we report for the first time on single intravenous The-0504 administration in the rat model. As describe above, The-0504 is a complex based on The-05, a modified ferritin which acts as carrier and includes, as payload, the cytotoxic compound Genz-644282. Two bioanalytical techniques were employed to follow the kinetic of the carrier, i.e., an ELISA protocol, using the carrier protein The-05 as standard and a polyclonal anti-The-05 antibody for detection, and an LC/MS method, using the Genz-644282 as reference item. Healthy rats injected with free Genz-644282 at 3.0 mg/kg showed hunched posture, slight to moderate piloerection and moderately decreased activity during the last days of the study. In sharp contrast, no clinical signs were recorded in animals treated with The-0504 at two different doses, 1.5 mg/kg and 3.0 mg/kg (Genz-644282 concentration), corresponding to about 30 mg/kg and 60 mg/kg as The-05 protein concentration, respectively. The dose of 3.0 mg/kg is the maximal concentration of The-0504 that we have previously shown to be safe in rat using multiple administrations (Falvo et al., 2021). Body

weights were within the expected range for this strain and age of animals. Test item was not detected in rat plasma before the intravenous administration.

Pharmacokinetics are illustrated by **figure 23**, that demonstrates at glance the much higher peak levels and persistence of The-0504 compared to free Genz-644282 (**Figure 23B**). The mean (N = 6) pharmacokinetic parameters determined from the mean concentration for the analytes are summarised in **table 3**. The concentrations of the two analytes, i.e., the payload (Genz-644282) and the carrier protein (The-05), were evaluated in all animals treated with the test item The-0504 and were detected up to the last sampling time point (144 h from administration). Since the values detected were still quite high at the end of the study, half-lives (T1/2) could only be estimated.

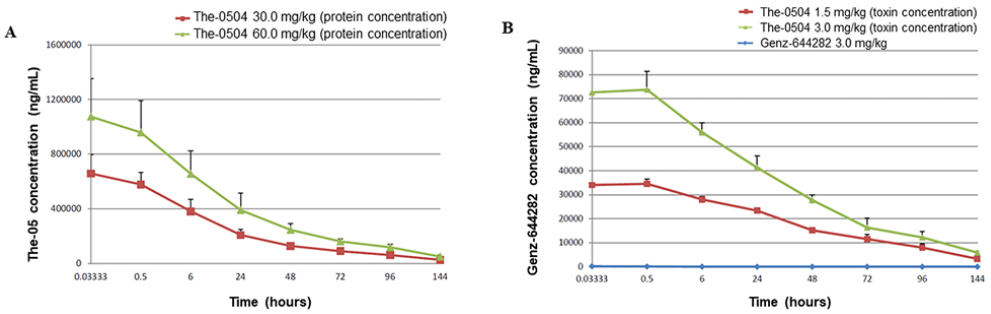

Figure 23. Mean plasma level of The-0504 following intravenous administration. **A**. The-05 protein concentration. **B**. Genz-644282 concentration.

Dose/Analyte	**C_{max} (ng/mL)**	**T_{max} (h)**	**AUC $_{(0\text{-inf})}$ (ng/mL*h)**	**$T_{1/2}$ (h)**
The-0504, 30 mg/kg in The-05 protein	657,833	0.03333	20,316,400	41.17
The-0504, 60 mg/kg in The-05 protein	1,073,430	0.03333	37,290,300	41.26
Free Genz-644282, 3.0 mg/kg	184	0.3333	983	15.02

The-0504, 3.0 mg/kg in Genz-644282	34,503	0.5	2,124,120	39.50
The-0504, 6.0 mg/kg in Genz-644282	73,713	0.5	3,812,180	48.48

Measured analyte is underlined

Table 3. Mean pharmacokinetic parameters after The-0504 injection in rats.

Mean Cmax values increased with increasing dose, in a dose proportional manner from 657,833 to 1,073,430 ng/mL (**Figure 23A**), and from 34, 503 to 73,713 ng/mL (**Figure 23B**), respectively for the analyte The-05 and Genz-644282 (**Table 3**). The exposure values showed a good dose correlation since the AUC(0-inf) ranged from 20,316,400 to 37,290,300 ng/mL*h, and from 2,124,120 to 3,812,180 ng/mL*h, respectively for the analyte The-05 and Genz-644282 (**Table 3**). Clearance values were very low, indicating that both the carrier protein The-05 and encapsulated Genz-644282 remained into the plasma compartment. As expected, free Genz-644282 was characterized by a faster clearance and a Cmax 400-fold lower in comparison to the Genz-644282 complexed with the carrier protein The-05 (**Table 3** and **Figure 23B**). Based on the above results and in agreement with the previously reported toxicological studies, it can be concluded that the test item The-0504 was well tolerated by Wistar Hannover rats, when administered intravenously at a concentration of 1.5 and 3.0 mg/kg as a single dose. At the selected dose levels, the test item remained in the plasma compartment and the exposure was from 2000 to 6000-fold higher than free Genz-644282. Furthermore, the half-life and kinetic profiles of the carrier (measured by ELISA method) and of the payload (measured by LC-MS/MS method) are essentially superimposable,

suggesting that the circulating protein-drug complex is stable up to 1 week after intravenous administration.

Due to the very long persistence of The-0504 in rat serum, a new set of *in vivo* experiments were designed for pancreatic PaCa44 tumor xenografts, involving administration once (and not twice) per week for three consecutive weeks. In this case, tumor-bearing mice were treated with The-0504 at 3.0 mg/kg or at 6.0 mg/kg in Genz-644282. The maximal dose of 6.0 mg/kg was applied in agreement with our previous toxicity data reporting the tolerability of The-0504 in mice at this concentration (Falvo et al., 2021). In Ref. (Falvo et al., 2021) the non-GLP toxicological evaluation in rats is also reported. The delayed The-0504 schedule still eradicated all tumor masses, although more slowly than in the experiment showed for reference in panel **B** of the **figure 24**, where a more frequent scheme of administration was applied in the same cancer model (PaCa44). Specifically, tumor growth immediately stalled after the first administration of The-0504 but significant regression occurred only between the second and the third injection. The relative TGI and ORR values at 3.0 and 6.0 mg/kg dose were both 100 % for the two injected doses (**Table 2**). Therefore, these results are quite identical of the experiment showed in panel B of the Fig. 7 where the more frequent scheme of administration was used. Here, The-0504 induced complete regression, with 100 % values of both TGI and ORR at 1.9 mg/kg dose, whereas free Genz-644282 resulted in much lower TGI and ORR values, 64.2 % and 16.6 %, respectively (**Table 2**).

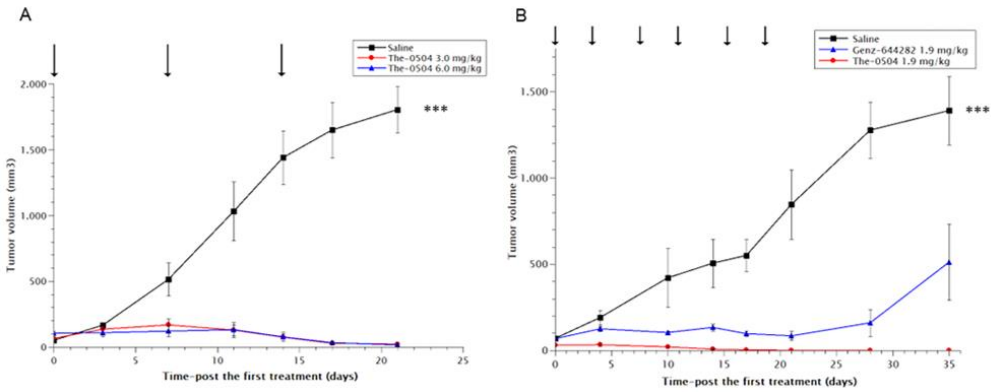

Figure 24. Anti-tumor activity of The-0504 in PaCa44 mouse xenografts treated by two different schedules. **A**. Once per week; **B**. twice per week. Three consecutive weeks in both cases. All p-values calculated by the Student's t-test. Control vs The-0504 1.9 mg/kg and 6.0 mg/kg: ***p < 0.0001: Control vs Genz-644282 and Genz-644282 vs The-0504 1.9 mg/kg: *p < 0.05. Control vs 3.0 mg/kg: **p < 0.005. Arrows: administrations. Panel **B** was adapted from Ref. (Falvo et al., 2021).

Mice did not show body weight loss, signs of pain or distress, or abnormal behaviour (not shown). To confirm this novel therapeutic scheme, we tested The-0504 also on MiaPaca2 tumor cells, using a lower dose of 1.5 mg/kg weekly in comparison with the previously used doses of 3.0 and 6.0 mg/kg weekly, or 2.0 mg/kg bi-weekly. As shown in **figure 25**, an excellent anticancer activity was observed, with appreciable TGI and ORR values of 92.2 and 66.6 %, respectively.

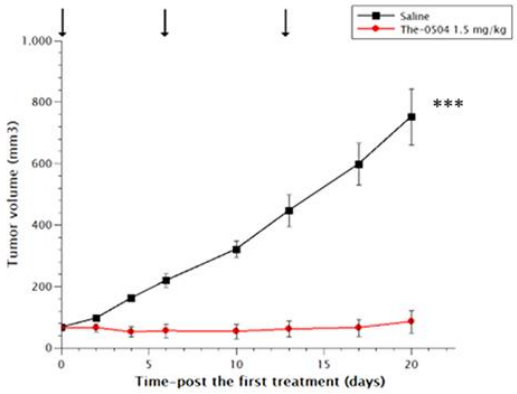

Figure 25. Anti-tumor activity of The-0504 in MiaPaca2 mouse xenografts. Control vs The-0504 1.5 mg/kg: ***p < 0.0001 (Student's t-test). Arrows: administrations.

A synopsis of all the data from the *in vivo* efficacy studies performed on The-0504 is provided in **table 2**. So far, the minimum efficacious dose (MED, total weekly dose) observed in the *in vivo* studies (**Figure 25**, **Table 2**) was 1.5 mg/kg.

4.2 Delivery of BioActive Peptides (BAPs)

4.2.1 Design and Production of THE-10

One of the main goals of this thesis was to assess whether a novel BAP-fusion protein based on an engineered human ferritin enhances the antitumor activity of co-administered drugs ('booster' effect). We aimed at assessing whether the booster effect takes place with different classes of anticancer agents, in different cells, in various experimental conditions, and to which extent. Therapeutic boosting may be of interest to expand the indications of approved drug as well as to refine efficacy data of drugs under clinical developments. The test compound, named THE-10, was derived by modification of our previously described PASylated protein HFt-MP-PASE (Falvo et al., 2018). The sequences selected for incorporation in the N-terminal domain of HFt-MP-PASE are linear versions of two previously reported cyclic BAPs: the PD-L1 binding peptide (PD-L1Pep-1), and another peptide binding integrin αVβ3/αVβ5 and NRP-1 (iRGD or Certepetide). THE-10 is shown in **figure 26.**

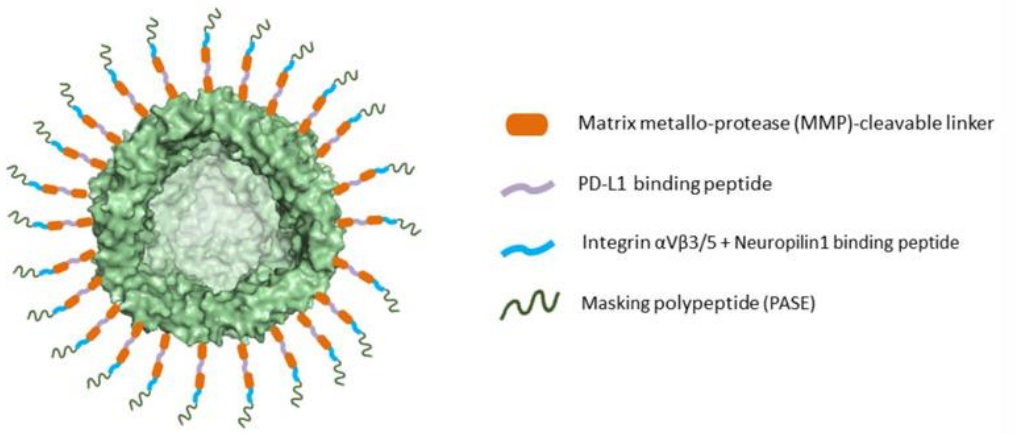

Figure 26. Schematic representation of the THE-10 construct, wherein the N terminus of each of the 24 monomers is genetically fused to a cleavable MMP peptide sequence, two bioactive peptides, and an outer PASE (masking) sequence.

4.2.2 THE-10: biochemical characterization and cleavable N-terminus

Purified (see methods) THE-10 was biochemically characterized and compared with THE-10 incubated at 37°C for two hours with a collagenase IV preparation containing matrix metalloproteases MMP-2 and 9. These are typically expressed in the tumor microenvironment. Size exclusion chromatography (SEC, **Figure 27A**) and sodium dodecyl sulfate–polyacrylamide gel electrophoresis (SDS-PAGE, **Figure 27B**) revealed the expected differences in elution volumes and profiles before and after cleavage. The latter were slight but clearly detectable and resulted in a shift in electrophoretic band migration profiles compatible with the anticipated drop of about 5 kD in each HFt subunit. Therefore, highly purified THE-10 is cleavable, e.g. BAPs are expected to be released at the TME in the presence of MMPs.

A

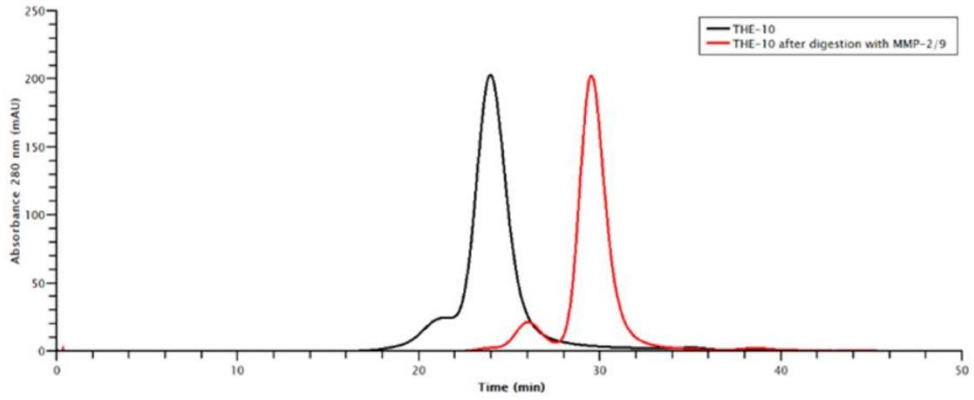

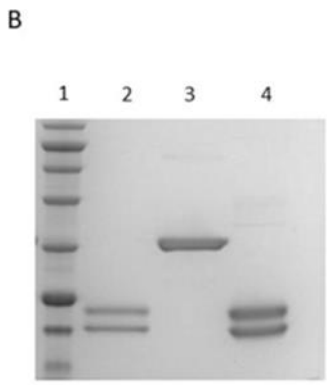

Figure 27. Purity and polypeptides removal *in vitro*. **A**. SEC profiles of THE-10 before (black line) and after (red line) PASE and BAP sequences removal by MMP-2/9 proteinase *in vitro*. **B**. SDS PAGE band migration profiles of THE-10 before and after MMP-2/9 digestion. Lane 1, protein marker; Lane 2, native HFt (5 µg); Lane 3, THE-10 (5 µg); Lane 4, THE-10 (5 µg) after *in vitro* digestion with 0.5 mg/mL MMP-2/9. SDS PAGE was stained with Coomassie brilliant blue R-250.

4.2.3 BAP-mediated receptor binding of THE-10

To determine whether BAPs confer receptor tropism, THE-10 binding was assessed by surface plasmon resonance (SPR) assay using recombinant αVβ3, neuropilin-1 (NRP-1) and PD-L1 as ligands (**Figure 28A** and **B**). All measured dissociation constants (K_D) were in the nanomolar range, indicating strong binding affinity between the THE-10 analyte and its ligands. Nevertheless, the two ligands show a different behaviour in the interaction with the functionalized construct. In fact, as shown in **figure 28A**, the interaction between THE-10 construct and αVβ3 prompted out a strongly biphasic interaction, characterized by two association rate constants (k_{on}) and two dissociation rate constants (k_{off}). Consequently, the αVβ3 SPR sensorgram required a heterogeneous ligand binding model compatible with the presence

of one analyte (THE-10) and two possible binding sites, with high and low affinity respectively (**Figure 28A**). Alternatively, a mixed population of the receptor may also be envisaged to interpret the kinetic data. However, the first interpretation is preferred, as the amplitude of the rapid dissociation phase is increasing with increasing concentration of the analyte, thus indicating that higher concentration of this species may populate more easily the alternative site at lower affinity. On the contrary, PD-L1 data fit a straightforward 1:1 interaction model (**Figure 28B**), with a very low K_D value consequent to the very slow k_{off} value. This indicates an extremely stable interaction between THE-10 and PD-L1. As to NRP-1, no significant SPR response could be detected (data not shown). This result may be expected, because binding of THE-10 to NRP-1 requires cleavage of the iRGD peptide incorporated in THE-10 construct, and exposure of the internal RGDK binding motif (C-end rule). Unfortunately, this cannot be modelled by *in vitro* SPR experiments, since it is mediated by an unknown TME protease *in vivo*. Regardless, SPR experiments clearly show that at least 2 of the 3 BAPs grafted onto the THE-10 fusion HFt nanovector retain full biological *in vitro* activity.

A

$k_{on}1(M^{-1}s^{-1})$	$k_{off}1(s^{-1})$	K_D1(nM)	$k_{on}2(M^{-1}s^{-1})$	$k_{off}2(s^{-1})$	K_D2(nM)
(1.33 ± 0.04) x 10^4	(57.86 ± 0.84) x 10^{-4}	435.4 ± 20.1	(17.25 ± 0.21) x 10^4	(0.53 ± 0.13) x 10^{-4}	0.31 ± 0.1

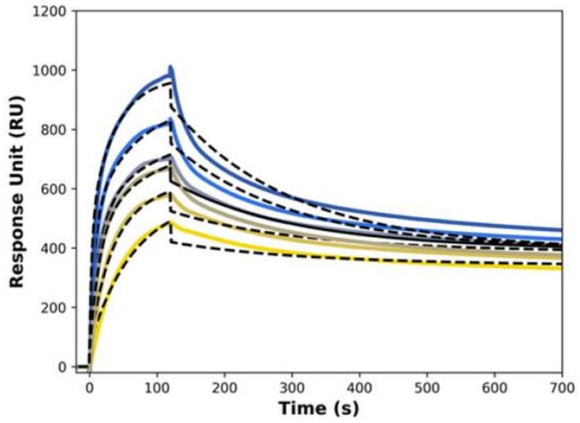

B

k_{on} (M^{-1} s^{-1})	K_{off} (s^{-1})	K_D (nM)
(1.45±0.01) x 10^4	(4.94±0.02) x 10^{-5}	3.41 ± 0.02

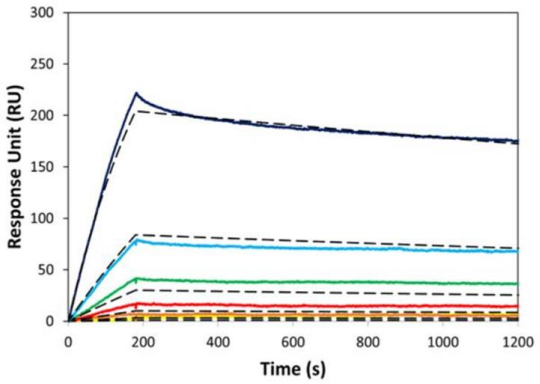

Figure 28. SPR experiments. Top: Thermodynamic and kinetic parameters of the interaction of THE-10 (analyte) with **A**. human αVβ3 and **B**. human PD-L1. Bottom: Sensorgrams showing the interaction of THE-10 with human his-tagged receptors immobilized onto a HisTag sensorchip. Sensorgrams show THE-10 injection,

followed by buffer injections to monitor analyte dissociation. **A**. Curves were fitted using a heterogeneous ligand binding model. **B**. Curves were fitted as single 1:1 interactions; fittings are shown as black dashed curves.

4.2.4 THE-10 enhances the internalization of a therapeutic antibody

As a first step to determine whether biochemical activity translates into biological activity, THE-10 was assessed for its ability to enhance the uptake and internalization of a co-administered anti-cancer drug (booster effect). The humanized therapeutic antibody Trastuzumab (TTZ) was selected as a test compound. TTZ binds the Human Epidermal Growth Factor Receptor 2 (HER2), that is typically overexpressed in breast cancer cells of the HER2-positive subtype, but is expressed at extremely low levels in most human tumors, including melanoma cells, which makes these tumors insensitive to anti-HER2 treatments with antibodies and small molecules. The melanoma cell line A375 recapitulates this typical HER2-negative phenotype, but it displays low and moderate expression of αVβ3 and NRP-1, respectively, which makes it suitable to test booster THE-10 activity, if any (**Figure 29**).

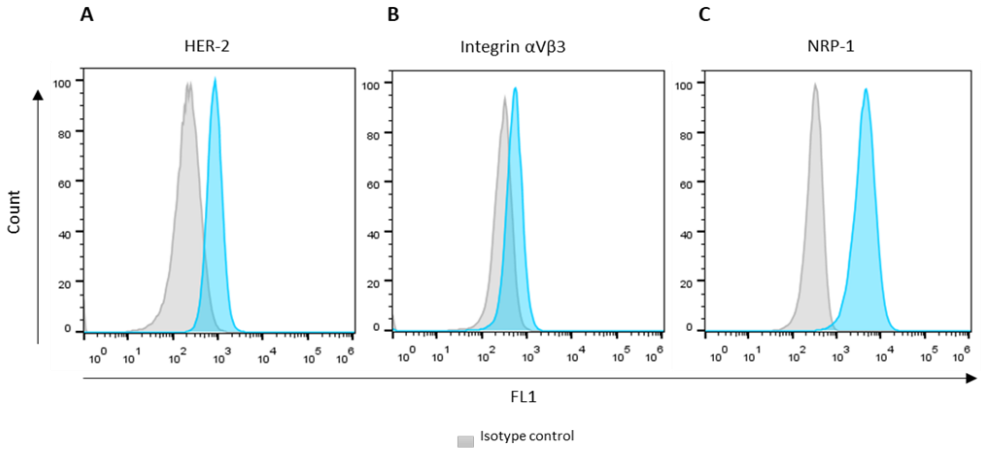

Figure 29. Flow cytometry of A375 human melanoma cells**.** Cells were surface stained with antibodies: **A**. anti-HER2, **B**. anti-CD51-CD6, **C**. anti-CD304 (1:20), and read in an Attune NxT flow cytometer.

On this basis, TTZ was conjugated to a pH-sensitive dye that turns red when the antibody is internalized into acidic intracellular vesicles. Time-lapse (every 60 min), live cell imaging of A375 melanoma cells growing for 48h under standard condition readily revealed that TTZ is poorly and slowly internalized, as expected, but addition of THE-10 to the culture medium accelerates uptake, and gradually enhances red fluorescence intensity, that reaches approximately four-fold the control values at endpoint (**Figure 30A** and compare panels **B** and **C**). In summary, THE-10 enhances cell uptake and internalization of a therapeutic antibody in a cell line with the right background of αVβ3 and NRP-1 receptors. This conclusively demonstrates functionally successful BAP grafting onto the THE-10 nanovector backbone.

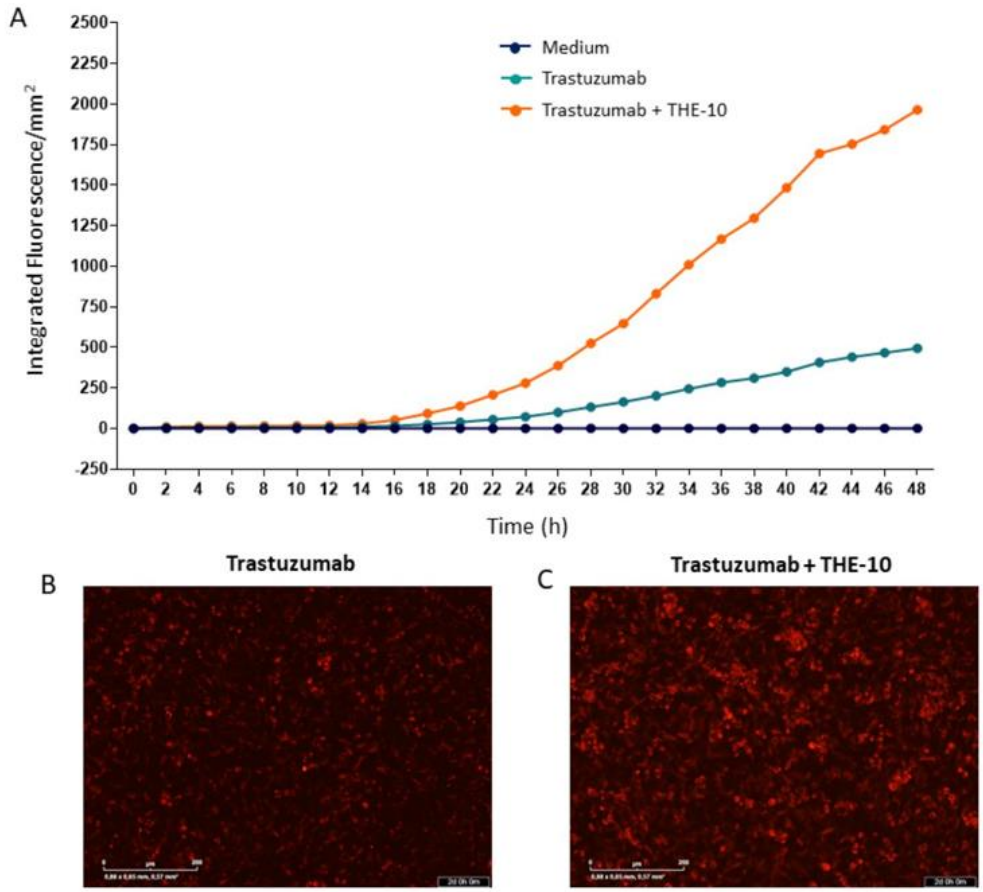

Figure 30. Kinetics of antibody Internalization by A375 melanoma cells. A375 cells were treated with pHrodo Deep Red labeled Trastuzumab (10 µg/mL), alone or combined with THE-10 (1 mg/mL), for 48 hours in an Incucyte Live-Cell system. **A**. A time course of red Integrated Fluorescence, corresponding to antibody internalized into acidic intracellular vesicles, is displayed (20X magnification) for the three conditions, with acquisition at 60 min intervals. Each point of the internalization kinetic is shown as the mean of 18 independent readings of 2 wells, which makes standard deviation negligible. **B, C**. Red images captured at time 48 h post treatment.

4.2.5 THE-10 enhances tumor cell killing by a therapeutic Antibody-Drug Conjugate (ADC)

To determine whether increased internalization translates into improved therapeutic efficacy, the same A375 human melanoma cells were exposed to the same antibody, albeit in a form conjugated to a toxic topoisomerase I inhibitor, e.g. Trastuzumab deruxtecan (T-DXd). T-DXd was selected because, unlike other naked antibodies and ADCs, it has remarkable unprecedented activity on HER2-low breast cancers (Modi et al., 2022), although results of clinical trials with HER2-low cancers from other histotypes are not yet available. T-DXd killing of A375 melanoma cells was dose-dependent, and at the lowest T-DXd dosage THE-10 enhanced killing approximately four times, whereas THE-10 alone displayed no significant effect (**Figure 31**). Therefore, THE-10 mediates a booster effect on a cytotoxic antibody to HER2 in a cell line expected to be unresponsive to anti-HER2 treatments but capable to internalize the antibody in presence of THE-10.

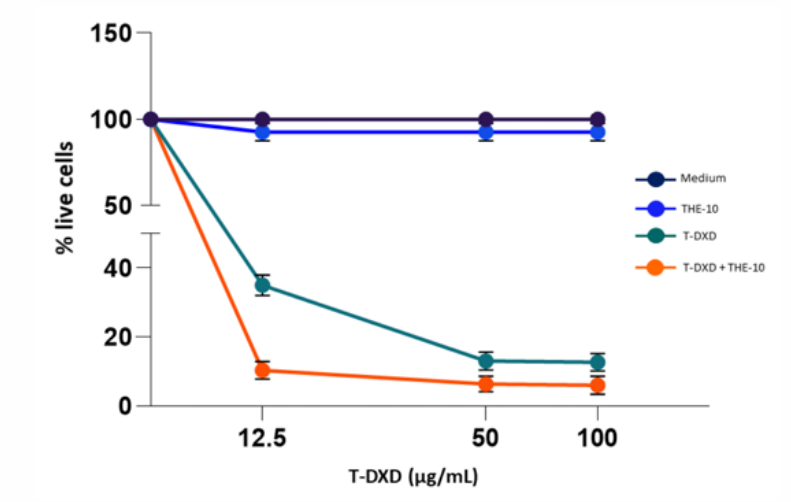

Figure 31. Booster effect of THE-10 on A375 melanoma cells. Cell killing after 5 days of treatment with Trastuzumab deruxtecan (T-DXD) and THE-10, alone or

combined. Each experimental condition was performed in triplicate. Bars correspond to mean ± SD from 3 replicates per condition.

4.2.6 THE-10 slows tumor growth in a colorectal cancer mouse model

A PD-L1 peptide (PD-L1pep1) fused to the N-terminal of the native human ferritin (HFt) was previously reported to block PD-1/PD-L1 interactions, inhibit the immune suppressive activity of PD-L1 and have some antitumor effects *in vivo* (Jeon et al., 2021). THE-10 contains a similar peptide, the only difference being the absence of the terminal N- and C-terminal cysteine residues. The antitumor activity of THE-10 was directly assessed in the same syngeneic mouse allograft model used by Jeon IS et al. Established CT26 mouse colon cancer grafts were treated by intravenous injection of THE-10 (120 mg/kg) or saline two times per week for a total of four injections. Treatment with THE-10 mildly inhibited tumor growth compared with control mice treated with saline (**Figure 32**). This mild antitumor efficacy was expected, and it is comparable to that reported for the HFt-PD-L1 fusion protein previously ascribed to the blocking PD-1/PD-L1 interaction and immunological restoring of T cell immune response against the tumor (Jeon et al., 2021). No significant differences in body weight were observed among experimental groups during treatment (not shown).

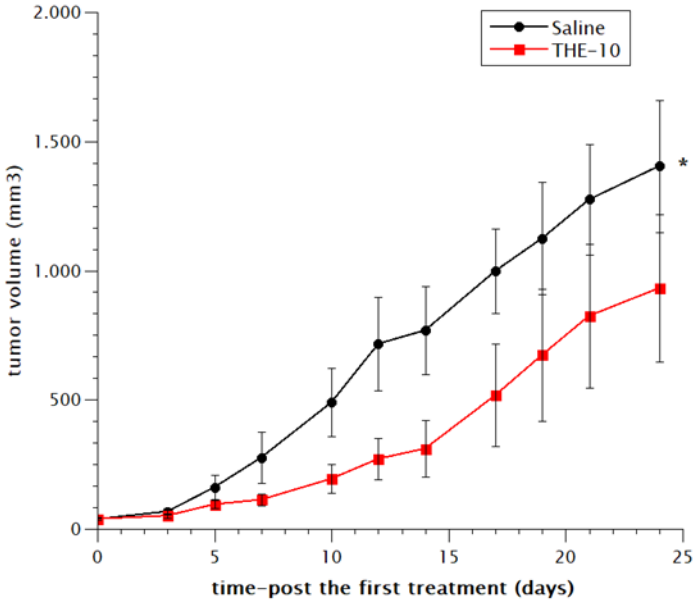

Figure 32. THE-10 antitumor effect on CT26 syngeneic mouse colon tumors. Growth curves representing the media of the tumor volume for each of the treated groups ± SEM (*p < 0.05, t-test).

4.2.7 THE-10 enhances the *in vivo* antitumor activity of two small drugs: Irinotecan and Gemcitabine

Irinotecan and gemcitabine are two key drugs employed worldwide for the treatment of several solid tumors. However, therapeutic resistance, short half-life, and side effects owing to toxicity limit their success in clinical practice. For this reason, we examined the ability of THE-10 to boost drug accumulation and anticancer effects in two murine models. The anticancer booster effect of combination therapy with Irinotecan plus THE-10 was evaluated in the syngeneic mouse colon (CT26) cancer model (**Figure 33A**). Four intravenous injections of THE-10 (120 mg/kg), followed by intra-peritoneal injections of

irinotecan (100 mg/kg), two times per week for a total of four injections, significantly reduced tumor growth as compared to injection of the sole Irinotecan ($p<0.05$; **Figure 33A**). Tumor Growth Inhibition (TGI) was 29.0 % for the Irinotecan-treated group and 63.0 % for the group treated by irinotecan plus THE-10 (**Table 4**). Similarly, co-administration of THE-10 (130 mg/Kg) with gemcitabine (100 mg/Kg) decreased growth of a syngeneic mouse pancreatic (KPC) tumor significantly more than gemcitabine monotherapy ($p<0.001$, **Figure 33B**), with TGI values of 82.2% vs 48.8% (**Table 4**).

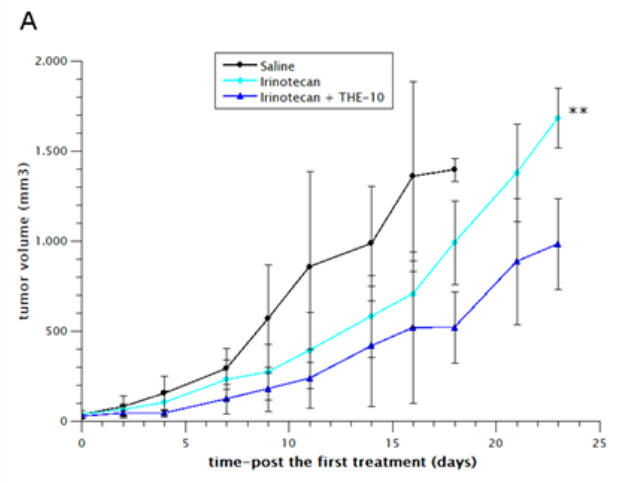

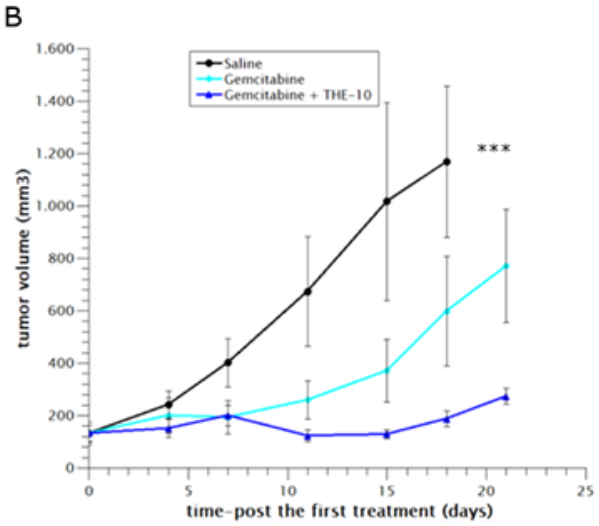

Figure 33. Tumor treatment studies involving co-administration of THE-10 with irinotecan or gemcitabine. **A**. Tumor growth curves of irinotecan and THE-10 combination therapy in CT26 colorectal cancer model. **B**. Tumor growth curves of gemcitabine and THE-10 combination therapy in KPC pancreatic cancer model. Statistical differences (t-test) are as follows. *p < 0.05: Irinotecan vs control, Irinotecan plus THE-10 vs control, Gemcitabine vs control, Gemcitabine plus THE-10 vs control; **p < 0.001: Irinotecan vs Irinotecan plus THE-10; ***p < 0.0001: Gemcitabine vs Gemcitabine plus THE-10.

4.2.8 THE-10 enhances the *in vivo* antitumor activity of the nanoferritin The-0504 in two different models of pancreatic cancer

The-0504 is a complex based on The-05, a genetically modified human ferritin which acts as a drug carrier. The-0504 encapsulates in its cavity, as payload, the cytotoxic drug Genz-644282, a non-camptothecin topoisomerase-I inhibitor. Recently, we evaluated The-0504 in solid tumor animal models. Delayed tumor growth and durable complete remissions were observed in combination with a manageable toxicity profile (Falvo et al., 2020; Falvo et

al., 2021, Fracasso et al., 2023). The-0504 is currently at an advance development stage for first-in-human trials in solid tumors.

This prompted us to evaluate THE-10 as an antitumor booster of The-0504. To this end, a murine model of pancreatic cancer was selected in which the activity of THE-0504 is very low, since THE-0504 binds the murine CD71 receptor much less than its human receptor orthologue (Marrocco et al., 2024). Syngeneic mouse pancreatic (KPC) cancers, about 250 mm^3 in volume, were treated by intravenous injection twice a week for three weeks. Mice received 200 μL of physiological saline, or The-0504 (1.0 mg/kg), or The-0504 (1.0 mg/kg) plus iRGD peptide (3.0 mg/Kg), or The-0504 (1.0 mg/kg) plus THE-10 (130 mg/Kg, corresponding to about 3.0 mg/kg in iRGD peptide). Tumor growth curves show the expected low antitumor activity of THE-0504 alone, a limited booster effect of the original cyclic iRGD peptide (CRGDKGPDC) that is currently in phase 2 clinical trial for pancreatic cancer, and a much greater, and remarkable, boost by THE-10 (**Figure 34**), as quantitatively estimated by TGI values (**Table 4**). Since the plasma half-lives of iRGD and parental The-05 are 15 min and about 40 hours respectively (Fracasso et al., 2023; Pang et al., 2014), these findings are consistent with a longer serum persistence and/or higher tumor accumulation/release of BAPs fused to HFt as compared to naked peptides.

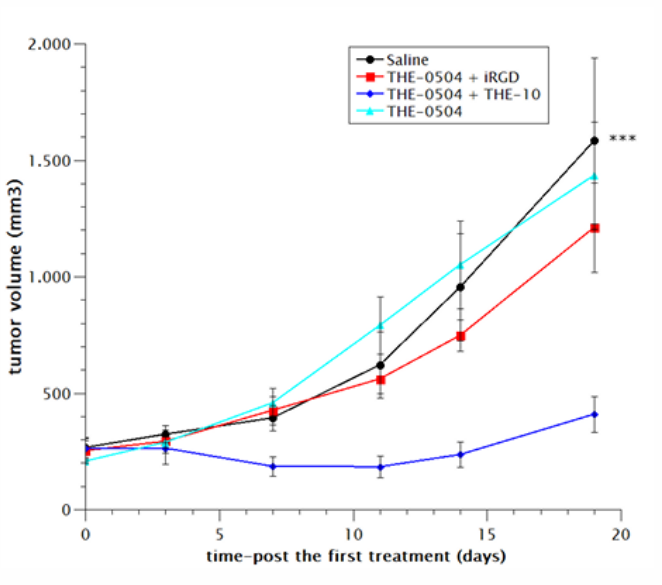

Figure 34. Tumor treatment studies involving co-administration of THE-0504 drug with THE-10 or iRGD peptide. Tumor growth curves in KPC pancreatic cancer model. Statistical differences (t-test) are as follows. **p < 0.001: THE-0504 vs control, THE-0504 plus THE-10 vs control, THE-0504 plus iRGD vs control; ***p < 0.0001: THE-0504 plus THE-10 vs THE-0504 plus iRGD.

The booster effect of THE-10 was assessed in a second pancreatic cancer model, that is instead susceptible to The-0504. In this case, the tumor (MiaPaca2) was of human origin and was grown as a xenograft. Mice were intravenously injected twice a week for three weeks with 200 µL of physiological saline, The-0504 (1.0 mg/kg), or The-0504 (1.0 mg/kg) plus THE-10 (130 mg/Kg). As shown in **figure 35**, THE-0504 alone greatly reduced tumor growth ($p < 0.001$), but despite this marked effect, addition of THE-10 resulted in a remarkable boost, revealed by an almost complete stall in tumor growth (**Figure 35A**, **Table 4**). This is best appreciated by considering the dramatic reduction (approximately four-fold) in the weight of

residual tumor masses excised from the animals at the end of the experiment compared with The-0504 alone (**Figure 35B**).

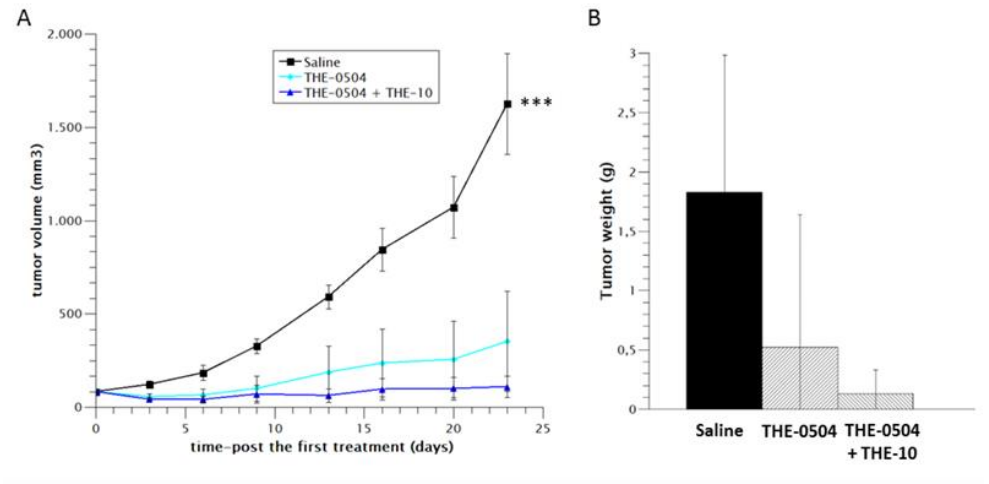

Figure 35. Tumor treatment study involving co-administration of THE-0504 drug with THE-10 or iRGD peptide. **A**. Tumor growth curves in MiaPaca2 pancreatic cancer model. **B**. Tumor weights of animals sacrificed at the end of the experiment. Statistical differences (t-test) are as follows. **p < 0.001: THE-0504 vs control; ***p < 0.0001: THE-0504 plus THE-10 vs control.

4.2.9 THE-10 enhances the *in vivo* antitumor activity of the Antibody-Drug Conjugate Sacituzumab govitecan in a murine model of pancreatic cancer

Sacituzumab govitecan (previously known as IMMU-132) is a first-in-class ADC that depends in its activity on the expression of the Trophoblast cell surface antigen-2 (Trop-2). IMMU-132 is indicated for the treatment of metastatic triple-negative breast cancer and metastatic urothelial cancer (Seligson et al., 2021). To test THE-10 boosting on IMMU-132 antitumor activity, the same murine pancreatic cancer graft (KPC) was selected, used in previous experiments. In this model, the activity of IMMU-132 alone was

expected to be absent or very low due to the lack of detectable Trop-2 expression in mice (Cardillo et al., 2015). Then, mice were intravenously injected three times, one every 3-4 days, with 200 µL of physiological saline, IMMU-132 (30.0 mg/kg), or IMMU-132 (30.0 mg/kg) plus THE-10 (130 mg/Kg). THE-10 was injected about 5-10 minutes before IMMU-132. As expected, IMMU-132 did not exert any significant therapeutic effect, whereas in combination with THE-10 it resulted in an excellent anticancer activity, with a remarkable TGI of 93.0 %, supported by reduction in residual tumor masses (**Figure 36**, **table 4**).

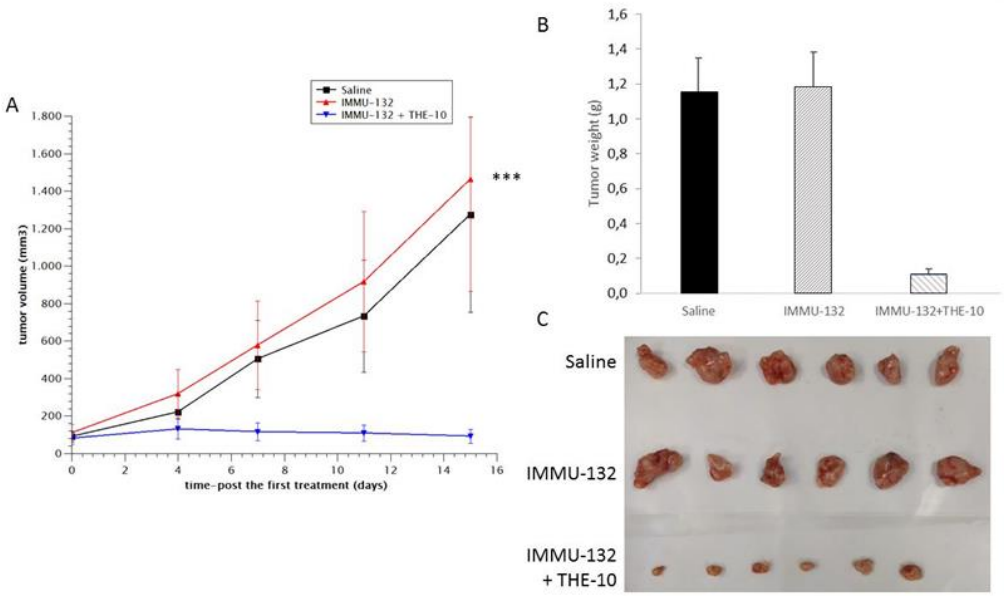

Figure 36. Tumor treatment study involving co-administration of Sacituzumab govitecan (IMMU-132) with THE-10. **A**. Tumor growth curves of IMMU-132 and THE-10 combination therapy in KPC pancreatic cancer model. **B**. Tumor weights and images from animals sacrificed at the end of the experiment. Statistical differences (t-test) are as follows. **p < 0.001: IMMU-132 vs control, IMMU-132 vs IMMU-132 plus THE-10; ***p < 0.0001: IMMU-132 plus THE-10 vs control.

In all *in vivo* experiments described above, no abnormal behaviour or body-weight loss were observed in mice treated with THE-10. This is in agreement with the fact that THE-10 lacks any chemotherapeutic molecules and therefore should not negatively affect the toxicological profile of the co-administered drug. Nevertheless, further detailed studies are needed to obtain the complete toxicological and toxicokinetic profile of THE-10.

TUMOR MODEL	**DRUG TYPE/COMBO** ***Tumor Growth Inhibition (TGI)***	
Colorectal (murine, CT26)	Irinotecan *29.0 %*	Irinotecan + THE-10 *63.0 %*
Pancreatic (murine, KPC)	Gemcitabine *48.8 %*	Gemcitabine + THE-10 *82.2 %*
Pancreatic (murine, KPC)	THE-0504 *9.4 %*	THE-0504 + THE-10 *74.2 %*
Pancreatic (murine, KPC)	THE-0504 *9.4 %*	THE-0504 + iRGD peptide *23.5 %*
Pancreatic (human, MiaPaca2)	THE-0504 *82.5 %*	THE-0504 + THE-10 *98.3 %*
Pancreatic (murine, KPC)	IMMU-132 *0 %*	IMMU-132 + THE-10 *93.0 %*

Table 4. Summary of the combination therapy of several drugs plus THE-10 in tumor-bearing mice models reported as Tumor Growth Inhibition percentage.

4.3 Delivery of small nucleic acids-siRNA

4.3.1 The personalized allele-specific FGFR2-targeting siRNA design strategy is able to selectively knockdown the mutant alleles in Crouzon patients' cells

To develop a personalized siRNA-based strategy targeting mutant FGFR2 allele, our collaborators (group of Policlinico Gemelli in Rome) enrolled a cohort of pediatric patients with Crouzon syndrome (CS) (n=3) carrying 3 different heterozygous gain-of-function (GoF) missense pathogenic variants in the FGFR2 gene (see **Table 5**).

Patient	Sex	Age	Variant NM_000141.5 (*FGFR2*)	Location (GRCh38)	Variant type	Protein change	Molecular consequence	Clinical significance[a]
#1	M	6y	c.983A>G (p.Tyr328Cys)	121517420	Single nucleotide variant	Y328C	Missense	Pathogenic

Table 5. *FGFR2* allelic variants**.** Table shows *FGFR2* allelic variants found in the Crouzon patient "number 1" enrolled in this study. [a]Based on the classification reported in ClinVar DataBase.

Each heterozygous FGFR2 mutation identified in CS patients was used to design siRNA sequences that fully matched the mutant FGFR2 mRNA while containing a single base difference (mismatch) with the wild-type FGFR2 transcripts to obtain allele-specific (AS)-siRNAs. Using internal procedures, our collaborators provided us a specific siRNA derived from patient#1, designed to carry the mismatch C:A at position 11, named si4. This siRNA exhibited the most reproducible allele-specific and inhibitory effect on the

expression of the mutant FGFR2 allele compared with controls treated with vehicle (not shown).

4.3.2 The FGFR2 mutant allele-specific siRNAs are capable of reprogramming Crouzon patients' cells

Functional effects of the siRNA molecule, previously developed for CS patient#1 (si4), have been investigated on FGFR2 signalling cascade. Due to the highest allele-specific inhibitory targeting of si4 and to the limited availability of a large number of primary cultures of mutant human calvarial-derived mesenchymal stromal cells (CMSCs) derived from patients, cells from patient#1 were chosen as the single use case for validation analyses. Firstly, silencing potency on FGFR2 expression was confirmed at protein level by immunoblotting analysis, revealing that allele-specific si4 downregulated total FGFR2 (t-FGFR2) protein levels by more than 2-fold (60%) compared with untreated cells (**Figure 37**). Moreover, these data demonstrated that si4 treatment reduced phospho-FGFR2 (p-FGFR2) levels by 34% compared with cells treated with solely lipofectamine (**Figure 37**).

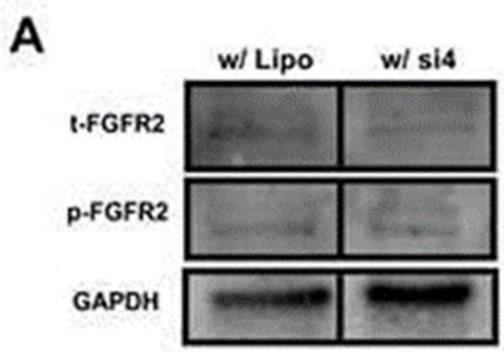

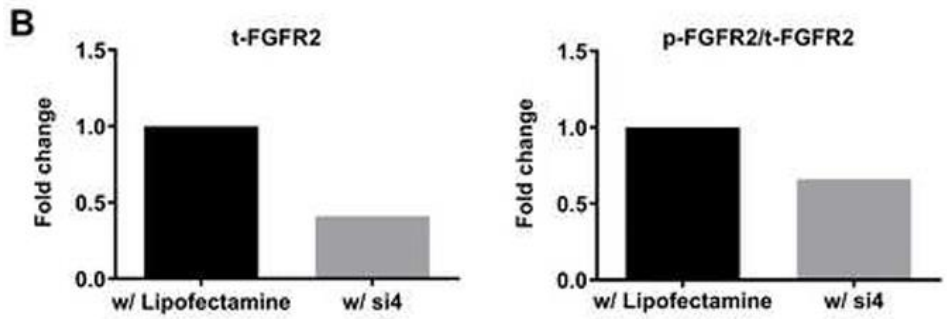

Figure 37. Effects of siRNAs on FGFR2 signalling pathway. **A**. Representative Western blot images of total FGFR2 (t-FGFR2), phospho-FGFR2 (p-FGFR2)/t-FGFR2, in patient#1-derived CMSCs (n=1) treated with selected siRNA (si4) for 48 hours, using Lipofectamine as transfection reagent. **B**. Relative densitometric bar graphs of t-FGFR2, (p-FGFR2)/t-FGFR2, in patient#1-derived CMSCs (n=1) treated with selected siRNA (si4) for 48 hours, using Lipofectamine as transfection reagent. Cells grown with only Lipofectamine were used as controls. t-FGFR2 expression levels were normalized to GAPDH and are represented as a fold changes to untreated control (w/ Lipofectamine). All phosphorylation levels were evaluated by the ratio of phosphoprotein to total protein.

4.3.3 CMSCs express higher levels of CD71 receptor and matrix metallopeptidases -2 and -9 during their osteogenesis

The potential application of ferritin-based nanoparticles as siRNA delivery systems has been investigated in *in vitro* culture of CMSCs to evaluate the capability of the HFt-HIS-PASE carrier to achieve cell-specific targeting. To this purpose, we first analyzed the expression of the ferritin receptor CD71, which mediates the entrance of ferritin within cells (**Figure 38A**). These results revealed a sustained expression of CD71 in CMSCs, showing an increased expression trend during their osteogenic differentiation (**Figure 38A**). In fact,

although CD71 levels remained stable after 5 days of osteogenic induction, its expression was upregulated by 0.6-fold at day 10 of osteogenesis and by 3-fold at day 15 compared with undifferentiated control cells (day 0). Moreover, we have analyzed the expression of the matrix metalloproteases MMP-2 and MMP-9, as the HFt-HIS-PASE constructs include the MP motif for MMP cleavage, inserted between each HFt subunit and the outer PASE polypeptide sequence acting as a shield (Falvo et al., 2018). Despite MMP2 mRNA levels decreased after 5 days of osteogenic induction of CMSCs, a significant increase in MMP2 expression was observed from day 10 to day 15 (**Figure 38B**). In contrast, MMP9 transcript levels remained stable during the initial 5 days of osteogenic differentiation of cells, while its expression was strongly upregulated throughout the subsequent 10-days of osteogenic induction (days 10 and 15). (**Figure 38B**)

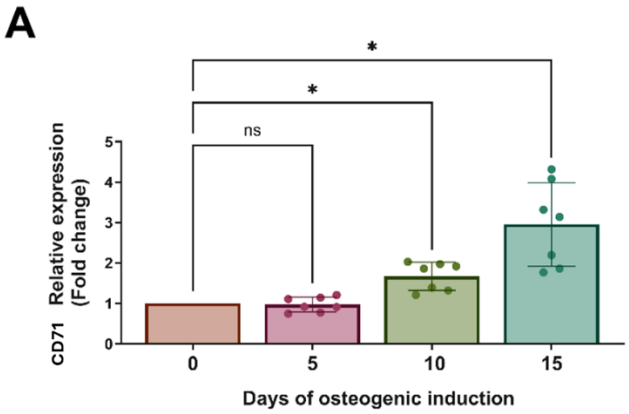

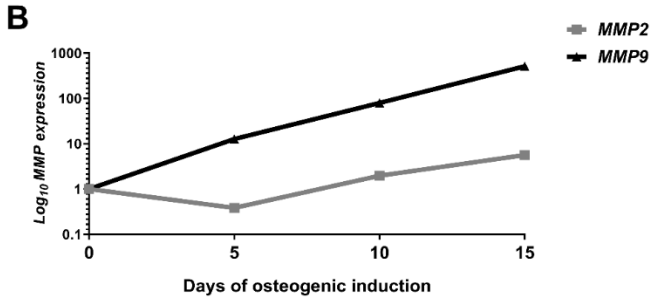

Figure 38. Expression analysis of *CD71* and *MMP2* and *MMP9*. **A**. The histogram shows the expression of ferritin receptor CD71 during different time points of osteogenic differentiation of CMSCs (0-5-10-15 days). Results were normalized to β-actin and are expressed as fold change calculated according to $2^{-\Delta\Delta Ct}$ method. Data are shown as mean (n=7) (graph bars) with SD (error bars). Statistical significance was determined with One-way ANOVA test; *p=0.0341 (0 *versus* 10 days), *p=0.0486 0341 (0 *versus* 15 days); ns. **B**. The graph shows *MMP-2* and *-9* expression levels during osteogenic induction of CMSCs (0-5-10-15 days). Results were normalized to β-actin and are expressed as fold change calculated according to $2^{-\Delta\Delta Ct}$ method. Data are presented as mean (n=7) in Log 10 scale.

4.3.4 The functionalized HFt-HIS-PASE nanoparticles (NPs) efficiently bind selected optimized siRNA

To develop a siRNA delivery system, we designed functionalized nanovectors based on HFt nanovector as a promising therapeutic strategy to target CS patient cells. To this purpose, we have synthesized a modified version of the recombinant HFt, named HFt-HIS-PASE. HFt-HIS-PASE contains a tag of five histidine residues to facilitate endosomal escape (He et al., 2020). HFt-HIS-PASE is shown in **Figure 39A**.

HFt-HIS-PASE was produced as soluble recombinant protein in *E. coli.* Typical yields were 50 mg of final pure protein per liter of bacteria culture.

The purity of all the preparations was confirmed by SDS-PAGE and size-exclusion chromatography (SEC), showing the single protein band as well as the elution profile of the HFt-HIS-PASE sample (**Figure 39C** and **39D**).

To conjugate the siRNA molecules to the HFt-HIS-PASE nanovector, we decided to use a short linker (SPDP; N -Succinimidyl 3-(2- pyridyldithio)-propionate), that can be cleaved in the reducing intracellular environment for payload release.

The characterization of complex HFt-HIS-PASE/si4 by agarose gel electrophoresis demonstrated the successful binding of siRNA on the external surface of the protein (**Figure 39B-C**). The HFt-HIS-PASE/si4 complex migrated differently, as appeared significantly delayed compared with that of naked si4 band when visualized by RNA-specific staining (**Figure 39B**). Additionally, the si4 molecule and HFt-HIS-PASE protein co-migrated as visualized by protein-specific staining (**Figure 39C**), confirming the formation of a siRNA-protein complex. To evaluate the amounts of si4 bound to the ferritin nanoparticles, the intensities of the relative agarose bands corresponding to RNA or protein molecules were quantified using the software Image J (https://imagej.net/ij/). Naked siRNA (NH_2-si4) or HFt-HIS-PASE molecules at a known concentration were used as reference standard. Overall, the procedure yielded a final siRNA: HFt-HIS-PASE molecular ratio of 2:1, that was about 10-fold higher in comparison to the canonical encapsulation approach. Purity and hydrodynamic volume of the complex HFt-HIS-PASE/si4 were determined by SEC (**Figure 39D**). HFt-HIS-PASE/si4 sample was found to have an elution volume and sizes very similar to the naked HFt-HIS-PASE protein (**Figure 39D**). In addition, no free siRNA was observed in the HFt-HIS-PASE/si4 sample, confirming that the siRNA molecules in solution co-eluted with the ferritin protein as a complex.

The absence of siRNA degradation was also assessed after three months for samples stored at 2-8°C. In addition, these samples stored for three months retained their silencing ability for the target gene (see below).

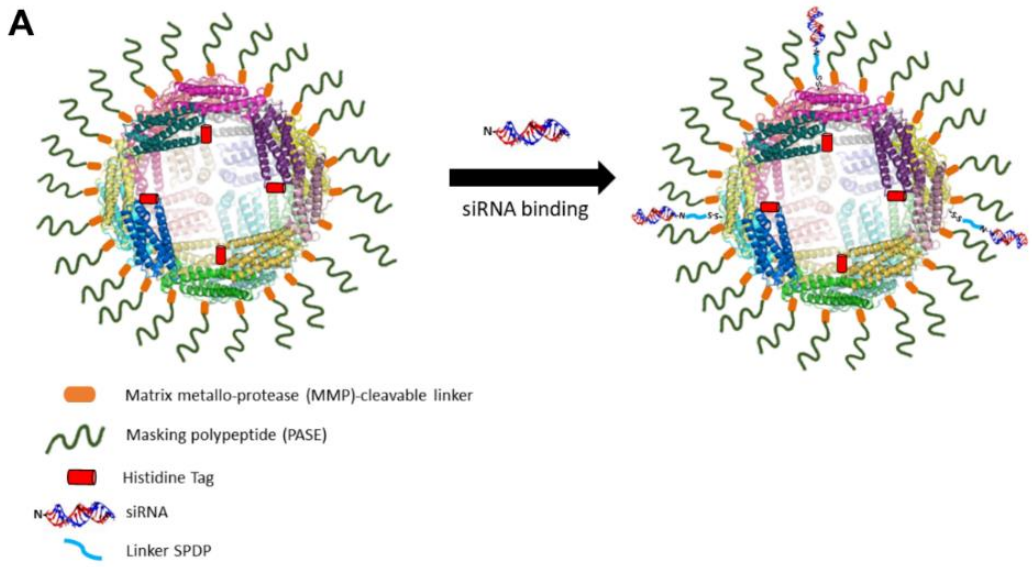

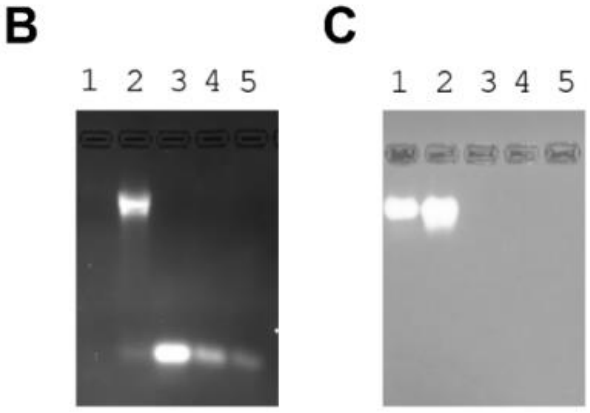

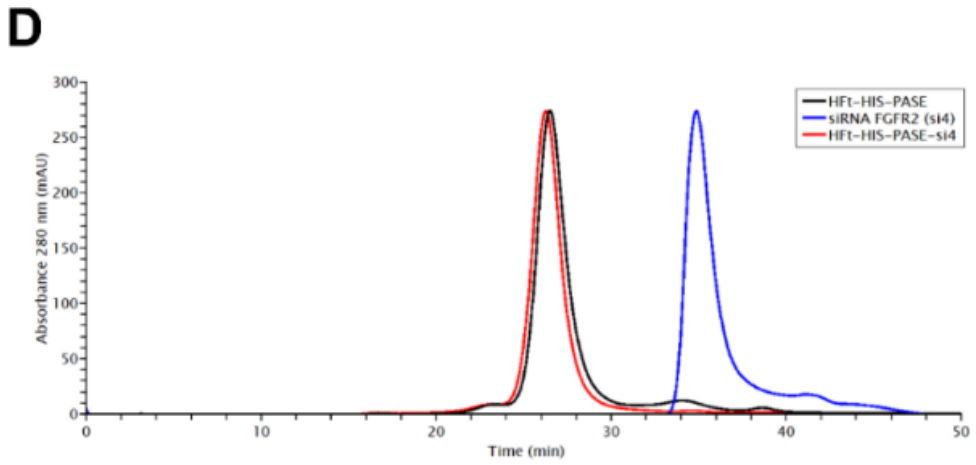

Figure 39. Development of HFt-HIS-PASE/NH_2-siRNA complex. **A.** Schematic representation of HFt-HIS-PASE and siRNA conjugation onto NP surface. Single domains and molecules are described in the legend at the bottom of the figure. To allow the internal surface of the protein to be visualized (lighter colors), only 18 monomers out of the 24 are shown. In addition, for clarity purposes, only 4 out of the 24 histidine tags are shown. The picture has been generated with Pymol and GNU Image Manipulation Programs. **B-D.** Agarose gel electrophoresis band migration profiles. Gel was double stained with Nuclei acid SYBR Gold staining for siRNAs visualization (**B**), and with Coomassie staining for ferritin protein visualization (**C**). Lane 1: HFt-HIS-PASE; Lane 2: HFt-HIS-PASE/si4 complex; Lane 3: si4 standard 2 µM; Lane 4: si4 standard 1 µM; Lane 5: si4 standard 0.5 µM. **D**. Size Exclusion Chromatography (SEC) analysis. SEC profiles of HFt-HIS-PASE (in black), HFt-HIS-PASE/si4 complex (in red) and si4 alone (in blue).

4.3.5 HFt-HIS-PASE nanoparticles are internalized by CMSCs and escape endosomal/lysosomal entrapment

To assess the uptake of HFt-HIS-PASE constructs in our cellular model, we analyzed and measured the internalization and intracellular trafficking of fluorescently labeled HFt-HIS-PASE (named HFt B) in CMSC cultures for 6

days, using the wild-type ferritin-based construct (named HFt A) as control. As shown in **Figure 40**, both HFt constructs were efficiently internalized in CMSCs, with HFt B exhibiting a two-fold increase in cellular uptake amount compared with HFt A after 15 minutes of incubation (**Figure 40B**). We observed a progressive increase in the internalization of HFt A throughout the initial 3-days of incubation (**Figure 40A-B**). Conversely, HFt B internationalization kinetics was much faster: it took as little as 15 minutes for HFt B to reach the same levels that HFt A reached after 24 hours (**Figure 40A-B**). After 3 days of incubation, both constructs exhibited comparable kinetics, indicating the attainment of a plateau phase in cellular uptake (**Figure 40A-B**). In addition, by analyzing the intracellular trafficking we noticed that both constructs were widely distributed within the CMSC cytoplasm. On this regard, HFt A showed partial co-localization within lysosomal compartments after 24 hours of incubation (**Figure 40C**), whereas HFt B fluorescence was not detectable in lysosomes (**Figure 40C**). Additionally, neither HFt A nor HFt B NPs were found to be distributed in the nucleus (data not shown). Overall, our data revealed that the engineered HFt B construct could be a more suitable siRNA delivery strategy, being able to enter CMSCs more rapidly than HFt A, without becoming entrapped in endo-lysosomal compartments once inside cell cytoplasm.

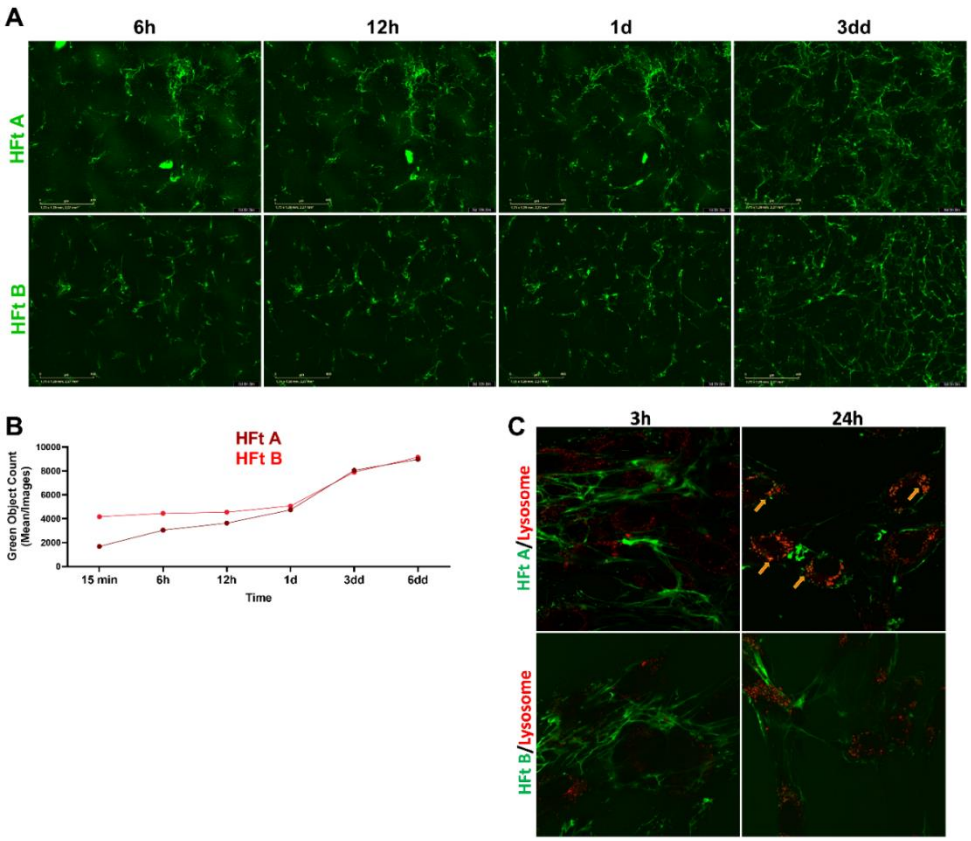

Figure 40. Analysis of cellular uptake and trafficking of HFt A and HFt B**. A.** Representative images of CMSCs treated with 1 mg/ml of fluorescently-labeled wild-type ferritin-based nanoparticles (named HFt A) and functionalized HFt-HIS-PASE for endosomal escape (named HFt B) for 6 days by Incucyte-Live cell analysis system (10X). **B.** The graph shows the quantification of green fluorescent signals detected in CMSCs treated with fluorescently-labeled HFt A and HFt B during different time points (15min, 6h, 12h, 1d, 3 dd and 6 dd). Each condition was conducted in triplicate (n=3 biological replicates) and 9 image/well has been analyzed. Data are shown as mean of green fluorescent objects detected inside cells for each condition. **C.** Representative confocal microscopy images showing the biodistribution of HFt A and HFt B in CMSCs after 3 and 24 hours of incubation (100X). Lysosomes were stained in red using Lysotracker Deep Red.

4.3.6 HFt-HIS-PASE exerts high proficiency to deliver and release NH_2-siRNA complexes in Crouzon patient cells

The sequence of siRNA previously selected for patient#1 (si4) has been optimized by design to include LNA bases to improve its stability and functionality. In addition, a chemical modification with an amine group was introduced at the 3' end of siRNA guide strand to allow the conjugation of si4 (NH_2-si4) on the cysteine residues present on the HFt-HIS-PASE surface. The ability of this naked modified siRNA (NH_2-si4) to stably silence the *FGFR2* mutant allele was confirmed in *in vitro* culture of patient#1 derived cells.

The final HFt-HIS-PASE/si4 complex was tested in patient#1 derived cells to assess the intracellular delivery and gene knockdown efficiency (**Figure 41**). Gene expression analysis demonstrated that the treatment with HFt-HIS-PASE/si4 was able to specifically knockdown the mutant *FGFR2* allele in patient#1 CMSC, compared to naked NPs. Specifically, upon released from the NPs into the cell cytoplasm, NH_2-si4 selectively downregulated mutant *FGFR2* allele levels by up to 65%, while the expression of the wild-type allele remained unchanged (**Figure 41**). By comparing the silencing effects of si4, we observed that the NH_2-si4 delivered by NPs had a higher allele-specific inhibitory proficiency compared to unmodified si4 delivered by a commercial transfection reagent (Lipofectamine) (see results above).

These findings highlighted the capability of HFt-HIS-PASE NPs to efficiently deliver and release therapeutic siRNAs within cell cytoplasm, enhancing their biological effects (**Figure 41**).

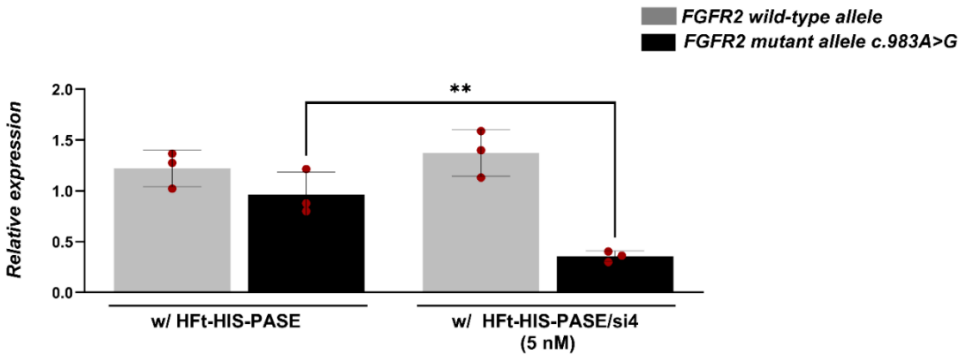

Figure 41. HFt-HIS-PASE/si4 investigation**.** The graph shows mutant (c.983A>G) and wild-type *FGFR2* expression levels in CMSCs derived from CS patient#1 treated with 5 nM of chemically modified siRNA 4 (NH_2-si4) delivered by HFt-HIS-PASE nanocarrier for 48h. Cells treated with naked HFt-HIS-PASE were used as controls. Results were normalized to β-actin and are expressed as fold change calculated according to $2^{-\Delta\Delta Ct}$ method. Data are presented as mean (n=3 biological replicates) with SD. Data were analyzed using GraphPad Prism, employing an unpaired t-test for statistical evaluation (** $p<0.0096$).

4.4 Delivery of Antisense Oligonucleotides (ASOs)

4.4.1 Identification of lncMB3-dependent transcriptome in a G3 MB cell line

To gain an understanding of the molecular networks through which lncMB3 operates in MB, our collaborators (Pietro Laneve's group at IBPM C.N.R. in Rome) initiated the identification of its target genes. This was achieved by the analysis of the transcriptome alteration following lncMB3 knockdown (KD) in the MYC-amplified D283 Med cell line, where the lncRNA was originally identified (Rea et al., 2021). According to GTex (https://gtexportal.org/home/) lncMB3 appears to be poorly expressed in healthy tissues.

LncMB3 loss-of-function was obtained with a reduction of approximately 70% 72 hours after multi-pulse transfections of an antisense Locked Nucleic Acid (LNA) oligonucleotide (Kurreck, 2002), GapmeR#1), designed to facilitate RNA silencing from the nucleus, where the lncRNA is 60% accumulated (Rea et al., 2021).

Our collaborators collected 3 independent replicates of RNA extracts which underwent polyA+ sequencing, on a Novaseq 6000 sequencing system (Illumina), with a depth of more than 20 M reads.

4.4.2 LncMB3 controls the TGF-β pathway in G3 MB

Attention was drawn to genes belonging to the TGF-β pathway. Aberrant TGF-β signalling results in the development of various diseases, including cancer (Baba et al., 2022). Its deregulation at the genetic level is supposed to be a driver event in G3 MB, influencing cell proliferation, differentiation, and survival (Morabito et al., 2019).

To better capture the alteration of the pathway, they completed the list of genes in the TGF-β cluster by including additional hits 1) known to be relevant to the cascade by literature and 2) found to be deregulated following lncMB3 KD according to the RNA-Seq analysis. A subset of 9 genes were identified whose protein products participate at various levels in the biochemical network, such as TGF-β/Activin signalling ligands (INHBE, Weiss & Attisano, 2013; THBS1, THBS3, Vanhoutte et al., 2024), receptors (ACVR1B, Schmierer & Hill, 2007; BAMBI, Onichtchouk et al., 1999), effectors (SMAD 3, 6 and 7, Schmierer & Hill, 2007) and downstream regulators (TFDP1, Chen et al., 2002). Interestingly, among them INHBE also emerged as the most significantly deregulated gene (padj < 0.001, -2 < LOGFC > 2, expressed > 50 CPM) according to the candidate selection driven by quantitative parameters. The gene cluster expression was analysed by qRT-PCR in D283 Med cells 72 hours after treatment with lncMB3-GapmeR, compared to scramble-treated cells. Our collaborators observed a substantial repression of genes with a positive function in the pathway, with a percentage of deregulation ranging from -20 to -80%. Consistently, two inhibitory components of the pathway were upregulated in the same conditions (**Figure 42**).

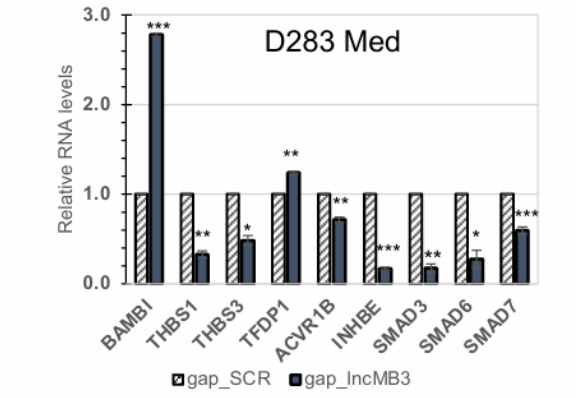

Figure 42. qRT-PCR validation analysis of TGF-β pathway genes in D283 Med cells treated for 72 hours with gap_SCR or gap_lncMB3 (GapmeR #1). Expression levels were compared to gap_SCR sample as control, set as 1. Data (means ± SEM) are expressed in arbitrary units and are relative to GAPDH mRNA levels. N = 3, * $p \leq 0.05$, ** $p \leq 0.01$ (two- tailed Student's t-test).

4.4.3 Production of HFt-HIS-PASE and its internalization in specific cells

LncMB3 targeting impacts on the TGF-β pathway, a crucial driver of G3 MB, leading to enhanced apoptosis in cancer cell lines. Furthermore, the modulation of the lncRNA affects chemotherapeutic treatments *in vitro* and potentiates this outcome. On these bases, we explored the potential use of lncMB3-directed GapmeRs to formulate innovative RNA/protein complexes based on HFt nanoparticles for selective cell delivery. To this scope, we have exploited the same ferritin construct HFt-HIS-PASE reported above for the siRNA delivery in Crouzon disease.

A preliminary assessment of *MMP 2, MMP 9*, and *CD71* mRNA expression in D283 Med cells was performed by qRT-PCR (**Figure 43**).

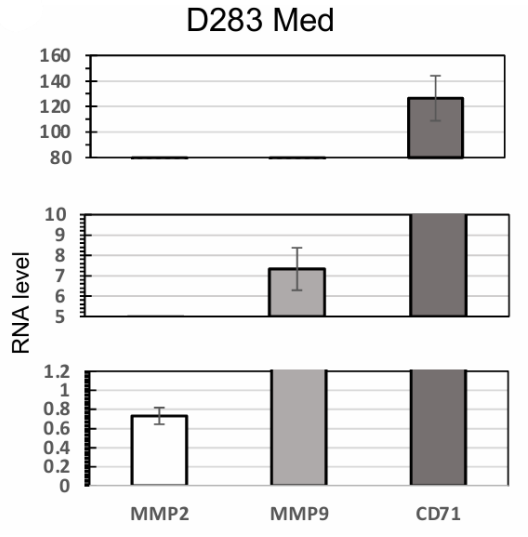

Figure 43. Levels of MMP 2, MMP 9 and CD71 in D283 cells.

Based on expression levels, D283 Med cells were selected for next experiments. We evaluated the ability of a fluorescent-labelled HFt-HIS-PASE nanovector (HFt-HIS-PASE-fluo) to recognise G3 MB cells. D283 Med cells were maintained for 48 hours with HFt-HIS-PASE-fluo at 200 nM. Twelve hours after administration, the number of green, HFt-HIS-PASE-fluo(+) cells was quantified relative to the total cell count (**Figure 44**).

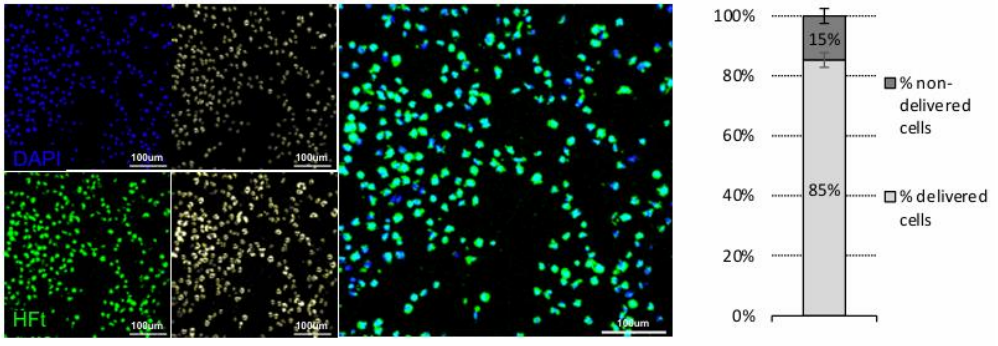

Figure 44. Production, analysis and application of HFt-HIS-PASE/GapmeR complexes. A. Left panel: representative image of colocalization analysis between fluorescein-HFt-HIS-PASE and DAPI in D283 Med cells, 12 hours after administration (magnification 20x). Fluorescein-HFt-HIS PASE (green) and DAPI (blue, nuclear staining) staining are on the left, object counts are in the middle and the merge of the two channels is on the right. Right panel: percentage of colocalization between fluorescein-HFt-HIS-PASE and DAPI in D283 Med cells. Data (mean + SEM) were obtained from 8 different fields.

D283 Med cells were targeted with a percentage of approximately 85%, confirming their affinity for HFt-HIS-PASE. Immunofluorescence was performed on the same samples 24 hours after HFt-HIS-PASE-fluo administration upon nuclear and cytoplasmic staining and analysed through confocal laser scanning microscopy. This analysis revealed the intracellular uptake of exogenous labelled ferritin (**Figure 45**, left panel) and nuclear-cytoplasmic distribution was evaluated and reported in **figure 45**, right panel.

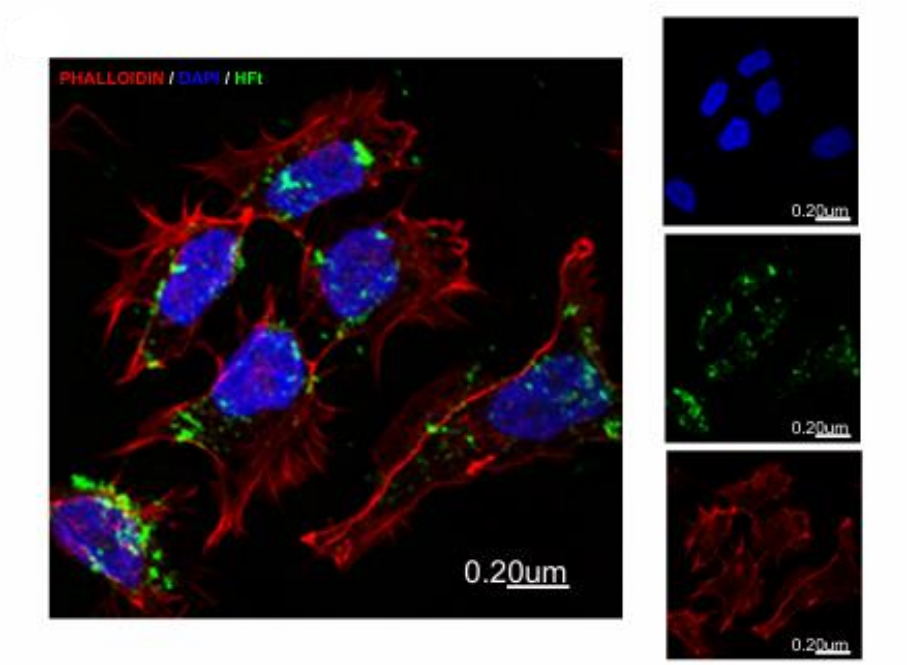

Figure 45. Representative immunofluorescence of fluorescein-HFt-HIS-PASE delivered for 24h (green), DAPI (blue, nucleus) a phalloidin (red, cytoplasm). Magnification 60x.

4.4.4 Targeting lncMB3 by HFt-GapmeR complexes

The generation and characterisation of a HFt-HIS-PASE-GapmeR complex was then undertaken. The lncMB3 GapmeR #1 was encapsulated within the internal cavity of the HFt-HIS-PASE using reversible, pH-dependent cage dissociation (acid pH) and re-association (neutral pH) in the presence of the bioactive payload (Falvo et al., 2021) (**Figure 46**).

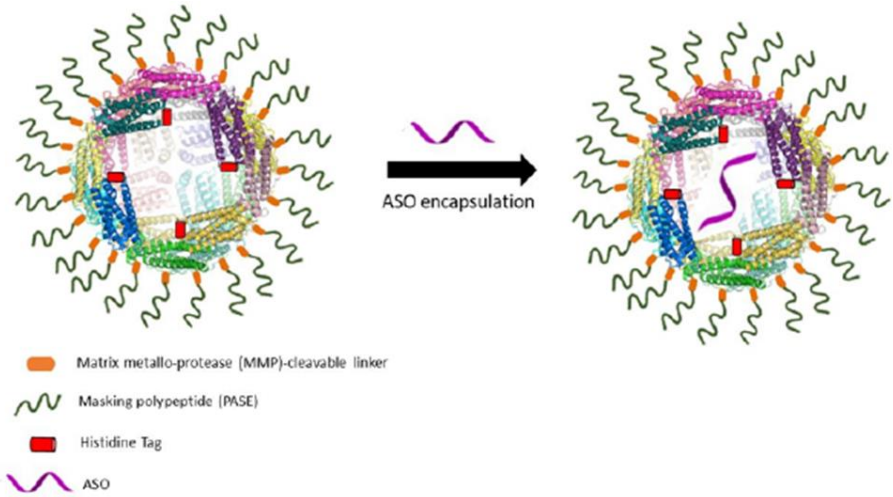

Figure 46. Schematic representation of ASO encapsulation in HFt-HIS-PASE NP. Single domains and molecules are described in the legend at the bottom of the figure. To allow the internal surface of the protein to be visualized (lighter colors), only 18 monomers out of the 24 are shown. In addition, for clarity purposes, only 4 out of the 24 histidine tags are shown. The picture has been generated with Pymol and GNU Image Manipulation Programs.

To demonstrate the successful loading of the GapmeR into the multiprotein cavity, the purified HFt-HIS-PASE-GapmeR complex was characterised by electrophoresis on 1.8% agarose gel. **Figure 47** reveals that the bands corresponding to the HFt-HIS-PASE-GapmeR complex or to the GapmeR alone migrated differently.

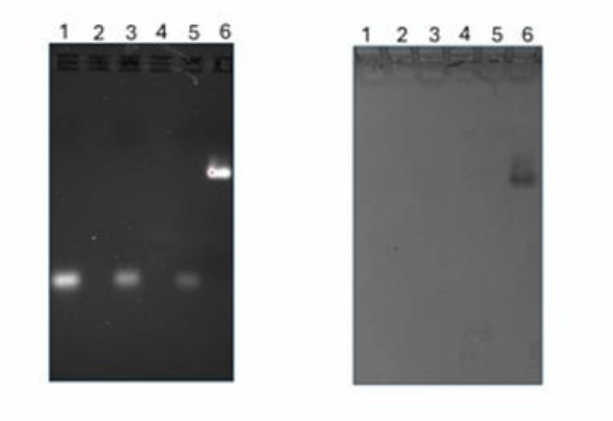

Figure 47. Band migration profiles on agarose gel electrophoresis. Gel was double stained with SYBR Gold for GapmeR visualization (left panel) and Coomassie Blue for ferritin visualization (right panel). *Lane 1*: GapmeR standard 2 µM; *Lane 3*: GapmeR standard 1 µM; *Lane 5*: GapmeR standard 0.5 µM; *Lane 6*: HFt-HIS-PASE-GapmeR complex.

Upon visualisation by DNA-specific staining (**Figure 47**, left panel), the nucleic acid appeared significantly delayed when associated with HFt-HIS-PASE, compared to the naked GapmeR. Furthermore, the HFt-HIS-PASE-GapmeR complex co-migrated with ferritin, since their respective bands match when visualised by protein-specific staining (**Figure 47**, right panel). Concerning complex stability, no evidence of nucleic acid degradation was observed after 1-hour and overnight incubation of HFt-HIS-PASE-GapmeR with Denarase at 37°C (**Figure 48**)**,** indicating that GapmeR molecules were encapsulated and protected from external injuries.

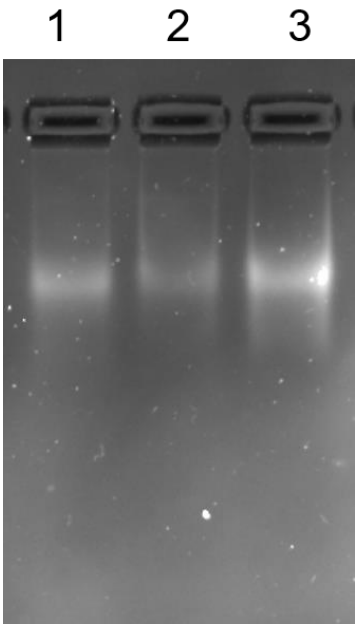

Figure 48. HFt-HIS-PASE-GapmeR complex stability in the presence of DNA/RNA nuclease (Denarase). HFt-HIS-PASE-GapmeR complex before and after Denarase treatment at 37°C visualized as band migration profiles on agarose gel electrophoresis. Lane 1: HFt-HIS-PASE-GapmeR complex; Lane 2: HFt-HIS-PASE-GapmeR complex after overnight incubation with Denarase; Lane 3: HFt-HIS-PASE-GapmeR complex after one hour incubation with Denarase. Gel was stained with SYBR Gold.

Moreover, no degradation was observed either after 3 months-storage of samples at 4°C, confirming that GapmeR is indeed encapsulated in the protein cavity and not merely bound to the protein external surface.

The encapsulation procedure yielded a final GapmeR:HFt-HIS-PASE molecular ratio of 0.5:1, as established applying the Image J software (https://imagej.net/ij/) to evaluate the amount of GapmeR bound to HFt nanoparticles. Purity and hydrodynamic volume of the complex HFt-HIS-

PASE-GapmeR were determined by size-exclusion chromatography. The HFt-HIS-PASE-GapmeR sample showed an elution volume and size very similar to the non-encapsulated HFt-HIS-PASE protein (**Figure 49**).

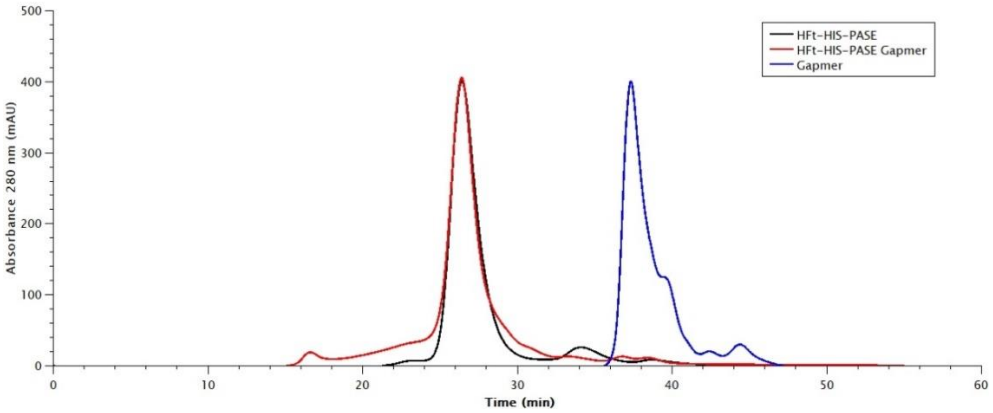

Figure 49. Size Exclusion Chromatography profile analysis of HFt-HIS-PASE (in black), HFt-HIS-PASE-GapmeR #1 complex (in red) and GapmeR #1 alone (in blue).

In addition, no free GapmeR was observed in the HFt-HIS-PASE-GapmeR sample, confirming that the GapmeR molecules in solution co-elute with ferritin.

To assess the biological activity of the complex, D283 Med cells were treated with a single dose of HFt-HIS-PASE nanocarrier alone or HFt-HIS-PASE-GapmeR complex at a concentration of 200 nM nanocarrier for each condition, and the expression of lncMB3 was assessed 48 hours after administration. A reduction of lncMB3 steady-state levels by approximately 35% was observed upon delivery of the encapsulated GapmeR #1, compared to mock-treated cells (**Figure 50**).

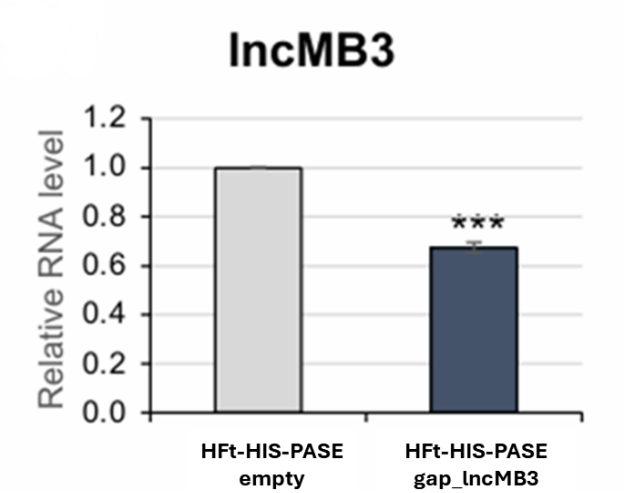

Figure 50. qRT-PCR analysis of lncMB3 RNA levels in D283 Med cells upon treatment with HFt-HIS-PASE-GapmeR #1 complexes, 48h after delivery, compared with empty HFt-HIS-PASE, set as 1. Data (means ± SEM) are expressed in arbitrary units and are relative to GAPDH mRNA levels. N = 3, *** $p \leq 0.001$ (two- tailed Student's t-test).

Similar results were observed when samples of HFt-HIS-PASE-GapmeR stored at 4°C for 3 months were retested.

The outcome of this setup simulates the effect of a standard single-pulse transfection of GapmeR #1 at 100 nM for 48 hours. Interestingly, in both conditions we did not appreciate any modulation of TGF-β pathway genes, or any decrease of cell proliferation or increase of apoptosis (data not shown), possibly due to insufficient downregulation of lncMB3 expression.

5. CONCLUSIONS

5.1 The-0504 therapeutic efficacy *in vitro* and *in vivo*

In this PhD thesis, we have rigorously evaluated the potential of a ferritin-based platform for drug delivery. Our primary focus was on the innovative HFt-based construct, The-0504 (Falvo et al., 2020; Falvo et al., 2021; Fracasso et al., 2023). This nanoformulation effectively encapsulates the anticancer drug Genz-644282, significantly enhancing its cytotoxic properties.

The therapeutic benefits in *in vivo* studies on mice are evident through both quantitative and qualitative improvements. Quantitatively, The-0504 induces DNA damage that is 1.5 times more effective than that achieved with free Genz-644282. Qualitatively, the nanoparticle formulation facilitates superior nuclear delivery, creating a positive feedback loop that sustains DNA damage over time. Additionally, the encapsulation of the drug prolongs its half-life in circulation and offers vital protection, leading to blood concentrations that are 400 times higher than those of the free drug in vivo.

These advantageous characteristics have allowed us to adjust the administration of The-0504 to weekly intervals without compromising the kinetics of tumor volume reduction or diminishing overall antitumor efficacy. Notably, The-0504 has shown remarkable results across a variety of tumor xenografts, achieving up to 100% objective responses in diverse histotypes, including epithelial, mesenchymal, and neuroendocrine origins. It has demonstrated effectiveness against aggressive and hard-to-treat molecular subtypes, such as triple-negative breast cancer xenografts.

These compelling results lay the groundwork for first-in-human trials, positioning The-0504 as a targeted, potentially low-toxicity chemotherapy option that could be effective across a wide range of malignancies.

5.2 Delivery of BioActive Peptides (BAPs)

The second aim of this thesis is to develop a new engineered HFt construct for the delivery of bioactive peptides (BAPs). We focused our attention on peptides that conduct a particular biological function. We developed a novel compound acting as a therapeutic booster for co-administered drugs in solid tumors. This nanoformulation, named THE-10, incorporates two BAPs at the N-terminus region of the human H-type ferritin (HFt). Specifically, the selected BAPs are two modified linear versions of previously described peptides: (a) iRGD, that binds integrin αVβ3/αVβ5 and NRP-1, and (b) PD L1Pep-1, that binds PD-L1. We produced this NP at high yields in *E. coli,* and we tested its binding to specific receptors. The presence of the two BAPs confers to THE-10 outstanding booster properties providing an immune checkpoint inhibitors-like effect and enhancing the anticancer effects (*in vitro* and/or animal models) of two ADCs (T-DXd and IMMU-132), one nanovector in the same therapeutic class (THE-0504), and two small molecules (gemcitabine and irinotecan), possibly with a preferential effect on large macromolecules. THE-10 hits some of the limits linked to naked BAPs. In fact, this NP could extend half-life in the bloodstream and conditional delivery into the TME (MMP cleavage) of BAPs. We demonstrated that THE-10 is able expand therapeutic indications of co-administered drugs and to improve the efficacy of drugs in their approved indication and/or lower dosages and side effects. In addition, THE-10 helps in drug repositioning, by expanding

indications to resistant tumor histotypes and/or settings, e.g. low expression of the tumor target. Interestingly, THE-10 applies several principles of precision oncology and target therapy, but it impacts on target therapy, chemotherapy and immunotherapy altogether. Additional preclinical studies are needed to evaluate the applicative spectrum of THE-10 and its possible limitations.

5.3 Delivery of small nucleic acids (siRNA and ASOs)

For the final objective of this PhD thesis, we aimed to harness the advantageous properties of engineered HFt for the transport of nucleic acids (NAs), which are essential for NA interference (NAi). The delivery of small molecules like siRNAs and ASOs faces several challenges, including rapid enzymatic degradation, poor pharmacokinetics, negative electrostatic charge hindering intracellular uptake, and high toxicity. To address these issues, we developed a functionalized nanovector, HFt-HIS-PASE, specifically designed for delivering selected siRNAs and ASOs. This construct includes a tag of five histidine residues to facilitate endosomal escape.

We produced this nanoparticle in high yields using *E. coli* and then functionalized it with nucleic acids. Notably, we collaborated with researchers from Policlinico Gemelli in Rome, who provided us a modified siRNA (si4, in the form of LNA) related to Crouzon syndrome. We conjugated the LNA-functionalized si4 to the external surface of HFt-HIS-PASE using an SPDP linker. The LNA enhances compatibility with the siRNA machinery and improves stability, while the SPDP linker is designed to dissociate the siRNA payload in the reducing intracellular environment, facilitating release. This resulted in a molecular ratio of siRNA to HFt-HIS-PASE of 2:1. Validation of

the therapeutic effects of the HFt-HIS-PASE-siRNA complex demonstrated its high efficiency in delivering and releasing siRNA to target cells, successfully modulating FGFR2 signaling and correcting the aberrant osteogenic commitment in FGFR2-mutated cells.

In collaboration with Pietro Laneve's group at IBPM C.N.R. in Rome, we also investigated the delivery of ASOs involved in Medulloblastoma pathology. Utilizing a pH disassembly/reassembly procedure, we encapsulated lncMB3 GapmeR #1 within the internal cavity of HFt-HIS-PASE, achieving a final molecular ratio of 0.5:1. When tested on D283 Med cells, the biological activity of this complex resulted in approximately a 35% reduction in lncMB3 steady-state levels compared to mock-treated cells after 48 hours of *in vitro* administration.

This research provides the first *in vitro* evidence for a non-invasive therapeutic approach for both Crouzon syndrome and Medulloblastoma. Moving forward, optimization of these NA delivery systems will be necessary to enhance yield and intracellular delivery, alongside further *in vitro* and *in vivo* studies. Once validated *in vivo*, the HFt-mediated NA delivery strategy could be swiftly translated into clinical applications. Given its inherent versatility, this delivery system holds promise for treating a range of conditions linked to gene-related diseases, including rare genetic syndromes, neurological disorders, and cancer therapies.

6. REFERENCES

1) Aggarwal BB, Vijayalekshmi RV, Sung B. Targeting inflammatory pathways for prevention and therapy of cancer: short-term friend, long-term foe. Clin Cancer Res. 2009 Jan 15;15(2):425-30. doi: 10.1158/1078-0432.CCR-08-0149.

2) Ahmed F, Raghava GP. Designing of highly effective complementary and mismatch siRNAs for silencing a gene. PLoS One. 2011;6(8):e23443. doi: 10.1371/journal.pone.0023443.

3) Alexis F, Pridgen EM, Langer R, Farokhzad OC. Nanoparticle technologies for cancer therapy. Handb Exp Pharmacol. 2010;(197):55-86. doi: 10.1007/978-3-642-00477-3_2.

4) Allen TM. Ligand-targeted therapeutics in anticancer therapy. Nat Rev Cancer. 2002 Oct;2(10):750-63. doi: 10.1038/nrc903.

5) Alshawwa SZ, Kassem AA, Farid RM, Mostafa SK, Labib GS. Nanocarrier Drug Delivery Systems: Characterization, Limitations, Future Perspectives and Implementation of Artificial Intelligence.Pharmaceutics.2022Apr18;14(4):883. doi:10.3390/pharmaceutics14040883.

6) Alshawwa SZ, Kassem AA, Farid RM, Mostafa SK, Labib GS. Nanocarrier Drug Delivery Systems: Characterization, Limitations, Future Perspectives and Implementation of Artificial Intelligence. Pharmaceutics. 2022 Apr 18;14(4):883. doi: 10.3390/pharmaceutics14040883.

7) Aman J, Margadant C. Integrin-Dependent Cell-Matrix Adhesion in Endothelial Health and Disease. Circ Res. 2023 Feb 3;132(3):355-378. doi: 10.1161/CIRCRESAHA.122.322332.

8) Arafat M, Sakkal M, Beiram R, AbuRuz S. Nanomedicines: Emerging Platforms in Smart Chemotherapy Treatment-A Recent Review. Pharmaceuticals(Basel).2024Feb28;17(3):315. doi:10.3390/ph17030315

9) Arap W, Pasqualini R, Ruoslahti E. Cancer treatment by targeted drug delivery to tumor vasculature in a mouse model. Science. 1998 Jan 16;279(5349):377-80.

10) Aubin-Tam ME. Conjugation of nanoparticles to proteins. Methods Mol Biol. 2013;1025:19-27. doi: 10.1007/978-1-62703-462-3_3.

11) Baba AB, Rah B, Bhat GR, Mushtaq I, Parveen S, Hassan R, Hameed Zargar M, Afroze D. Transforming Growth Factor-Beta (TGF-β) Signaling in Cancer-A Betrayal Within. Front Pharmacol. 2022 Feb 28;13:791272. doi: 10.3389/fphar.2022.791272

12) Baban DF, Seymour LW. Control of tumour vascular permeability. Adv Drug Deliv Rev. 1998 Oct 5. Doi: 10.1016/s0169-409x(98)00003-9.

13) Baban DF, Seymour LW. Control of tumour vascular permeability. Adv Drug Deliv Rev. 1998 Oct 5;34(1):109-119. doi: 10.1016/s0169-409x(98)00003-9.

14) Bahşi A, Tekin AM, Bahşi I. The Most Frequently Cited References in the Articles Published in the Journal of Craniofacial

Surgery Between 1995 and 2020. J Craniofac Surg. 2022 Jan-Feb 01;33(1):251-253. doi: 10.1097/SCS.0000000000008025.

15) Bao G, Mitragotri S, Tong S. Multifunctional nanoparticles for drug delivery and molecular imaging. Annu Rev Biomed Eng. 2013;15:253-82. doi: 10.1146/annurev-bioeng-071812-152409.

16) Barba M, Di Pietro L, Massimi L, Geloso MC, Frassanito P, Caldarelli M, Michetti F, Della Longa S, Romitti PA, Di Rocco C, Arcovito A, Parolini O, Tamburrini G, Bernardini C, Boyadjiev SA, Lattanzi W. Corrigendum to "BBS9 gene in nonsyndromic craniosynostosis: Role of the primary cilium in the aberrant ossification of the suture osteogenic niche" [Bone 112 (July 2018) 58-70]. Bone. 2019 Apr;121:293. doi: 10.1016/j.bone.2019.02.004. Epub 2019 Feb 15. Erratum for: Bone. 2018 Jul;112:58-70. doi: 10.1016/j.bone.2018.04.013.

17) Baronzio G, Schwartz L, Kiselevsky M, Guais A, Sanders E, Milanesi G, Baronzio M, Freitas I. Tumor interstitial fluid as modulator of cancer inflammation, thrombosis, immunity and angiogenesis. Anticancer Res. 2012 Feb;32(2):405-14.

18) Batista-Duharte, A., Sendra, L., Herrero, M. J., Téllez-Martínez, D., Carlos, I. Z., and Aliño, S. F. (2020). Progress in the use of antisense oligonucleotides for vaccine improvement. Biomolecules 10 (2), 316. doi:10.3390/biom10020316

19) Bedi D, Gillespie JW, Petrenko VA Jr, Ebner A, Leitner M, Hinterdorfer P, Petrenko VA. Targeted delivery of siRNA into breast cancer cells via phage fusion proteins. Mol Pharm. 2013 Feb 4;10(2):551-9. doi: 10.1021/mp3006006.

20) Bellini M, Mazzucchelli S, Galbiati E, Sommaruga S, Fiandra L, Truffi M, Rizzuto MA, Colombo M, Tortora P, Corsi F, Prosperi D. Protein nanocages for self-triggered nuclear delivery of DNA-targeted chemotherapeutics in Cancer Cells. J Control Release. 2014 Dec 28;196:184-96. doi: 10.1016/j.jconrel.2014.10.002.

21) Bellini M, Mazzucchelli S, Galbiati E, Sommaruga S, Fiandra L, Truffi M, Rizzuto MA, Colombo M, Tortora P, Corsi F, Prosperi D. Protein nanocages for self-triggered nuclear delivery of DNA-targeted chemotherapeutics in Cancer Cells. J Control Release. 2014 Dec 28;196:184-96. doi: 10.1016/j.jconrel.2014.10.002.

22) Bennett MJ, Lebrón JA, Bjorkman PJ. Crystal structure of the hereditary haemochromatosis protein HFE complexed with transferrin receptor. Nature. 2000 Jan 6;403(6765):46-53. doi: 10.1038/47417.

23) Bhavyata (Pandya) Shesh, James R. Connor, A novel view of ferritin in cancer, Biochimica et Biophysica Acta (BBA) - Reviews on Cancer, Volume 1878, Issue 4, 2023, 188917. Doi: https://doi.org/10.1016/j.bbcan.2023.188917.ù

24) Birrer MJ, Moore KN, Betella I, Bates RC. Antibody-Drug Conjugate-Based Therapeutics: State of the Science. J Natl Cancer Inst. 2019 Jun 1;111(6):538-549. doi: 10.1093/jnci/djz035.

25) Bok S, Yallowitz AR, Sun J, McCormick J, Cung M, Hu L, Lalani S, Li Z, Sosa BR, Baumgartner T, Byrne P, Zhang T, Morse KW, Mohamed FF, Ge C, Franceschi RT, Cowling RT, Greenberg BH, Pisapia DJ, Imahiyerobo TA, Lakhani S, Ross ME, Hoffman CE,

Debnath S, Greenblatt MB. A multi-stem cell basis for craniosynostosis and calvarial mineralization. Nature. 2023 Sep;621(7980):804-812. doi: 10.1038/s41586-023-06526-2.

26) Calcabrini A, Meschini S, Stringaro A, Cianfriglia M, Arancia G, Molinari A. Detection of P-glycoprotein in the nuclear envelope of multidrug resistant cells. Histochem J. 2000 Oct;32(10):599-606. doi: 10.1023/a:1026732405381.

27) Cardillo TM, Govindan SV, Sharkey RM, Trisal P, Arrojo R, Liu D, Rossi EA, Chang CH, Goldenberg DM. Sacituzumab Govitecan (IMMU-132), an Anti-Trop-2/SN-38 Antibody-Drug Conjugate: Characterization and Efficacy in Pancreatic, Gastric, and Other Cancers. Bioconjug Chem. 2015 May 20;26(5):919-31. doi: 10.1021/acs.bioconjchem.5b00223.

28) Carter PJ, Lazar GA. Next generation antibody drugs: pursuit of the 'high-hanging fruit'. Nat Rev Drug Discov. 2018 Mar;17(3):197-223. doi: 10.1038/nrd.2017.227.

29) Ceci P, Morea V, Fornara M, Bellapadrona, G, Falvo E, and Ilari A. Biomimetic materials synthesis by ferritin-related, cage-shaped proteins. Adv. Topics in Biomineralization, 2012: Jong Seto (Ed.), doi: 10.5772/31309

30) Chang X, Lv C, Zhao G. A Dual Function of Ferritin (Animal and Plant): Its Holo Form for Iron Supplementation and Apo Form for Delivery Systems. Annu Rev Food Sci Technol. 2023 Mar 27;14:113-133. doi: 10.1146/annurev-food-060721-024902

31) Chehelgerdi M, Chehelgerdi M, Allela OQB, Pecho RDC, Jayasankar N, Rao DP, Thamaraikani T, Vasanthan M, Viktor P,

Lakshmaiya N, Saadh MJ, Amajd A, Abo-Zaid MA, Castillo-Acobo RY, Ismail AH, Amin AH, Akhavan-Sigari R. Progressing nanotechnology to improve targeted cancer treatment: overcoming hurdles in its clinical implementation. Mol Cancer. 2023 Oct 9;22(1):169. doi: 10.1186/s12943-023-01865-0.

32) Chen H, Zhang S, Xu C, Zhao G. Engineering protein interfaces yields ferritin disassembly and reassembly under benign experimental conditions. Chem Commun (Camb). 2016 Jun 11;52(46):7402-5. doi: 10.1039/c6cc03108k.

33) Chen W, Wahl SM. TGF-beta: receptors, signaling pathways and autoimmunity. Curr Dir Autoimmun. 2002;5:62-91. doi: 10.1159/000060548.

34) Cho K, Wang X, Nie S, Chen ZG, Shin DM. Therapeutic nanoparticles for drug delivery in cancer. Clin Cancer Res. 2008 Mar 1;14(5):1310-6. doi: 10.1158/1078-0432.CCR-07-1441.

35) Choi, Y., Nam, GH., Kim, G.B. *et al.* Nanocages displaying SIRP gamma clusters combined with prophagocytic stimulus of phagocytes potentiate anti-tumor immunity. Cancer Gene Ther 28, 960–970 (2021). Doi: https://doi.org/10.1038/s41417-021-00372-y

36) Collotta D, Bertocchi I, Chiapello E, Collino M. Antisense oligonucleotides: a novel Frontier in pharmacological strategy. Front Pharmacol. 2023 Nov 17;14:1304342. doi: 10.3389/fphar.2023.1304342.

37) Conti, G.; Pitea, M.;Ossanna, R.; Opri, R.; Tisci, G.; Falvo,E.; Innamorati, G.; Ghanem, E.; Sbarbati, A.; Ceci, P.; et al. Mitoxantrone-Loaded Nanoferritin Slows Tumor Growth and

Improves the Overall Survival Rate in a Subcutaneous Pancreatic Cancer Mouse Model. Biomedicines 2021, 9, 1622. https://doi.org/10.3390/ biomedicines9111622

38) Corry DB, Kiss A, Song LZ, Song L, Xu J, Lee SH, Werb Z, Kheradmand F. Overlapping and independent contributions of MMP2 and MMP9 to lung allergic inflammatory cell egression through decreased CC chemokines. FASEB J. 2004 Jun;18(9):995-7. doi: 10.1096/fj.03-1412fje.

39) Daliri EB, Oh DH, Lee BH. Bioactive Peptides. Foods. 2017 Apr 26;6(5):32. doi: 10.3390/foods6050032.

40) Damiani V, Falvo E, Fracasso G, Federici L, Pitea M, De Laurenzi V, Sala G, Ceci P. Therapeutic Efficacy of the Novel Stimuli-Sensitive Nano-Ferritins Containing Doxorubicin in a Head and Neck Cancer Model. Int J Mol Sci. 2017 Jul 18;18(7):1555. doi: 10.3390/ijms18071555.

41) Danhier F, Feron O, Préat V. To exploit the tumor microenvironment: Passive and active tumor targeting of nanocarriers for anti-cancer drug delivery. J Control Release. 2010 Dec 1;148(2):135-46. doi: 10.1016/j.jconrel.2010.08.027.

42) Daniels TR, Bernabeu E, Rodríguez JA, Patel S, Kozman M, Chiappetta DA, Holler E, Ljubimova JY, Helguera G, Penichet ML. The transferrin receptor and the targeted delivery of therapeutic agents against cancer. Biochim Biophys Acta. 2012 Mar;1820(3):291-317. doi: 10.1016/j.bbagen.2011.07.016.

43) de la Rica R, Matsui H. Applications of peptide and protein-based materials in bionanotechnology. Chem Soc Rev. 2010 Sep;39(9):3499-509. doi: 10.1039/b917574c.

44) de Visser KE, Joyce JA. The evolving tumor microenvironment: From cancer initiation to metastatic outgrowth. Cancer Cell. 2023 Mar 13;41(3):374-403. doi: 10.1016/j.ccell.2023.02.016.

45) Debnath S, Yallowitz AR, McCormick J, Lalani S, Zhang T, Xu R, Li N, Liu Y, Yang YS, Eiseman M, Shim JH, Hameed M, Healey JH, Bostrom MP, Landau DA, Greenblatt MB. Discovery of a periosteal stem cell mediating intramembranous bone formation. Nature. 2018 Oct;562(7725):133-139. doi: 10.1038/s41586-018-0554-8.

46) Din FU, Aman W, Ullah I, Qureshi OS, Mustapha O, Shafique S, Zeb A. Effective use of nanocarriers as drug delivery systems for the treatment of selected tumors. Int J Nanomedicine. 2017 Oct 5;12:7291-7309. doi: 10.2147/IJN.S146315.

47) Ding Y, Li S, Nie G. Nanotechnological strategies for therapeutic targeting of tumor vasculature. Nanomedicine (Lond). 2013 Jul;8(7):1209-22. doi: 10.2217/nnm.13.106.

48) Domínguez-Vera JM, Fernández B, Gálvez N. Native and synthetic ferritins for nanobiomedical applications: recent advances and new perspectives. Future Med Chem. 2010 Apr;2(4):609-18. doi: 10.4155/fmc.09.171.

49) Du C, Gong H, Zhao H, Wang P. Recent progress in the preparation of bioactive peptides using simulated gastrointestinal digestion processes. Food Chem. 2024 Sep 30;453:139587. doi: 10.1016/j.foodchem.2024.139587.

50) Ebrahimnia M, Alavi S, Vaezi H, Karamat Iradmousa M, Haeri A. Exploring the vast potentials and probable limitations of novel and

nanostructured implantable drug delivery systems for cancer treatment. EXCLI J. 2024 Feb 1;23:143-179. doi: 10.17179/excli2023-6747.

51) Endoh T, Ohtsuki T. Cellular siRNA delivery using cell-penetrating peptides modified for endosomal escape. Adv Drug Deliv Rev. 2009 Jul 25;61(9):704-9. doi: 10.1016/j.addr.2009.04.005.

52) Essa S, Rabanel JM, Hildgen P. Characterization of rhodamine loaded PEG-g-PLA nanoparticles (NPs): effect of poly(ethylene glycol) grafting density. Int J Pharm. 2011 Jun 15;411(1-2):178-87. doi: 10.1016/j.ijpharm.2011.02.039.

53) Falvo E, Arcovito A, Conti G, Cipolla G, Pitea M, Morea V, Damiani V, Sala G, Fracasso G, Ceci P. Engineered Human Nanoferritin Bearing the Drug Genz-644282 for Cancer Therapy. Pharmaceutics. 2020 Oct 20;12(10):992. doi: 10.3390/pharmaceutics12100992.

54) Falvo E, Damiani V, Conti G, Boschi F, Messana K, Giacomini P, Milella M, De Laurenzi V, Morea V, Sala G, Fracasso G, Ceci P. High activity and low toxicity of a novel CD71-targeting nanotherapeutic named The-0504 on preclinical models of several human aggressive tumors. J Exp Clin Cancer Res. 2021 Feb 10;40(1):63. doi: 10.1186/s13046-021-01851-8.

55) Falvo E, Malagrinò F, Arcovito A, Fazi F, Colotti G, Tremante E, Di Micco P, Braca A, Opri R, Giuffrè A, Fracasso G, Ceci P. The presence of glutamate residues on the PAS sequence of the stimuli-sensitive nano-ferritin improves *in vivo* biodistribution

and mitoxantrone encapsulation homogeneity. J Control Release. 2018 Apr 10;275:177-185. doi: 10.1016/j.jconrel.2018.02.025.

56) Falvo E, Tremante E, Arcovito A, Papi M, Elad N, Boffi A, Morea V, Conti G, Toffoli G, Fracasso G, Giacomini P, Ceci P. Improved Doxorubicin Encapsulation and Pharmacokinetics of Ferritin-Fusion Protein nanocarriers Bearing Proline, Serine, and Alanine Elements. Biomacromolecules. 2016 Feb 8;17(2):514-22. doi: 10.1021/acs.biomac.5b01446.

57) Falvo E, Tremante E, Fraioli R, Leonetti C, Zamparelli C, Boffi A, Morea V, Ceci P, Giacomini P. Antibody-drug conjugates: targeting melanoma with cisplatin encapsulated in protein-cage nanoparticles based on human ferritin. Nanoscale. 2013 Dec 21;5(24):12278-85. doi: 10.1039/c3nr04268e.

58) Fan D, Cao Y, Cao M, Wang Y, Cao Y, Gong T. Nanomedicine in cancer therapy. Signal Transduct Target Ther. 2023 Aug 7;8(1):293. doi: 10.1038/s41392-023-01536-y.

59) Fan K, Cao C, Pan Y, Lu D, Yang D, Feng J, Song L, Liang M, Yan X. Magnetoferritin nanoparticles for targeting and visualizing tumour tissues. Nat Nanotechnol. 2012 Jun 17;7(7):459-64. doi: 10.1038/nnano.2012.90.

60) Fan K, Gao L, Yan X. Human ferritin for tumor detection and therapy. Wiley Interdiscip Rev Nanomed Nanobiotechnol. 2013 Jul-Aug;5(4):287-98. doi: 10.1002/wnan.1221.

61) Fares F, Ganem S, Hajouj T, Agai E. Development of a long-acting erythropoietin by fusing the carboxyl-terminal peptide of human chorionic gonadotropin beta-subunit to the coding sequence of

human erythropoietin. Endocrinology. 2007 Oct;148(10):5081-7. doi: 10.1210/en.2007-0026.

62) Ferrari R, Colombo C, Casali C, Lupi M, Ubezio P, Falcetta F, D'Incalci M, Morbidelli M, Moscatelli D. Synthesis of surfactant free PCL-PEG brushed nanoparticles with tunable degradation kinetics. Int J Pharm. 2013 Sep 10;453(2):551-9. doi: 10.1016/j.ijpharm.2013.06.020.

63) Fire A, Xu S, Montgomery MK, Kostas SA, Driver SE, Mello CC. Potent and specific genetic interference by double-stranded RNA in Caenorhabditis elegans. Nature. 1998 Feb 19;391(6669):806-11. doi: 10.1038/35888.

64) Fracasso G, Falvo E, Colotti G, Fazi F, Ingegnere T, Amalfitano A, Doglietto GB, Alfieri S, Boffi A, Morea V, Conti G, Tremante E, Giacomini P, Arcovito A, Ceci P. Selective delivery of doxorubicin by novel stimuli-sensitive nano-ferritins overcomes tumor refractoriness. J Control Release. 2016 Oct 10;239:10-8. doi: 10.1016/j.jconrel.2016.08.010.

65) Fracasso G, Falvo E, Tisci G, Sala G, Colotti G, Cingarlini S, Tito C, Bibbo S, Frusteri C, Tremante E, Giordani E, Giacomini P, Ceci P. Widespread in vivo efficacy of The-0504: A conditionally-activatable nanoferritin for tumor-agnostic targeting of CD71-expressing cancers. Heliyon. 2023 Oct 6;9(10):e20770. doi: 10.1016/j.heliyon.2023.e20770.

66) Friedman AD, Claypool SE, Liu R. The smart targeting of nanoparticles. Curr Pharm Des. 2013;19(35):6315-29. doi: 10.2174/13816128113199990375.

67) Gammella E, Buratti P, Cairo G, Recalcati S. The transferrin receptor: the cellular iron gate. Metallomics. 2017 Oct 18;9(10):1367-1375. doi: 10.1039/c7mt00143f.

68) Griffin RJ, Avery E, Xia CQ. Predicting Approximate Clinically Effective Doses in Oncology Using Preclinical Efficacy and Body Surface Area Conversion: A Retrospective Analysis. Front Pharmacol. 2022 Apr 26;13:830972. doi: 10.3389/fphar.2022.830972.

69) Gullotti E, Yeo Y. Extracellularly activated nanocarriers: a new paradigm of tumor targeted drug delivery. Mol Pharm. 2009 Jul-Aug;6(4):1041-51. doi: 10.1021/mp900090z.

70) Harari D, Kuhn N, Abramovich R, Sasson K, Zozulya AL, Smith P, Schlapschy M, Aharoni R, Köster M, Eilam R, Skerra A, Schreiber G. Enhanced in vivo efficacy of a type I interferon superagonist with extended plasma half-life in a mouse model of multiple sclerosis. J Biol Chem. 2014 Oct 17;289(42):29014-29. doi: 10.1074/jbc.M114.602474.

71) Harrison PM, Arosio P. The ferritins: molecular properties, iron storage function and cellular regulation. Biochim Biophys Acta. 1996 Jul 31;1275(3):161-203. doi: 10.1016/0005-2728(96)00022-9.

72) He J, Xu S, Mixson AJ. The Multifaceted Histidine-Based Carriers for Nucleic Acid Delivery: Advances and Challenges. Pharmaceutics. 2020 Aug 14;12(8):774. doi: 10.3390/pharmaceutics12080774.

73) Heldin CH, Rubin K, Pietras K, Ostman A. High interstitial fluid pressure - an obstacle in cancer therapy. Nat Rev Cancer. 2004 Oct;4(10):806-13. doi: 10.1038/nrc1456.

74) Hobbs SK, Monsky WL, Yuan F, Roberts WG, Griffith L, Torchilin VP, Jain RK. Regulation of transport pathways in tumor vessels: role of tumor type and microenvironment. Proc Natl Acad Sci U S A. 1998 Apr

75) Hong S, Choi DW, Kim HN, Park CG, Lee W, Park HH. Protein-Based Nanoparticles as Drug Delivery Systems. Pharmaceutics. 2020 Jun 29;12(7):604. doi: 10.3390/pharmaceutics12070604.

76) Houghton PJ, Lock R, Carol H, Morton CL, Gorlick R, Anders Kolb E, Keir ST, Reynolds CP, Kang MH, Maris JM, Billups CA, Zhang MX, Madden SL, Teicher BA, Smith MA. Testing of the topoisomerase 1 inhibitor Genz-644282 by the pediatric preclinical testing program. Pediatr Blood Cancer. 2012 Feb;58(2):200-9. doi: 10.1002/pbc.23016.

77) Howell M, Wang C, Mahmoud A, Hellermann G, Mohapatra SS, Mohapatra S. Dual-function theranostic nanoparticles for drug delivery and medical imaging contrast: perspectives and challenges for use in lung diseases. Drug Deliv Transl Res. 2013 Aug 1;3(4):352-63. doi: 10.1007/s13346-013-0132-4.

78) Huang H, Qiao R, Zhao D, Zhang T, Li Y, Yi F, Lai F, Hong J, Ding X, Yang Z, Zhang L, Du Q, Liang Z. Profiling of mismatch discrimination in RNAi enabled rational design of allele-specific siRNAs. Nucleic Acids Res. 2009 Dec;37(22):7560-9. doi: 10.1093/nar/gkp835.

79) Huang X, Chisholm J, Zhuang J, Xiao Y, Duncan G, Chen X, Suk JS, Hanes J. Protein nanocages that penetrate airway mucus and tumor tissue. Proc Natl Acad Sci U S A. 2017 Aug 8;114(32):E6595-E6602. doi: 10.1073/pnas.1705407114.

80) Inoue I , Chiba M , Ito K , Okamatsu Y , Suga Y , Kitahara Y , Nakahara Y , Endo Y , Takahashi K , Tagami U , Okamoto N . One-step construction of ferritin encapsulation drugs for cancer chemotherapy. Nanoscale. 2021 Jan 28;13(3):1875-1883. doi: 10.1039/d0nr04019c.

81) Inoue I, Zheng B, Watanabe K, Ishikawa Y, Shiba K, Yasueda H, Uraoka Y, Yamashita I. A novel bifunctional protein supramolecule for construction of carbon nanotube-titanium hybrid material. Chem Commun (Camb). 2011 Dec 21;47(47):12649-51. doi: 10.1039/c1cc15221a.

82) Jain RK, Stylianopoulos T. Delivering nanomedicine to solid tumors. Nat Rev Clin Oncol. 2010 Nov;7(11):653-64. doi: 10.1038/nrclinonc.2010.139.

83) Jain RK. Delivery of molecular and cellular medicine to solid tumors. Adv Drug Deliv Rev. 2001 Mar 1;46(1-3):149-68. doi: 10.1016/s0169-409x(00)00131-9.

84) Jain RK. Transport of molecules in the tumor interstitium: a review. Cancer Res. 1987 Jun 15;47(12):3039-51.

85) Jain RK. Transport of molecules, particles, and cells in solid tumors. Annu Rev Biomed Eng. 1999;1:241-63. doi: 10.1146/annurev.bioeng.1.1.241.

86) Jeon IS, Yoo JD, Gurung S, Kim M, Lee C, Park EJ, Park RW, Lee B, Kim S. Anticancer nanocage platforms for combined immunotherapy designed to harness immune checkpoints and deliver anticancer drugs. Biomaterials. 2021 Mar;270:120685. doi: 10.1016/j.biomaterials.2021.120685.

87) Jones A, Harris AL. New developments in angiogenesis: a major mechanism for tumor growth and target for therapy. Cancer J Sci Am. 1998 Jul-Aug;4(4):209-17.

88) Juliano R, Alam MR, Dixit V, Kang H. Mechanisms and strategies for effective delivery of antisense and siRNA oligonucleotides. Nucleic Acids Res. 2008 Jul;36(12):4158-71. doi: 10.1093/nar/gkn342.

89) Kanapathipillai M, Brock A, Ingber DE. Nanoparticle targeting of anti-cancer drugs that alter intracellular signaling or influence the tumor microenvironment. Adv Drug Deliv Rev. 2014 Dec 15;79-80:107-18. doi: 10.1016/j.addr.2014.05.005.

90) Kang YF, Sun C, Zhuang Z, Yuan RY, Zheng Q, Li JP, Zhou PP, Chen XC, Liu Z, Zhang X, Yu XH, Kong XW, Zhu QY, Zhong Q, Xu M, Zhong NS, Zeng YX, Feng GK, Ke C, Zhao JC, Zeng MS. Rapid Development of SARS-CoV-2 Spike Protein Receptor-Binding Domain Self-Assembled Nanoparticle Vaccine Candidates. ACS Nano. 2021 Feb 23;15(2):2738-2752. doi: 10.1021/acsnano.0c08379.

91) Karati D, Kumar D. A Comprehensive Review on Targeted Cancer Therapy: New Face of Treatment Approach. Curr Pharm

Des. 2023;29(41):3282-3294.doi: 10.2174/0113816128272203231121034814.

92) Karlsson J, Rui Y, Kozielski KL, Placone AL, Choi O, Tzeng SY, Kim J, Keyes JJ, Bogorad MI, Gabrielson K, Guerrero-Cazares H, Quiñones-Hinojosa A, Searson PC, Green JJ. Engineered nanoparticles for systemic siRNA delivery to malignant brain tumours. Nanoscale. 2019 Nov 14;11(42):20045-20057. doi: 10.1039/c9nr04795f.

93) Kawasaki K, Rekhtman N, Quintanal-Villalonga Á, Rudin CM. Neuroendocrine neoplasms of the lung and gastrointestinal system: convergent biology and a path to better therapies. Nat Rev Clin Oncol. 2023 Jan;20(1):16-32. doi: 10.1038/s41571-022-00696-0.

94) Khoshnejad M, Parhiz H, Shuvaev VV, Dmochowski IJ, Muzykantov VR. Ferritin-based drug delivery systems: Hybrid nanocarriers for vascular immunotargeting. J Control Release. 2018 Jul 28;282:13-24. doi: 10.1016/j.jconrel.2018.02.042.

95) Köber C, Schmiedek F, Habermas T. Characterizing lifespan development of three aspects of coherence in life narratives: a cohort-sequential study. Dev Psychol. 2015 Feb;51(2):260-75. doi: 10.1037/a0038668.

96) Kocarnik JM, Compton K, Dean FE, Fu W, Gaw BL, Harvey JD, Henrikson HJ, Lu D, Pennini A, Xu R, Ababneh E, Abbasi-Kangevari M, et al., Cancer Incidence, Mortality, Years of Life Lost, Years Lived With Disability, and Disability-Adjusted Life Years for 29 Cancer Groups From 2010 to 2019: A Systematic

Analysis for the Global Burden of Disease Study 2019. JAMA Oncol. 2022 Mar 1;8(3):420-444. doi: 10.1001/jamaoncol.2021.6987.

97) Komori T. Regulation of Proliferation, Differentiation and Functions of Osteoblasts by Runx2. Int J Mol Sci. 2019 Apr 4;20(7):1694. doi: 10.3390/ijms20071694.

98) Kotagiri N, Lee JS, Kim JW. Selective pathogen targeting and macrophage evading carbon nanotubes through dextran sulfate coating and PEGylation for photothermal theranostics. J Biomed Nanotechnol. 2013 Jun;9(6):1008-16. doi: 10.1166/jbn.2013.1531.

99) Kreuter J. Nanoparticles--a historical perspective. Int J Pharm. 2007 Feb 22;331(1):1-10. doi: 10.1016/j.ijpharm.2006.10.021.

100) Krishna R, Mayer LD. Multidrug resistance (MDR) in cancer. Mechanisms, reversal using modulators of MDR and the role of MDR modulators in influencing the pharmacokinetics of anticancer drugs. Eur J Pharm Sci. 2000 Oct;11(4):265-83. doi: 10.1016/s0928-0987(00)00114-7.

101) Kurreck J, Wyszko E, Gillen C, Erdmann VA. Design of antisense oligonucleotides stabilized by locked nucleic acids. Nucleic Acids Res. 2002 May 1;30(9):1911-8. doi: 10.1093/nar/30.9.1911.

102) Kurtzberg L.S., S. Roth, R. Krumbholz, J. Crawford, C. Bormann, S. Dunham, M. Yao, C. Rouleau, R.G. Bagley, X.-J. Yu, F. Wang, S.M. Schmid, E.J. LaVoie, B.A. Teicher, Genz-644282, a Novel Non-Camptothecin Topoisomerase I Inhibitor for Cancer

Treatment, Clinical Cancer Research. 17 (2011) 2777–2787. https://doi.org/10.1158/1078-0432.CCR-10-0542.

103) Kurtzberg LS, Roth S, Krumbholz R, Crawford J, Bormann C, Dunham S, Yao M, Rouleau C, Bagley RG, Yu XJ, Wang F, Schmid SM, Lavoie EJ, Teicher BA. Genz-644282, a novel non-camptothecin topoisomerase I inhibitor for cancer treatment. Clin Cancer Res. 2011 May 1;17(9):2777-87. doi: 10.1158/1078-0432.CCR-10-0542.

104) Kwon C, Kang YJ, Jeon S, Jung S, Hong SY, Kang S. Development of protein-cage-based delivery nanoplatforms by polyvalently displaying β-cyclodextrins on the surface of ferritins through copper(I)-catalyzed azide/alkyne cycloaddition. Macromol Biosci. 2012 Nov;12(11):1452-8. doi: 10.1002/mabi.201200178.

105) Lammers T, Kiessling F, Hennink WE, Storm G. Drug targeting to tumors: principles, pitfalls and (pre-) clinical progress. J Control Release. 2012 Jul 20;161(2):175-87. doi: 10.1016/j.jconrel.2011.09.063.

106) LaRocque J, Bharali DJ, Mousa SA. Cancer detection and treatment: the role of nanomedicines. Mol Biotechnol. 2009 Jul;42(3):358-66. doi: 10.1007/s12033-009-9161-0.

107) Lattanzi W, Barba M, Novegno F, Massimi L, Tesori V, Tamburrini G, Galgano S, Bernardini C, Caldarelli M, Michetti F, Di Rocco C. Lim mineralization protein is involved in the premature calvarial ossification in sporadic craniosynostoses. Bone. 2013 Jan;52(1):474-84. doi: 10.1016/j.bone.2012.09.004.

108) Lawrence CM, Ray S, Babyonyshev M, Galluser R, Borhani DW, Harrison SC. Crystal structure of the ectodomain of human transferrin receptor. Science. 1999 Oct 22;286(5440):779-82. doi: 10.1126/science.286.5440.779.

109) Lawson DM, Artymiuk PJ, Yewdall SJ, Smith JM, Livingstone JC, Treffry A, Luzzago A, Levi S, Arosio P, Cesareni G, et al. Solving the structure of human H ferritin by genetically engineering intermolecular crystal contacts. Nature. 1991 Feb 7;349(6309):541-4. doi: 10.1038/349541a0

110) Leamon CP, Reddy JA. Folate-targeted chemotherapy. Adv Drug Deliv Rev. 2004 Apr 29;56(8):1127-41. doi: 10.1016/j.addr.2004.01.008.

111) Lebrón JA, Bennett MJ, Vaughn DE, Chirino AJ, Snow PM, Mintier GA, Feder JN, Bjorkman PJ. Crystal structure of the hemochromatosis protein HFE and characterization of its interaction with transferrin receptor. Cell. 1998 Apr 3;93(1):111-23. doi: 10.1016/s0092-8674(00)81151-4.

112) Lee NK, Lee EJ, Kim S, Nam GH, Kih M, Hong Y, Jeong C, Yang Y, Byun Y, Kim IS. Ferritin nanocage with intrinsically disordered proteins and affibody: A platform for tumor targeting with extended pharmacokinetics. J Control Release. 2017 Dec 10;267:172-180. doi: 10.1016/j.jconrel.2017.08.014.

113) Li L, Fang CJ, Ryan JC, Niemi EC, Lebrón JA, Björkman PJ, Arase H, Torti FM, Torti SV, Nakamura MC, Seaman WE. Binding and uptake of H-ferritin are mediated by human

transferrin receptor-1. Proc Natl Acad Sci U S A. 2010 Feb 23;107(8):3505-10. doi: 10.1073/pnas.0913192107.

114) Links M, Brown R. Clinical relevance of the molecular mechanisms of resistance to anti-cancer drugs. Expert Rev Mol Med. 1999 Oct 25. doi: 10.1017/S1462399499001099X.

115) Liu T, Li L, Cheng C, He B, Jiang T. Emerging prospects of protein/peptide-based nanoassemblies for drug delivery and vaccine development. Nano Res. 2022;15(8):7267-7285. doi: 10.1007/s12274-022-4385-4.

116) Lobatto ME, Fuster V, Fayad ZA, Mulder WJ. Perspectives and opportunities for nanomedicine in the management of atherosclerosis. Nat Rev Drug Discov. 2011 Oct 21;10(11):835-52. doi: 10.1038/nrd3578. Erratum in: Nat Rev Drug Discov. 2011 Dec;10(12):963

117) Lu J, Gao X, Wang S, He Y, Ma X, Zhang T, Liu X. Advanced strategies to evade the mononuclear phagocyte system clearance of nanomaterials. Exploration (Beijing). 2023 Jan 5;3(1):20220045. doi: 10.1002/EXP.20220045.

118) Maeda H, Wu J, Sawa T, Matsumura Y, Hori K. Tumor vascular permeability and the EPR effect in macromolecular therapeutics: a review. J Control Release. 2000 Mar 1;65(1-2):271-84. doi: 10.1016/s0168-3659(99)00248-5

119) Maeda H. The enhanced permeability and retention (EPR) effect in tumor vasculature: the key role of tumor-selective macromolecular drug targeting. Adv Enzyme Regul. 2001;41:189-207. doi: 10.1016/s0065-2571(00)00013-3.

120) Malam Y, Loizidou M, Seifalian AM. Liposomes and nanoparticles: nanosized vehicles for drug delivery in cancer. Trends Pharmacol Sci. 2009 Nov;30(11):592-9. doi: 10.1016/j.tips.2009.08.004.

121) Manivasagan P, Ashokkumar S, Manohar A, Joe A, Han HW, Seo SH, Thambi T, Duong HS, Kaushik NK, Kim KH, Choi EH, Jang ES. Biocompatible Calcium Ion-Doped Magnesium Ferrite Nanoparticles as a New Family of Photothermal Therapeutic Materials for Cancer Treatment. Pharmaceutics. 2023 May 21;15(5):1555. doi: 10.3390/pharmaceutics15051555.

122) Manohar A., Vattikuti S.V.P., Manivasagan P., Jang E.S., Abdelghani H.T.M., Kim K.H., Synthesis and characterization of CeO2/MgFe2O4 nanocomposites for electrochemical study and their cytotoxicity in normal human dermal fibroblast (HDF) and human breast cancer (MDA-MB-231) cell lines, J. Alloys Compd. 968 (2023), 171932, https://doi.org/10.1016/J.JALLCOM.2023.171932.

123) Manohar A., Vijayakanth V., Chintagumpala K., Manivasagan P., Jang E.S., Kim K.H., Zn- doped MnFe2O4 nanoparticles for magnetic hyperthermia and their cytotoxicity study in normal and cancer cell lines, Colloids Surf. A Physicochem. Eng. Asp. 675 (2023), https://doi.org/10.1016/j.colsurfa.2023.132037.

124) Marrocco, F., Falvo, E., Mosca, L. et al. Nose-to-brain selective drug delivery to glioma via ferritin-based nanovectors reduces tumor growth and improves survival rate. Cell Death Dis 15, 262 (2024). Doi: https://doi.org/10.1038/s41419-024-06653-2

125) Martinez JO, Chiappini C, Ziemys A, Faust AM, Kojic M, Liu X, Ferrari M, Tasciotti E. Engineering multi-stage nanovectors for controlled degradation and tunable release kinetics. Biomaterials. 2013 Nov;34(33):8469-77. doi: 10.1016/j.biomaterials.2013.07.049.

126) Maruyama K, Ishida O, Takizawa T, Moribe K. Possibility of active targeting to tumor tissues with liposomes. Adv Drug Deliv Rev. 1999 Nov 10;40(1-2):89-102. doi: 10.1016/s0169-409x(99)00042-3.

127) Matsumura Y, Maeda H. A new concept for macromolecular therapeutics in cancer chemotherapy: mechanism of tumoritropic accumulation of proteins and the antitumor agent smancs. Cancer Res. 1986 Dec;46(12 Pt 1):6387-92.

128) Miraoui H, Oudina K, Petite H, Tanimoto Y, Moriyama K, Marie PJ. Fibroblast growth factor receptor 2 promotes osteogenic differentiation in mesenchymal cells via ERK1/2 and protein kinase C signaling. J Biol Chem. 2009 Feb 20;284(8):4897-904. doi: 10.1074/jbc.M805432200.

129) Mitchell MJ, Billingsley MM, Haley RM, Wechsler ME, Peppas NA, Langer R. Engineering precision nanoparticles for drug delivery. Nat Rev Drug Discov. 2021 Feb;20(2):101-124. doi: 10.1038/s41573-020-0090-8.

130) Modi S, Jacot W, Yamashita T, Sohn J, Vidal M, Tokunaga E, Tsurutani J, Ueno NT, Prat A, Chae YS, Lee KS, Niikura N, Park YH, Xu B, Wang X, Gil-Gil M, Li W, Pierga JY, Im SA, Moore

HCF, Rugo HS, Yerushalmi R, Zagouri F, Gombos A, Kim SB, Liu Q, Luo T, Saura C, Schmid P, Sun T, Gambhire D, Yung L, Wang Y, Singh J, Vitazka P, Meinhardt G, Harbeck N, Cameron DA; DESTINY-Breast04 Trial Investigators. Trastuzumab Deruxtecan in Previously Treated HER2-Low Advanced Breast Cancer. N Engl J Med. 2022 Jul 7;387(1):9-20. doi: 10.1056/NEJMoa2203690.

131) Montemiglio LC, Testi C, Ceci P, Falvo E, Pitea M, Savino C, Arcovito A, Peruzzi G, Baiocco P, Mancia F, Boffi A, des Georges A, Vallone B. Cryo-EM structure of the human ferritin-transferrin receptor 1 complex. Nat Commun. 2019 Mar 8;10(1):1121. doi: 10.1038/s41467-019-09098-w.

132) Morabito M, Larcher M, Cavalli FM, Foray C, Forget A, Mirabal-Ortega L, Andrianteranagna M, Druillennec S, Garancher A, Masliah-Planchon J, Leboucher S, Debalkew A, Raso A, Delattre O, Puget S, Doz F, Taylor MD, Ayrault O, Bourdeaut F, Eychène A, Pouponnot C. An autocrine ActivinB mechanism drives TGFβ/Activin signaling in Group 3 medulloblastoma. EMBO Mol Med. 2019 Aug;11(8):e9830. doi: 10.15252/emmm.201809830.

133) Nie S, Xing Y, Kim GJ, Simons JW. Nanotechnology applications in cancer. Annu Rev Biomed Eng. 2007;9:257-88. doi: 10.1146/annurev.bioeng.9.060906.152025.

134) Niland S, Eble JA. Neuropilins in the Context of Tumor Vasculature. Int J Mol Sci. 2019 Feb 1;20(3):639. doi: 10.3390/ijms20030639.

135) Obozina AS, Komedchikova EN, Kolesnikova OA, Iureva AM, Kovalenko VL, Zavalko FA, Rozhnikova TV, Tereshina ED, Mochalova EN, Shipunova VO. Genetically Encoded Self-Assembling Protein Nanoparticles for the Targeted Delivery *In Vitro* and *In Vivo*. Pharmaceutics. 2023 Jan 10;15(1):231. doi: 10.3390/pharmaceutics15010231.

136) Onichtchouk D, Chen YG, Dosch R, Gawantka V, Delius H, Massagué J, Niehrs C. Silencing of TGF-beta signalling by the pseudoreceptor BAMBI. Nature. 1999 Sep 30;401(6752):480-5. doi: 10.1038/46794.

137) Overall CM, Kleifeld O. Tumour microenvironment - opinion: validating matrix metalloproteinases as drug targets and anti-targets for cancer therapy. Nat Rev Cancer. 2006 Mar;6(3):227-39. doi: 10.1038/nrc1821.

138) Paciotti GF, Myer L, Weinreich D, Goia D, Pavel N, McLaughlin RE, Tamarkin L. Colloidal gold: a novel nanoparticle vector for tumor directed drug delivery. Drug Deliv. 2004 May-Jun;11(3):169-83. doi: 10.1080/10717540490433895.

139) Pang HB, Braun GB, She ZG, Kotamraju VR, Sugahara KN, Teesalu T, Ruoslahti E. A free cysteine prolongs the half-life of a homing peptide and improves its tumor-penetrating activity. J Control Release. 2014 Feb 10;175:48-53. doi: 10.1016/j.jconrel.2013.12.006.

140) Papisov MI. Theoretical considerations of RES-avoiding liposomes: Molecular mechanics and chemistry of liposome

interactions. Adv Drug Deliv Rev. 1998 Jun 8;32(1-2):119-138. doi: 10.1016/s0169-409x(97)00135-x.

141) Park J, Zhang Y, Vykhodtseva N, Jolesz FA, McDannold NJ. The kinetics of blood brain barrier permeability and targeted doxorubicin delivery into brain induced by focused ultrasound. J Control Release. 2012 Aug 20;162(1):134-42. doi: 10.1016/j.jconrel.2012.06.012.

142) Patel H., J. Li, L. Bo, R. Mehta, C.R. Ashby, S. Wang, W. Cai, Z.S. Chen, Nanotechnologybased delivery systems to overcome drug resistance in cancer, Med. Rev. 4 (2024). Doi: https://doi.org/10.1515/mr-2023-0058.

143) Patel HM, Moghimi SM. Serum-mediated recognition of liposomes by phagocytic cells of the reticuloendothelial system - The concept of tissue specificity. Adv Drug Deliv Rev. 1998 Jun 8;32(1-2):45-60. doi: 10.1016/s0169-409x(97)00131-2.

144) Peer D, Karp JM, Hong S, Farokhzad OC, Margalit R, Langer R. Nanocarriers as an emerging platform for cancer therapy. Nat Nanotechnol. 2007 Dec;2(12):751-60. doi: 10.1038/nnano.2007.387.

145) Pérez-Herrero E, Fernández-Medarde A. Advanced targeted therapies in cancer: Drug nanocarriers, the future of chemotherapy. Eur J Pharm Biopharm. 2015 Jun;93:52-79. doi: 10.1016/j.ejpb.2015.03.018.

146) Perrault SD, Chan WC. In vivo assembly of nanoparticle components to improve targeted cancer imaging. Proc Natl Acad Sci U S A. 2010 Jun 22;107(25):11194-9. doi: 10.1073/pnas.1001367107.

147) Pozzi D, Colapicchioni V, Caracciolo G, Piovesana S, Capriotti AL, Palchetti S, De Grossi S, Riccioli A, Amenitsch H, Laganà A. Effect of polyethyleneglycol (PEG) chain length on the bio-nano-interactions between PEGylated lipid nanoparticles and biological fluids: from nanostructure to uptake in cancer cells. Nanoscale. 2014 Mar 7;6(5):2782-92. doi: 10.1039/c3nr05559k.

148) Quintero-Fabián S, Arreola R, Becerril-Villanueva E, Torres-Romero JC, Arana-Argáez V, Lara-Riegos J, Ramírez-Camacho MA, Alvarez-Sánchez ME. Role of Matrix Metalloproteinases in Angiogenesis and Cancer. Front Oncol. 2019 Dec 6;9:1370. doi: 10.3389/fonc.2019.01370.

149) Rea J, Carissimo A, Trisciuoglio D, Illi B, Picard D, Remke M, Laneve P, Caffarelli E. Identification and Functional Characterization of Novel MYC-Regulated Long Noncoding RNAs in Group 3 Medulloblastoma. Cancers (Basel). 2021 Jul 30;13(15):3853. doi: 10.3390/cancers13153853.

150) Rizzolio S, Tamagnone L. Multifaceted role of neuropilins in cancer. Curr Med Chem. 2011;18(23):3563-75. doi: 10.2174/092986711796642544.

151) Roberts, T. C., Langer, R., and Wood, M. J. A. (2020). Advances in oligonucleotide drug delivery. Nat. Rev. Drug Discov. 19 (10), 673–694. doi:10.1038/s41573-020-0075-7.

152) Romberg B, Hennink WE, Storm G. Sheddable coatings for long-circulating nanoparticles. Pharm Res. 2008 Jan;25(1):55-71. doi: 10.1007/s11095-007-9348-7. Epub 2007 Jun 6.

153) Rose SD, Kim DH, Amarzguioui M, Heidel JD, Collingwood MA, Davis ME, Rossi JJ, Behlke MA. Functional polarity is

introduced by Dicer processing of short substrate RNAs. Nucleic Acids Res. 2005 Jul 26;33(13):4140-56. doi: 10.1093/nar/gki732.

154) Rossin R, Pan D, Qi K, Turner JL, Sun X, Wooley KL, Welch MJ. 64Cu-labeled folate-conjugated shell cross-linked nanoparticles for tumor imaging and radiotherapy: synthesis, radiolabeling, and biologic evaluation. J Nucl Med. 2005 Jul;46(7):1210-8.

155) Rubin MA. Targeted therapy of cancer: new roles for pathologists--prostate cancer. Mod Pathol. 2008 May;21 Suppl 2:S44-55. doi: 10.1038/modpathol.2008.11.

156) Rubin P, Casarett G. Microcirculation of tumors. I. Anatomy, function, and necrosis. Clin Radiol. 1966 Jul;17(3):220-9.

157) Sakhrani NM, Padh H. Organelle targeting: third level of drug targeting. Drug Des Devel Ther. 2013 Jul 17;7:585-99. doi: 10.2147/DDDT.S45614.

158) Salmaso S, Caliceti P. Self assembling nanocomposites for protein delivery: supramolecular interactions of soluble polymers with protein drugs. Int J Pharm. 2013 Jan 2;440(1):111-23. doi: 10.1016/j.ijpharm.2011.12.029.

159) Sant S, Poulin S, Hildgen P. Effect of polymer architecture on surface properties, plasma protein adsorption, and cellular interactions of pegylated nanoparticles. J Biomed Mater Res A. 2008 Dec 15;87(4):885-95. doi: 10.1002/jbm.a.31800.

160) Santucci C, Mignozzi S, Malvezzi M, Boffetta P, Collatuzzo G, Levi F, La Vecchia C, Negri E. European cancer mortality predictions for the year 2024 with focus on colorectal cancer. Ann

Oncol. 2024 Mar;35(3):308-316. doi: 10.1016/j.annonc.2023.12.003.

161) Schlapschy M, Binder U, Börger C, Theobald I, Wachinger K, Kisling S, Haller D, Skerra A. PASylation: a biological alternative to PEGylation for extending the plasma half-life of pharmaceutically active proteins. Protein Eng Des Sel. 2013 Aug;26(8):489-501. doi: 10.1093/protein/gzt023.

162) Schmierer B, Hill CS. TGFbeta-SMAD signal transduction: molecular specificity and functional flexibility. Nat Rev Mol Cell Biol. 2007 Dec;8(12):970-82. doi: 10.1038/nrm2297.

163) Schwarz DS, Ding H, Kennington L, Moore JT, Schelter J, Burchard J, Linsley PS, Aronin N, Xu Z, Zamore PD. Designing siRNA that distinguish between genes that differ by a single nucleotide. PLoS Genet. 2006 Sep 8;2(9):e140. doi: 10.1371/journal.pgen.0020140.

164) Seligson JM, Patron AM, Berger MJ, Harvey RD, Seligson ND. Sacituzumab Govitecan-hziy: An Antibody-Drug Conjugate for the Treatment of Refractory, Metastatic, Triple-Negative Breast Cancer. Ann Pharmacother. 2021 Jul;55(7):921-931. doi: 10.1177/1060028020966548.

165) Shamsi MH, Kraatz HB. Probing nucleobase mismatch variations by electrochemical techniques: exploring the effects of position and nature of the single-nucleotide mismatch. Analyst. 2010 Sep;135(9):2280-5. doi: 10.1039/c0an00184h.

166) Shi P, Cheng Z, Zhao K, Chen Y, Zhang A, Gan W, Zhang Y. Active targeting schemes for nano-drug delivery systems in

osteosarcoma therapeutics. J Nanobiotechnology. 2023 Mar 22;21(1):103. doi: 10.1186/s12951-023-01826-1.

167) Shubik P. Vascularization of tumors: a review. J Cancer Res Clin Oncol. 1982. doi: 10.1007/BF00409698.

168) Sooryakumar D, Dexheimer TS, Teicher BA, Pommier Y. Molecular and cellular pharmacology of the novel noncamptothecin topoisomerase I inhibitor Genz-644282. Mol Cancer Ther. 2011 Aug;10(8):1490-9. doi: 10.1158/1535-7163.MCT-10-1043.

169) Soutschek J, Akinc A, Bramlage B, Charisse K, Constien R, Donoghue M, Elbashir S, Geick A, Hadwiger P, Harborth J, John M, Kesavan V, Lavine G, Pandey RK, Racie T, Rajeev KG, Röhl I, Toudjarska I, Wang G, Wuschko S, Bumcrot D, Koteliansky V, Limmer S, Manoharan M, Vornlocher HP. Therapeutic silencing of an endogenous gene by systemic administration of modified siRNAs. Nature. 2004 Nov 11;432(7014):173-8. doi: 10.1038/nature03121.

170) Strohl WR. Fusion Proteins for Half-Life Extension of Biologics as a Strategy to Make Biobetters. BioDrugs. 2015 Aug;29(4):215-39. doi: 10.1007/s40259-015-0133-6.

171) Subhan MA, Yalamarty SSK, Filipczak N, Parveen F, Torchilin VP. Recent Advances in Tumor Targeting via EPR Effect for Cancer Treatment. J Pers Med. 2021 Jun 18;11(6):571. doi: 10.3390/jpm11060571.

172) Sudimack J, Lee RJ. Targeted drug delivery via the folate receptor. Adv Drug Deliv Rev. 2000 Mar 30;41(2):147-62. doi: 10.1016/s0169-409x(99)00062-9.

173) Sun T, Zhang YS, Pang B, Hyun DC, Yang M, Xia Y. Engineered nanoparticles for drug delivery in cancer therapy. Angew Chem Int Ed Engl. 2014 Nov 10;53(46):12320-64. doi: 10.1002/anie.201403036.

174) Sung H, Ferlay J, Siegel RL, Laversanne M, Soerjomataram I, Jemal A, Bray F. Global Cancer Statistics 2020: GLOBOCAN Estimates of Incidence and Mortality Worldwide for 36 Cancers in 185 Countries. CA Cancer J Clin. 2021 May;71(3):209-249. doi: 10.3322/caac.21660.

175) Talekar M, Kendall J, Denny W, Garg S. Targeting of nanoparticles in cancer: drug delivery and diagnostics. Anticancer Drugs. 2011 Nov;22(10):949-62. doi: 10.1097/CAD.0b013e32834a4554.

176) Tesarova B, Dostalova S., Smidova V., Goliasova Z., Skubalova Z., et al., Surface-PASylation of ferritin to form stealth nanovehicles enhances *in vivo* therapeutic performance of encapsulated ellipticine, Applied Materials Today,Volume 18,2020. Doi: https://doi.org/10.1016/j.apmt.2019.100501.

177) Thomas CR, Ferris DP, Lee JH, Choi E, Cho MH, Kim ES, Stoddart JF, Shin JS, Cheon J, Zink JI. Noninvasive remote-controlled release of drug molecules in vitro using magnetic actuation of mechanized nanoparticles. J Am Chem Soc. 2010 Aug 11;132(31):10623-5. doi: 10.1021/ja1022267.

178) Ulldemolins A, Seras-Franzoso J, Andrade F, Rafael D, Abasolo I, Gener P, Schwartz S Jr. Perspectives of nano-carrier drug delivery systems to overcome cancer drug resistance in the clinics. Cancer Drug Resist. 2021 Mar 19;4(1):44-68. doi: 10.20517/cdr.2020.59.

179) Vanhoutte D, Schips TG, Minerath RA, Huo J, Kavuri NSS, Prasad V, Lin SC, Bround MJ, Sargent MA, Adams CM, Molkentin JD. Thbs1 regulates skeletal muscle mass in a TGFβ-Smad2/3-ATF4-dependent manner. Cell Rep. 2024 May 28;43(5):114149. doi: 10.1016/j.celrep.2024.114149.

180) Vannucci L, Falvo E, Failla CM, Carbo M, Fornara M, Canese R, Cecchetti S, Rajsiglova L, Stakheev D, Krizan J, Boffi A, Carpinelli G, Morea V, Ceci P. In Vivo Targeting of Cutaneous Melanoma Using an Melanoma Stimulating Hormone-Engineered Human Protein Cage with Fluorophore and Magnetic Resonance Imaging Tracers. J Biomed Nanotechnol. 2015 Jan;11(1):81-92. doi: 10.1166/jbn.2015.1946.

181) Vannucci L, Falvo E, Fornara M, Di Micco P, Benada O, Krizan J, Svoboda J, Hulikova-Capkova K, Morea V, Boffi A, Ceci P. Selective targeting of melanoma by PEG-masked protein-based multifunctional nanoparticles. Int J Nanomedicine. 2012;7:1489-509. doi: 10.2147/IJN.S28242.

182) Vannucci, L, Falvo, E, Ceci, P. Multifunctional Protein-Based Nanoparticles for Cancer Theranosis. 2014, A. Prokop et al. (eds.), Intracellular Delivery II, Fundamental Biomedical Technologies 7. doi: 10.1007/978-94-017-8896-0_12.

183) Vasir JK, Labhasetwar V. Targeted drug delivery in cancer therapy. Technol Cancer Res Treat. 2005 Aug. doi: 10.1177/153303460500400405.

184) Wang L., N. Wang, W. Zhang, X. Cheng, Z. Yan, G. Shao, X. Wang, R. Wang, C. Fu, Therapeutic peptides: current applications and future directions, Signal Transduct. Target. Ther. 7 (2022). https://doi.org/10.1038/s41392-022-00904-4.

185) Wang W, Liu Z, Zhou X, Guo Z, Zhang J, Zhu P, Yao S, Zhu M. Ferritin nanoparticle-based SpyTag/SpyCatcher-enabled click vaccine for tumor immunotherapy. Nanomedicine. 2019 Feb;16:69-78. doi: 10.1016/j.nano.2018.11.009.

186) Wang Z, Chui WK, Ho PC. Nanoparticulate delivery system targeted to tumor neovasculature for combined anticancer and antiangiogenesis therapy. Pharm Res. 2011 Mar;28(3):585-96. doi: 10.1007/s11095-010-0308-2.

187) Weiss A, Attisano L. The TGFbeta superfamily signaling pathway. Wiley Interdiscip Rev Dev Biol. 2013 Jan-Feb;2(1):47-63. doi: 10.1002/wdev.86.

188) Wu Y, Sefah K, Liu H, Wang R, Tan W. DNA aptamer-micelle as an efficient detection/delivery vehicle toward cancer cells. Proc Natl Acad Sci U S A. 2010 Jan 5;107(1):5-10. doi: 10.1073/pnas.0909611107.

189) Xiao K, Li Y, Luo J, Lee JS, Xiao W, Gonik AM, Agarwal RG, Lam KS. The effect of surface charge on *in vivo* biodistribution of PEG-oligocholic acid based micellar nanoparticles. Biomaterials. 2011 May;32(13):3435-46. doi: 10.1016/j.biomaterials.2011.01.021.

190) Xie J, Xu C, Kohler N, Hou Y, Sun S. Controlled PEGylation of monodisperse Fe3O4 nanoparticles for reduced non-specific uptake by macrophage cells. Adv Mater; 2007; 19(20):3163.

191) Xin Q, Wang D, Wang S, Zhang L, Liang Q, Yan X, Fan K, Jiang B. Tackling Esophageal Squamous Cell Carcinoma with ITFn-Pt(IV): A Novel Fusion of PD-L1 Blockade, Chemotherapy, and T-cell Activation. Adv Healthc Mater. 2024 Apr;13(11):e2303623. doi: 10.1002/adhm.202303623.

192) Yu MK, Park J, Jon S. Targeting strategies for multifunctional nanoparticles in cancer imaging and therapy. Theranostics. 2012. doi: 10.7150/thno.3463.

193) Yuan Z, Wang B, Teng Y, Ho W, Hu B, Boakye-Yiadom KO, Xu X, Zhang XQ. Rational design of engineered H-ferritin nanoparticles with improved siRNA delivery efficacy across an *in vitro* model of the mouse BBB. Nanoscale. 2022 May 5;14(17):6449-6464. doi: 10.1039/d1nr07880a.

194) Zhang H, Vandesompele J, Braeckmans K, De Smedt SC, Remaut K. Nucleic acid degradation as barrier to gene delivery: a guide to understand and overcome nuclease activity. Chem Soc Rev. 2024 Jan 2;53(1):317-360. doi: 10.1039/d3cs00194f. PMID: 38073448.

195) Zhang L, Li L, Di Penta A, Carmona U, Yang F, Schöps R, Brandsch M, Zugaza JL, Knez M. H-Chain Ferritin: A Natural Nuclei Targeting and Bioactive Delivery Nanovector. Adv Healthc Mater. 2015 Jun 24;4(9):1305-10. doi: 10.1002/adhm.201500226.

196) Zhen Z, Tang W, Chen H, Lin X, Todd T, Wang G, Cowger T, Chen X, Xie J. RGD-modified apoferritin nanoparticles for efficient drug delivery to tumors. ACS Nano. 2013 Jun 25;7(6):4830-7. doi: 10.1021/nn305791q.

197) Zhu S, Chen W, Masson A, Li YP. Cell signaling and transcriptional regulation of osteoblast lineage commitment, differentiation, bone formation, and homeostasis. Cell Discov. 2024 Jul 2;10(1):71. doi: 10.1038/s41421-024-00689-6.

7. APPENDIX

Publications produced during this Ph.D thesis:

- Grandioso A, Tollis P, Pellegrini FR, Falvo E, Palma A, Migliaccio F, Belvedere A, Rea J, **Tisci G**, Carissimo A, Bozzoni I, Trisciuoglio D, Ballarino M, Ceci P, Laneve P. **"A circuit involving the lncRNA MB3 and the driver genes MYC and OTX2 inhibits apoptosis in Group 3 Medulloblastoma by regulating the TGF-β pathway via HMGN5".** Nature Communications. 2024 November, "*submitted*".

- Tiberio F, Salvati M, Polito L, **Tisci G**, Vita A, Parolini O, Massimi L, Di Pietro L, Ceci P, Tamburrini P, Arcovito A, Falvo E, Lattanzi W. **"Targeted allele-specific FGFR2 knockdown via human recombinant ferritin nanoparticles for personalized treatment of Crouzon syndrome".** Molecular Therapy Nucleic Acids (MTNA). 2024 July, "*submitted, under revision*".

- **Tisci G**, Rajsiglova L, Bibbo S, Zicchedda G, Falvo E, De Laurenzi V, Sala G, Colotti G, Arcovito A, Giacon N, Vannucci L, Giacomini P and Pierpaolo Ceci. **"Boosting of targeted therapy, chemotherapy and immunotherapy by a novel noncytotoxic nanovector THE-10 based on recombinant human ferritin"**. International Journal of Biological Macromolecules. 2024 July, "*submitted, under revision*".

- Marrocco F, Falvo E, Mosca L, **Tisci G**, Arcovito A, Reccagni A, Limatola C, Bernardini R, Ceci P, D'Alessandro G, Colotti G. **"Nose-to-brain selective drug delivery to glioma via ferritin-based nanovectors reduces tumor growth and improves survival rate."**

Cell Death Disease. 2024 April 13;15(4):262. doi: 10.1038/s41419-024-06653-2.

- Fracasso G, Falvo E, **Tisci G**, Sala G, Colotti G, Cingarlini S, Tito C, Bibbo S, Frusteri C, Tremante E, Giordani E, Giacomini P, Ceci P. **"Widespread in vivo efficacy of The-0504: A conditionally-activatable nanoferritin for tumor-agnostic targeting of CD71-expressing cancers."** Heliyon 2023 October 6;9(10):e20770. doi: 10.1016/j.heliyon.2023.e20770.

- Conti G, Pitea M, Ossanna R, Opri R, **Tisci G**, Falvo E, Innamorati G, Ghanem E, Sbarbati A, Ceci P, Fracasso G. **"Mitoxantrone-Loaded Nanoferritin Slows Tumor Growth and Improves the Overall Survival Rate in a Subcutaneous Pancreatic Cancer Mouse Model."** Biomedicines 2021 November 5;9(11):1622. doi: 10.3390/biomedicines9111622.